SURFACE MICROSTRUCTURE OF BACTERIAL BIOFILMS AND STRATEGIES TO CONTROL THEIR SUPERHYDROPHOBICITY

A dissertation submitted by Carolina Falcón García
for the degree of Dr. -Ing.

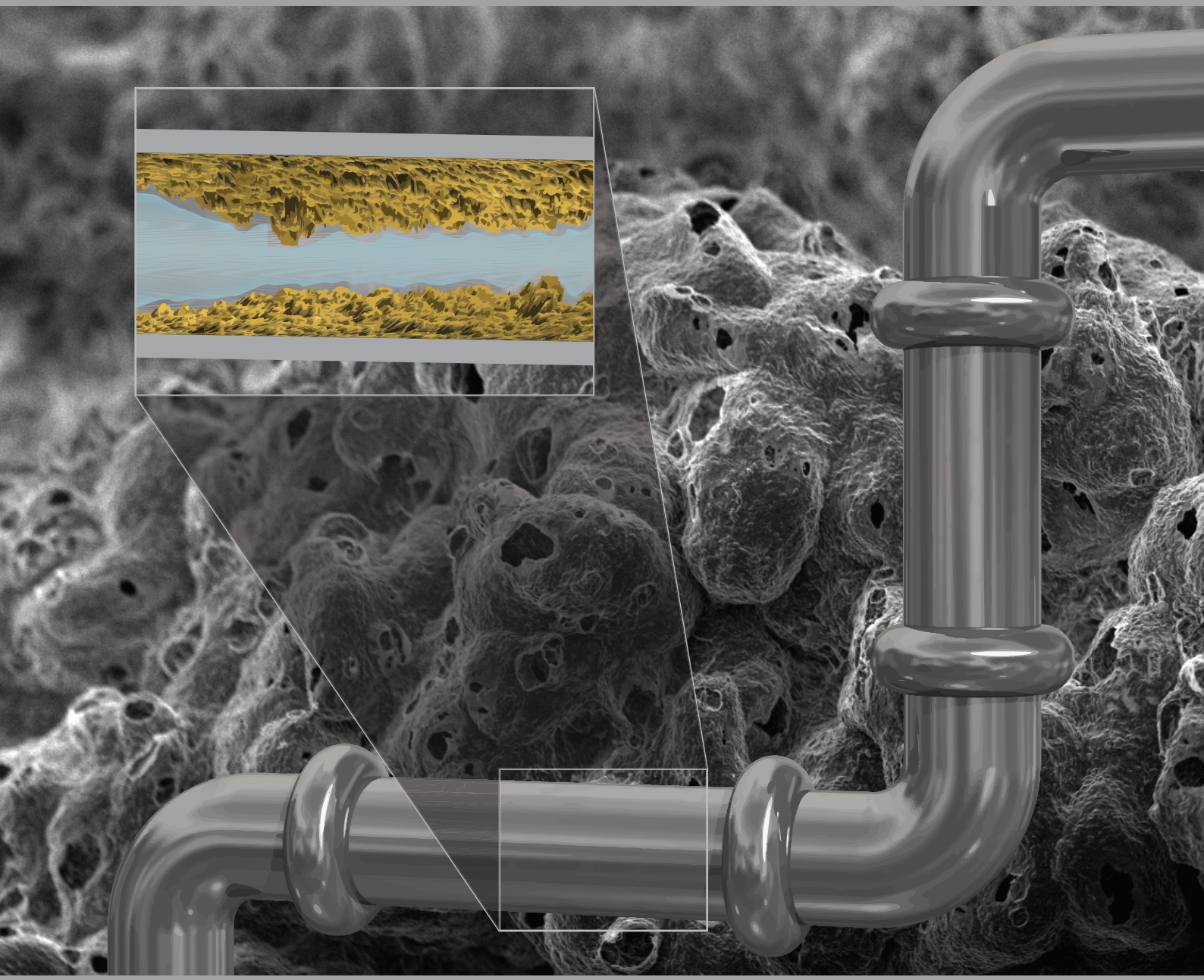

TECHNISCHE UNIVERSITÄT MÜNCHEN

Technische Universität München

Fakultät für Maschinenwesen

Professur für Biomechanik

Surface microstructure of bacterial biofilms and strategies to control their superhydrophobicity

Carolina Falcón García

Vollständiger Abdruck der von der Fakultät für Maschinenwesen der Technischen Universität München zur Erlangung des akademischen Grades eines

Doktor-Ingenieurs (Dr.-Ing.)

genehmigten Dissertation.

Vorsitzender:	Prof. Dr.-Ing. Dirk Weuster-Botz
Prüfer der Dissertation:	1. Prof. Dr. rer. nat. Oliver Lieleg 2. Prof. Dr. rer. nat. Andreas Bausch

Die Dissertation wurde am 03.09.2019 bei der Technischen Universität München eingereicht und durch die Fakultät für Maschinenwesen am 19.02.2020 angenommen.

Summary

Bacteria, the most abundant organisms on earth, have a complex coping mechanism to survive diverse environmental conditions. When bacteria encounter a surface (solid or liquid) they secrete macromolecules that embed the cells forming a 3D-mentional hydrated matrix, known as *biofilms*. Biofilms are the most common form of life for bacteria as, in this form, they are further protected from chemical, physical and mechanical attacks than in their planktonic form. In fact, biofilm bacteria are 100-1000 times more resistant to antibiotics than their planktonic counterparts. Part of this resistance is a physical one: certain bacteria produce biofilms with (super)-omniphobic surfaces; that is, surfaces able to resist wetting from water, oils, and even organic solvents. As virtually every surface can be colonized by bacteria, biofilm-forming microorganisms pose a great threat in areas where they are not desired, i.e. in industrial pipes; surfaces and packaging in food industry; instrumentation, catheters and implants in medical settings, etc. Clearly, in such cases –especially when the bacteria are pathogenic– it is crucial to remove the biofilm material and inactivate the bacteria within, as well as any remaining cells on the surface. However, current disinfection and biofilm control strategies rely on methods and compositions based on aqueous solutions, and in the case of biofilms with liquid repellent surfaces, those efforts are often futile. In order to fight the robust nature of bacterial biofilms, it is essential to recognize the detailed mechanisms that bacteria employ to defend themselves from the environment.

In this dissertation, macroscopic biofilm colonies formed by different bacterial strains are characterized in terms of their physical material properties with the aim to elucidate the origin of their liquid repellency. First, using the model organism *Bacillus subtilis* NCIB 3610, it is demonstrated that, depending on both the growth medium used for biofilm generation and the location on the biofilm colony, a hydrophilic and two hydrophobic biofilm variants can be found, i.e., water repellent surfaces with either strong or weak water droplet adhesion. Using a combination of imaging techniques, those different wetting behaviors are correlated with structural differences of the biofilm surfaces, which can be quantified with metrological parameters. Furthermore, it is demonstrated that the two hydrophobic biofilm variants can be described by different physical wetting regimes which are related to the lotus and rose petal effect, and that the distinct wetting properties of the biofilms are accompanied by alterations in the biofilm matrix composition. Additionally, and inspired by the latter, the impact of matrix composition on surface roughness is studied using light profilometry and mutant strains of NCIB 3610 lacking expression of specific matrix components. It is revealed that both, the polysaccharide and the surface layer protein BslA, contribute to the final biofilm surface roughness; which in turn, has a great impact on the liquid repellency of those bio-surfaces.

Next, the relation between surface topography and wetting behavior is verified for other bacterial strains, cultivation conditions, and even biofilm forms. The quantification of the biofilm surface topography by a metrological parameter allows for the creation of a phase diagram where a separation between hydrophilic, lotus-like biofilms, and rose-like biofilms can be clearly distinguished. It is demonstrated that the existence of lotus-like and rose-like superhydrophobicity is not limited to *Bacillus subtilis* biofilms but also occurs for other

biofilm-forming strains, regardless of the cultivation conditions at which they are generated. Even for biofilm pellicles, –biofilms formed at the liquid-air interface, which form smoother surfaces, a similar trend is described: rougher biofilms show hydrophobic behavior, whereas smoother ones are hydrophilic. Furthermore, the relation between surface topography and wetting behavior is employed to support findings in evolutionary processes of *Bacillus subtilis* bacteria. The same characterization techniques are proven powerful in differentiating the products of evolutionary diversification –often called morphotypes, by metrological parameters. Also here, the distinct wetting behavior described previously could be distinguished, and the ancestor strain could be quantitatively and gradually discriminated from its evolved diversified products.

Once the physical mechanisms underlying biofilm surface superhydrophobicity are identified, two strategies aiming at disrupting their outstanding liquid repellency are suggested. First, it is demonstrated how exposing the surface of mature biofilm colonies formed by three different bacterial species to concentrated ethanol, saline, or glucose solutions results in topographical changes that enable their wettability. Essentially, their highly complex surface features are "*deflated*" through an osmotic effect induced by the highly concentrated treating agents. As a result of this surface smoothening and reduced liquid repellency, the biofilms become susceptible to erosion by water, and the bacteria within pre-treated biofilms can now be inactivated with antibiotic solutions. Second, Cu^{2+} and Zn^{2+} ions –in low concentrations–, are proposed as biofilm treatment agents at both early and late stages of biofilm formation. Using a combination of microbiological and biophysical methods, it is demonstrated that both metal ions cause an unspecific reduction of the expression of biofilm matrix promoting genes. This is accompanied by changes in both, the biofilm surface roughness and wetting behavior. As a result, biofilms grown in the presence of metal ions are significantly more susceptible to treatment with aqueous antibiotic solutions. Interestingly, a similar effect is observed when the metal ions are diffused through the substrate on which mature biofilms have already been grown.

Taken together, these findings emphasize the importance of environmental conditions and biofilm matrix composition on the final macro- and microscopic morphology of bacterial biofilm colonies, and that such micromorphology –specifically the surface topography– has a great impact on biofilm surface wetting. Unraveling the complexity of the surface allowed to correlate the biofilm wetting behavior with known physical wetting regimes, which in turn, opens the door for designing new multi-facetted approaches to target biofilms. For instance, it is demonstrated that by smoothening the biofilm surface roughness, one can reduce their wetting resistance and that reducing their wetting resistance, enhances mechanical removal of the biomaterial and chemical inactivation of the microorganisms. The strategies presented here are applicable to many settings where biofilms have already been established, and depending on the agent used, they can be affordably scaled up.

Table of contents

1 Introduction

1.1 [a]Superhydrophobicity of bacterial biofilms

In nature, a broad range of biological materials have evolved to repel liquids. Lotus [1] and rice leaves [2], rose petals [3], gecko's feet [4], the legs of the water strider [5], and insect wings [6] have revealed well-orchestrated physical mechanisms that dictate their wetting resistance. Their extraordinary surface properties make them attractive for environmental [7], industrial [8, 9], technological [10], and biomedical [11, 12] applications.

Lotus-like superhydrophobic surfaces (SHS) (Fig. 1) possess contact angles towards water larger than 150°, low contact angle hysteresis, and are characterized by the formation of a composite solid-liquid-air interface -a key mechanism that allows impacting [13, 14] and condensed water droplets to bounce-off or roll-off easily [15] (Cassie-Baxter wetting state [16]). Artificial superhydrophobic materials mimic surface structures found on biological templates [17-19]: SHS inspired by the lotus leaf exhibit roughness features on both the nano- and micro-scale, and are often combined with low surface energy materials or coatings [2, 20-22].

Another type of superhydrophobic behavior is found on rose petals (Fig. 1). Here, static contact angles with water are similarly high, but water droplets remain adhered to the petal surface when tilted [3]. There are also surfaces which prevent ice adhesion [23] (icephobic surfaces) and others can repel both polar and apolar liquids [24, 25] (omniphobic surfaces).

An example of a biological surface which repels not only water but even water/solvent mixtures is given by bacterial biofilms (Fig. 1). Biofilms are viscoelastic materials comprising bacteria and secreted macromolecules. By embedding themselves into a biopolymer matrix, the bacteria are protected from harsh environmental conditions. Biofilms formed by the model bacterium *Bacillus subtilis* resist liquid wetting up to 80% ethanol [26], a mechanism which severely limits its antibacterial efficiency. Although this remarkable wetting resistance of biofilms may be a key reason why bacteria are that resilient towards antimicrobials [27], biocides, and solvents; the underlying physical principles giving rise to this superhydrophobic behavior have not been thoroughly explored. In particular, a direct correlation of physical wetting regimes as described by Wenzel [28] and Cassie-Baxter [16] with differences in the wetting behavior of biofilms has not been established. This is mainly due to a lack of suitable measuring methods that allow for quantitatively comparing the surfaces of soft biological materials such as biofilms.

[a] This section follows in part the publication: "*Surface topology affects wetting behavior of Bacillus subtilis biofilms*" published on 2017, in npj biofilms and microbiomes.

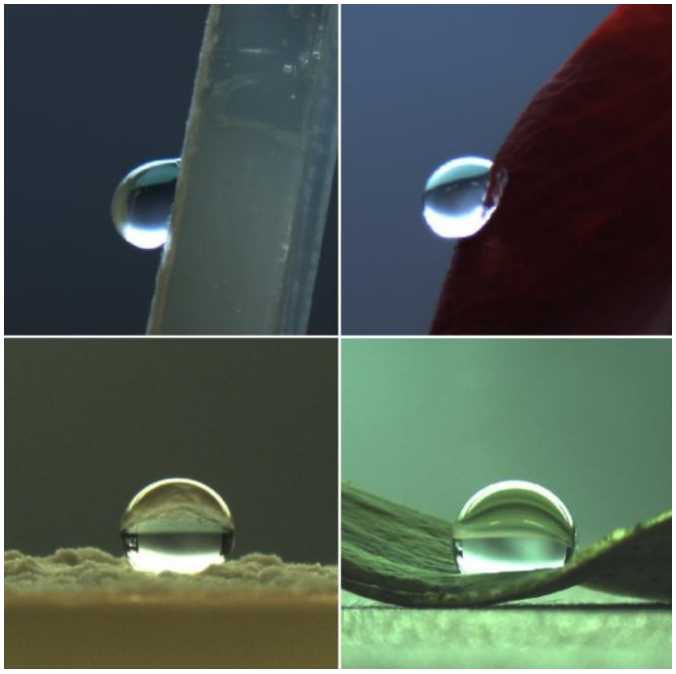

Figure 1 *Bacterial biofilms and plants are examples of surfaces found in nature with superhydrophobic properties.* Top: rose-like surfaces. Bottom: lotus-like surfaces. Pictures on the left correspond to bacterial biofilms and the ones on the right to a rose petal (top) and a lotus leaf (bottom).

A topographical characterization of surfaces is commonly performed using scanning electron microscopy (SEM) imaging. However, for soft biological materials such as bacterial biofilms, the required sample preparation procedure may alter the material properties. Also, SEM images are mostly limited to providing qualitative information. A complementary technique for the topographical characterization of biofilm surfaces is confocal fluorescence microscopy. With this technique, a 3D image of the material is obtained that provides information on biofilm thickness, surface area coverage, and surface roughness [29, 30]. However, a more detailed analysis of the surface topography of bacterial biofilms is typically not performed. Recently, white light profilometry has been shown to possess great potential as a new non-destructive imaging technique for the visualization of bacterial biofilms *in situ* [31]. Still, data obtained with this technique has so far mainly been analyzed in terms of sample thickness and roughness [32-34]. In contrast, the surface topography of lotus leaves and rose petals has already been quantified in great detail, e.g. using both traditional and more complex metrological parameters [35].

Here, using a combination of imaging techniques, a profounder characterization of biofilm surfaces is performed in order to describe the physical mechanisms underlying their superhydrophobicity. Using the bacterium *B. subtilis* NCIB 3610 for the formation of biofilms, their modes of wetting behavior are explored in relation to their surface topographical features and matrix composition. Furthermore, superhydrophobic biofilm variants, which exhibit either, low and high adhesion towards water, are further characterized in relation to the lotus and rose petal effects.

1.1.1 [b]The biofilm matrix and surface roughness

The biofilm matrix can be composed of various extracellular polymeric substances (EPS) such as proteins, exopolysaccharides, lipids or nucleic acids [36-38]. The EPS promotes biofilm adhesion to surfaces, provides the mechanical stability of the biofilm, and protects cells within the biofilm from chemical and mechanical stresses and invasion of foreign bacteria [36, 39]. Biofilm formation comprises four phases: the attachment of single cells to surfaces, followed by two-dimensional cell growth and the formation of microcolonies, followed by three-dimensional growth of the entire biofilm colony and biofilm maturation, and finally biofilm dispersal [40]. In the past years, the main matrix composition has been resolved for many bacterial biofilms [37, 41-45]. Improvements in computational analyses allowed the quantification of biofilm structure [29, 46-48] and recent technical advances in high-resolution optical microscopy enabled the investigation of the extracellular matrix structure [49, 50], even at the single cell level [51]. Together, those studies provided crucial information that is urgently needed to prevent or control biofilm formation [52, 53], such as the fundamental role of the biofilm matrix in establishing emergent biofilm properties [54]. One example of such properties is their remarkable wetting resistance.

Quantitative aspects of biofilm formation have been addressed theoretically [55-58], but studies investigating how EPS production influences the final biofilm dimensions are just emerging [56, 59, 60]. For example, it has been suggested that the physical mechanism responsible for the spreading of biomass in *Bacillus subtilis* biofilms is the pressure generated by bacterial division [33]. However, it remains unclear how the different molecular components of the biofilm matrix quantitatively modulate *B. subtilis* biofilm growth. Deletion mutants which are unable to produce selected biofilm matrix components can be a helpful tool to unravel the contribution of specific biomolecules on the macroscopic biofilm properties. For instance, the matrix of *B. subtilis* NCIB 3610 biofilms has been described to be mainly composed of two proteins: BslA and TasA, and an exopolysaccharide [61-63]; the use of deletion mutants of this strain has enabled to suggest one or more particular functions for each of this components. The hydrophobin protein (BslA) forms a coat on the biofilm surface, thus critically contributing to its water repellency [62, 64-66]; the exopolysaccharide produced by the *epsA-O* operon, which expression is required for the BslA protein to localize to the biofilm matrix, bundles the cells [61, 62, 67]; and the amyloid fibers formed by the TasA protein connect the cells within the matrix, thus rendering the structure of the biofilm more compact and stable [67, 68]. However, due to the superhydrophobic behavior observed on biofilm colonies formed by the NCIB 3610 strain, it is difficult to attribute this property to one protein only.

Here, the development of biofilm surface roughness is quantified for two *B. subtilis* wild type strains (B-1 and NCIB 3610) that differ in their biofilm matrix composition [61-63, 69], and a biofilm defective *B. subtilis* strain (BD630) which is unable to produce a biofilm on solid LB agar surfaces. Using light profilometry and deletion mutant strains of NCIB 3610, the

[b] This section follows in part the publication: "*Matrix composition determines the dimensions of Bacillus subtilis NCIB 3610 biofilm colonies grown on LB agar*" published on 2017, in RSC Advances.

individual contribution of each main matrix component on the development of surface roughness features on mature biofilm colonies grown on LB agar is studied.

1.1.2 [c]Biofilms can be formed by different bacterial strains and on different substrates

Depending on the bacterial species –and even the strains within a species, the macromolecular composition of the biofilm matrix can be very different. For instance, the key matrix components of biofilms formed by the bacterial species: *Bacillus*, *Pseudomonas*, *Burkholderia*[70], *Staphylococcus*, and *Streptococcus*, have been identified [71]. Although, they can be broadly classified in two groups based on their matrix composition: mainly polysaccharide, or mainly protein elements; all those bacterial species secrete a unique mixture of EPS. As it has been shown that the material properties of biofilms are affected by their matrix compositions [67, 71], it is no surprise that bacteria from different origins can form biofilms with different physical and mechanical properties. Environmental conditions and the substrate where the biofilms grow on, have also been shown to affect the final properties of these biomaterials, even when they are formed by the same bacteria [67, 71-73].

For instance, whereas many bacteria produce biofilms on surfaces under water-saturated conditions (in liquid) [29, 48, 51], *Bacillus subtilis* bacteria can form biofilms on solid nutrient surfaces in air: biofilm colonies, or at liquid-air interfaces: biofilm pellicles [40, 74, 75]. When cultivated in liquid under static conditions, *B. subtilis* initially grows suspended, but an increasing cell density results in decreasing oxygen concentration in the bottom layers of the medium. Using aerotaxis, cells actively swim towards the liquid-air interface and colonize in the form of a densely packed pellicle [76]. As with biofilm colonies, pellicle formation requires a secretion of EPS; however, here, when bacteria are not able to secrete one of the matrix components, they cannot colonize the liquid-air interface, and as a result, pellicles cannot be formed [77]. Similar to biofilm colonies formed by *B. subtilis* NCIB 3610, the biofilm matrix of pellicles formed by this strain is mainly composed of the amyloid fiber forming protein TasA and the exopolysaccharide [61]. Although created by the same bacterial strain, the two biofilm forms: colonies and pellicles, show different characteristics [73, 78].

Here, the microscopic surface of pellicle biofilms formed by *B. subtilis* NCIB 3610 and derivative strains, is studied in detail to explore if the relation between surface topography and wetting behavior observed on biofilm colonies, extends to this biofilm form. Moreover, colonies formed by biofilm-forming bacteria from different origins are characterized to explore whether the existence of lotus-like and rose-like superhydrophobicity is limited to *B. subtilis* biofilms, or if it is a more generic feature. For this, the surface topography of these biofilms is quantified by a metrological parameter and their wetting resistance is determined by the contact angle. The latter approach aims to categorize the different bio-surfaces, regardless of their origin or the environmental conditions at which they are generated.

[c] This section follows in part the publication: "*Topographical alterations render bacterial biofilms susceptible to chemical and mechanical stress*" published on 2018, in Biomaterials Science.

1.1.3 [d]Surface characterization of biofilms formed by products of evolutionary processes

The study of biofilms can follow different directives depending on the interest in hand and the research area where such interest belongs to. Whereas some studies focus on their malicious properties and strategies to fight them, others consider them a complex microbial puzzle provided by nature to decipher. For instance, the rapid evolution of microbes constitutes a tremendous challenge to modern medicine and, at the same time, a privilege to microbial ecology [78]. The former is due to the virulent power of microbial biofilms and their rapid adaptation, i.e. evolution of antibiotic resistance; the latter is due to large population sizes coupled with short generation times; thus, bacterial adaptation can be observed in a course of days or months allowing for its investigation [78, 79]. Hence, in order to tap into the convoluted world of microbial biofilms, a wide array of experimental techniques have been used, adapted and developed.

Experimental evolution studies continuously deepen our understanding of microbial adaptation, revealing common evolutionary scenarios such as diversification [80-84], where microbes develop into distinct variants. In bacterial biofilms, such a scenario appears to be very common as they represent structured environments that offer alternative niches varying in nutrient and oxygen content [79, 85]. Evolutionary diversification tends to improve biofilm productivity as newly emerged variants specialize in occupying different niches, thereby reducing competition [80, 82, 86, 87]. Several studies have already proven that diversification is a rapid, general and significant process in microbial evolution. However, those studies are viewed from a purely ecological angle and are assessed mostly with microbiological methods only. The use of techniques from other research areas can provide a multi-disciplinary approach with a novel take on traditional processes. Here, light profilometry is used for the quantitative study of diversification during the evolution of *Bacillus subtilis* biofilms.

1.2 [c] [e]Strategies to tackle the surface superhydrophobicity of biofilms

Biofilm surface liquid repellency has recently gained increasing attention [26, 62, 66, 73, 77, 78, 88, 89]. This is due to the improved protection bacteria experience within biofilms when a strong wetting resistance is present on the biofilm surface. Forming biofilms is a key survival strategy of bacteria; unlike their planktonic counterparts, such surface-attached microorganisms are well-shielded and protected from the environment. Bacterial biofilms can be beneficial for nature and mankind: certain plants employ a coat of harmless biofilms such as those generated by *Bacillus subtilis* to protect themselves from pathogenic microorganisms [90, 91]; industrial

[d] This section follows in part the publication: "*Evolution of exploitative interactions during diversification in Bacillus subtilis biofilms*" published on 2018, in FEMS Microbiology Ecology.
[c] This section follows in part the publication: "*Topographical alterations render bacterial biofilms susceptible to chemical and mechanical stress*" published on 2018, in Biomaterials Science.
[e] This section follows in part the publication: "*Effect of metal ions on B. subtilis NCIB 3610 biofilm surface hydrophobicity and antibiotic susceptibility*" submitted on 2019.

processes such as waste water treatment [90, 92, 93], bioremediation [94, 95], and non-toxic leaching of copper from ore [96] rely on bacterial biofilms to take effect. However, in most industrial and medical settings, bacterial biofilms have a negative impact on the function of processes and devices, and they can also be a source for inflammation and disease which is difficult to fight [97-99]. As a consequence, there is increasing effort to develop efficient methods to eradicate this biomaterial [53, 100-102].

Typical biofilm control strategies either aim at preventing bacterial attachment and thus biofilm formation [103-105], chemically inactivating the bacteria within the biofilm or removing the whole biomaterial from surfaces by mechanical forces. Studies aiming at disrupting the protective biofilm matrix (chemical route Fig. 2) mainly focus on the enzymatic degradation of EPS components or the disassembly of the matrix architecture by antibodies, microbial surfactants or nucleic acid binding proteins [102, 106]. Similarly, biological macromolecules (i.e. mucin glycoproteins or the alginate oligomer OligoG) have been proposed to promote the disassembly of *Pseudomonas aeruginosa* biofilms [107, 108]. However, such efforts are mostly strain specific and –when involving antibodies or purified biomolecules– expensive. This makes it difficult to implement them on large scales, i.e. for industrial applications.

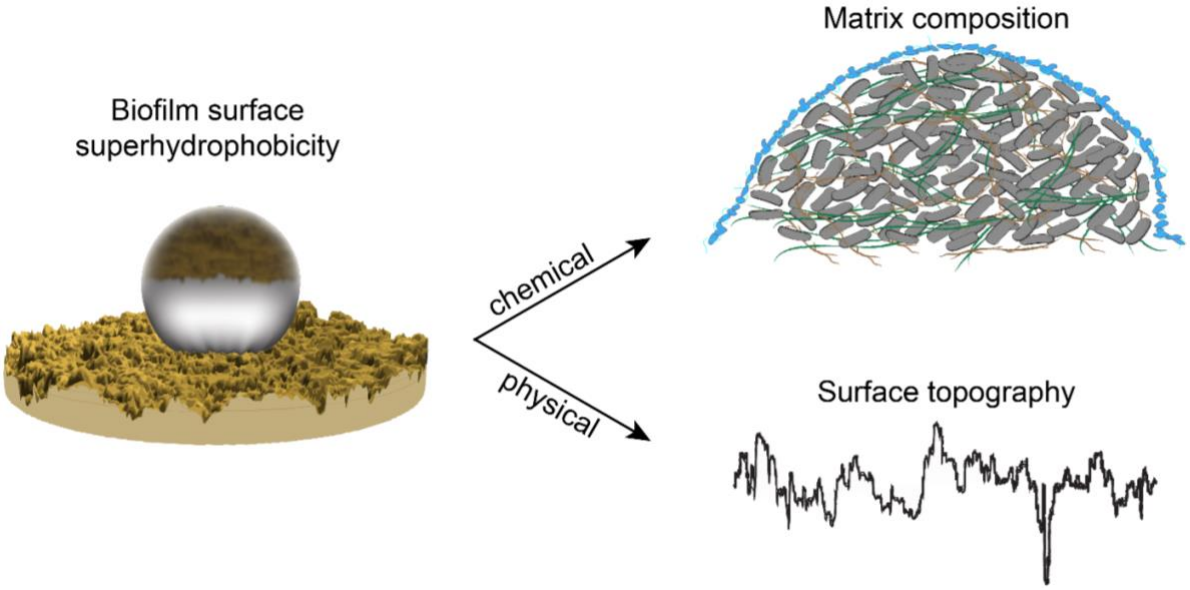

Figure 2 *The proposed routes to tackle biofilm surface superhydrophobicity*. A chemical approach relies on targeting specific matrix biomolecules to expose the biofilm bacteria. A physical approach is more general, and relies on targeting the biofilm surface topography to reduce the liquid repellency that protects the embedded cells.

A simpler way to gain access to biofilm bacteria would be to weaken or remove the superhydrophobic properties of the biofilm surface (physical route Fig. 2). Here, a method employing concentrated ethanol, saline or glucose solutions is proposed to treat the surfaces of superhydrophobic biofilms in order to reduce their micro-roughness features. Three different biofilm forming bacterial species are tested: *Bacillus subtilis* B-1, *Burkholderia thailandensis*, and *Pseudomonas putida*. Using light profilometry and wetting tests, putative changes in the surface topography and liquid repellency of the treated biofilms are assessed. Furthermore, the

impact of such treatment on the mechanical stability and antibiotic resistance of biofilms is also studied.

Of course, there are also biofilm control strategies which are applied before a biofilm has been established. Examples include the inhibition of EPS synthesis (by targeting signaling pathways) or preventing the colonization of surfaces by bacteria in the first place (by means of surface patterning and/or antimicrobial coatings) [102, 109]. In this context, metal ions such as Cu^{2+} and Zn^{2+} have been widely explored as biofilm inhibitors and antimicrobial agents [110-112]. For instance, antimicrobial metallic surfaces made of Copper are suggested to induce lipid peroxidation in bacteria thus causing impaired membrane function [113]. Zinc oxide nanoparticles have been shown to inhibit bacterial growth and biofilm formation [114].

Inspired by those findings, low concentrations of $CuSO_4$ and $ZnCl_2$ are used here for the treatment of *B. subtilis* NCIB 3610 biofilms, both at early and late stages of biofilm formation. Using a combination of microbiological and biophysical methods, the expression of biofilm matrix components, and biofilm surface characteristics are assessed after the metal exposure. Exposure to metal ions for mature biofilm colonies is achieved by diffusing the ionic solutions through the substrate they grow on (i.e. their underlying agar layer). The impact of metal ion exposure is studied in terms of the antibiotic susceptibility of biofilms.

2 [abcde]Materials & Methods

2.1 Bacterial strains and cultivation conditions

2.1.1 Strains

Different derivative strains of the species *Bacillus subtilis* were used throughout this dissertation and these are presented in Table 1 along with their specifications and references. Additionally, the species *Pseudomonas putida* (mt-2KT2440) and *Bhurkolderia thailandensis* (E264) were used, which were obtained from the Leibniz-Institut DSMZ Gmbh.

Table 1 *Bacillus subtilis strains*

Strain	Description	Main matrix composition/specification	Resistance	Ref.
NCIB 3610	Wild type	Proteins TasA & BslA, exopolysaccharide	None	[115]
natto	27E3	Mainly γ-polyglutamate	None	[116]
B-1	Wild type	Mainly γ-polyglutamate	None	[69]
CA017	*tasA::kan*	Protein BslA, exopolysaccharide	Kanamycin 50 μg/mL	[63]
N24	*bslA::cat*	Protein TasA, exopolysaccharide	Chloramphenicol 5 μg/mL	[62]
ZK3660	*epsA-O::tet*	Proteins TasA & (BslA)	Tetracycline 12.5 μg/mL	[61]
bslA/tasA	*bslA::cat, tasA::kan*	Exopolysaccharide	Chloramphenicol 5 μg/mL, kanamycin 50 μg/mL	[67]
BD630	Wild type	Unable to form proper a biofilm including exopolysaccharide	None	[117]
DK1042	NCIB 3610 $comI^{Q12I}$	Competent derivative of NCIB 3610, used to probe promoter activity	None	[118]
TB34	$P_{hyperspank}$-*gfp*	Transcriptional reporter carrying a promoter fusion to the *gfp* gene	Spectinomycin 100 μg/mL	[119]

[a] This section follows in part the publication: "*Surface topology affects wetting behavior of Bacillus subtilis biofilms*" published on 2017, in npj biofilms and microbiomes.
[b] This section follows in part the publication: "*Matrix composition determines the dimensions of Bacillus subtilis NCIB 3610 biofilm colonies grown on LB agar*" published on 2017, in RSC Advances.
[c] This section follows in part the publication: "*Topographical alterations render bacterial biofilms susceptible to chemical and mechanical stress*" published on 2018, in Biomaterials Science.
[d] This section follows in part the publication: "*Evolution of exploitative interactions during diversification in Bacillus subtilis biofilms*" published on 2018, in FEMS Microbiology Ecology.
[e] This section follows in part the publication: "*Effect of metal ions on B. subtilis NCIB 3610 biofilm surface hydrophobicity and antibiotic susceptibility*" submitted on 2019.

Strain	Description	Main matrix composition/specification	Resistance	Ref.
TB363	P_{eps}-*gfp*	Transcriptional reporter of *epsA-O* carrying a promoter fusion to the *gfp* gene	Kanamycin 5 µg/mL	[75]
TB373	P_{tapA}-*gfp*	Transcriptional reporter of *tapA* carrying a promoter fusion to the *gfp* gene	Kanamycin 5 µg/mL	[75]
TB685	P_{blsA}-*gfp*	Transcriptional reporter of *bslA* carrying a promoter fusion to the *gfp* gene	Chloramphenicol 5 µg/mL	[120]

2.1.2 Bacterial cultivation

Bacteria were kept in frozen glycerol stocks until use. Unless specified, liquid cultures of all strains were prepared as follows: 10-15 mL of sterile 2.5% (w/v) Lysogeny broth (LB medium, Table 2) containing the corresponding antibiotic when necessary, were inoculated with the frozen bacterial/glycerol stock. Then, the bacterial solution was incubated at 37 °C and 90-100 rpm in a shaking incubator (Sartorius, Göttingen, Germany) overnight. For cultivation of the bacterial species *Burkholderia thailandensis*, CASO broth was used instead (Table 2). For studying the effect of the matrix composition in biofilms surface roughness (section 3.1.4), the cultivation conditions consisted of 5 mL of inoculated LB medium incubated at 37 °C and 300 rpm agitation.

2.2 Biofilm formation and sample treatment

2.2.1 Biofilm growth on agar

2.2.1.1 Agar substrates

Most studies conducted in this dissertation make use of biofilms grown on semi-solid nutrient-rich substrates, the latter were generated by mixing the different nutrient media (Table 2) with 1.5% (w/v) Agar-Agar (Carl Roth, Karlsruhe, Germany). Unless specified, the mixture was autoclaved and ~22 mL of the still hot liquid was poured into standard petri dishes, then they were left to cure for ~30 min with the lid slightly open under laminar flow. The "*agar plates*" as referred for simplicity, were kept at 4 °C prior to use. The biofilms grown on the different agar variants are referred to as "LB biofilm", "LBGM biofilm," and "MSgg biofilm" throughout this dissertation.

Table 2 *Nutrient media compositions*

Nutrient media	Composition	Reference
LB – "standard medium"	1% (w/v) tryptone, 1% (w/v) NaCl and 0.5% (w/v) yeast extract	Luria/Miller LB (Carl Roth, Karlsruhe, Germany)
LBGM – "nutrient rich"	2.5% (w/v) LB medium (from Carl Roth) enriched with 100 µM Manganese(II)sulfate (MnSO4), and 1% (v/v) glycerol	[121]
MSgg – "minimal medium"	5 mM potassium phosphate, 100 mM Mops, 2 mM $MgCl_2$, 700 µM $CaCl_2$, 50 µM $MnCl_2$, 50 µM $FeCl_3$, 1 µM $ZnCl_2$, 2 µM thiamine, 0.5% (v/v) glycerol, 0.5 % (w/v) glutamate, 50 µg/mL tryptophan, 50 µg/ml phenylalanine, and 50 µg/mL threonine	Adapted from Branda *et al.* [115]
CASO	1.5% (w/v) peptone from casein, 0.5% (w/v) peptone from soymeal, 0.5% (w/v) NaCl	Casein-Soja-Pepton (Merck KGaA, Darmstadt, Germany)
LB + metal ions	LB medium (from Fischer Scientific) + 1.5 mM $CuSO_4$ or 1.5 mM $Al_2(SO_4)_3$ or 0.5 mM $ZnCl_2$	Luria-Bertani LB (Fischer Scientific, New Hampshire, USA)
LBGM + metal ions	LBGM medium + 1.5 mM $CuSO_4$ or 1.5 mM $Al_2(SO_4)_3$ or 0.5 mM $ZnCl_2$	[121]

Media containing metal ions were generated by bringing the temperature of the autoclaved media down to RT (or 60 °C when mixed with agar for agar plates) and afterwards adding the metal ions from sterile stocks forming a homogenous liquid mixture.

2.2.1.2 Biofilm colonies

Typically, bacterial biofilm colonies were generated by spotting 5 µL drops of bacterial liquid culture (as prepared in 2.1.2) to the "*dry*" agar surfaces. Three equally spaced drops were placed per agar plate, and once the droplet had dried, the inoculated agar plates were placed in an incubator with the lid down at 30 or 37 °C for 24 or 48 h. Agar plates were "*dried*" by leaving them slightly open under the laminar flow for ~30 min prior to inoculation if signs of condensation were observed.

For studying the effect of the matrix composition on the biofilm surface roughness (section 3.1.4) the procedure was as follows: before inoculation, the bacterial cultures (as prepared in 2.1.2) were diluted to an OD_{600} of 0.05 and grown until an OD_{600} of 0.1 was reached, representing the beginning of the exponential growth phase. The cultures were again diluted to an OD_{600} of 0.05 and 18 droplets of 0.5 µL per bacterial strain were applied to an LB agar plate (Table 2). This allowed for investigating biofilm colony growth starting from single cells distributed across the agar plate until full growth of biofilm colonies was established (max 17 h).

For testing the effect of different environmental conditions on the surface hydrophobicity of biofilms (section 3.2.1), the influence of two different levels of humidity during biofilm cultivation were studied: low (~22%) and high (>80%). Moreover, the low humidity condition

was studied in two different ways: first, the agar plates containing the samples were placed directly into the incubator, and second, the samples were grown inside closed bags (without air exchange with the incubator environment). These samples were incubated at 30 °C for both 24 h and 48 h.

Biofilm colonies produced for osmotic treatment (section 4.1) were incubated for 24 h at 37 °C.

2.2.1.3 Continuous biofilm layers

Continuous layers of biofilm material were generated specifically for the erosion assays described in section 2.4.1; here, 200 µL of bacterial liquid culture (as prepared in 2.1.2) was spread across the entire surface of an agar plate using a *Drigalsky* spatula while the agar plate was rotated on a stage, until the bacterial liquid culture was evenly distributed. These samples were incubated for 24 h at 37 °C.

2.2.2 Osmotic treatment of biofilm colony surfaces

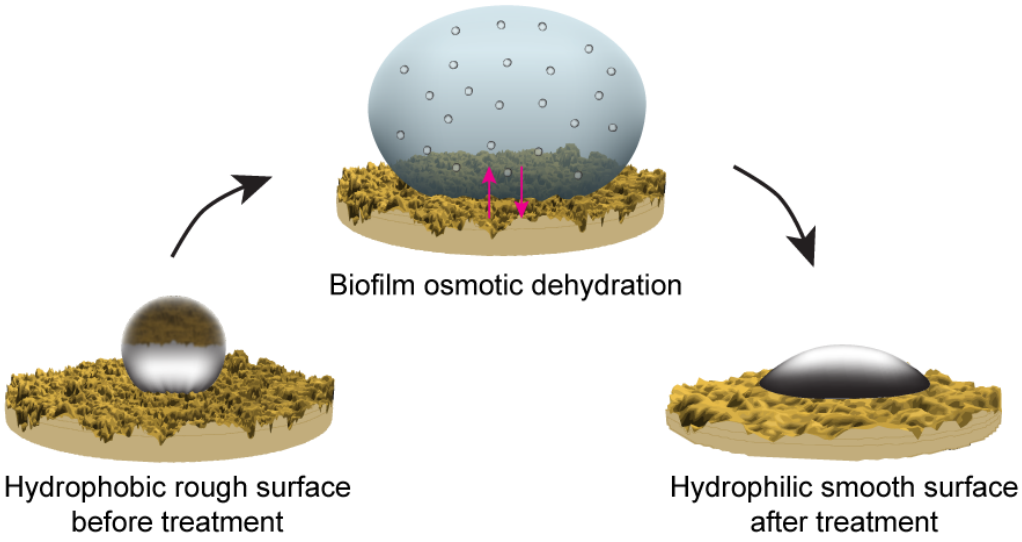

Figure 3 *Treatment of biofilm surfaces with an osmotic agent.*

Treatment of biofilm surfaces with osmotic agents was performed on superhydrophobic biofilms formed by the following species: *B. subtilis* B-1, *P. putida* and *B. thailandensis*. The treatment consisted of applying a 150–250 µL droplet (depending on the size of the biofilm colony) of each osmotic agent onto the biofilm surface, while ensuring that the size of the liquid droplet was big enough to cover the entire surface, but small enough that it would not fall off during the treatment (Fig. 3). The samples were left covered and undisturbed during a set treatment time (depending on the strain and the osmotic agent used). Afterwards, the osmotic agent was carefully removed from the surface with the aid of a pipette. The treated biofilm surface was left to air-dry for a few minutes and then analyzed. The osmotic agents used were aqueous solutions of: 80% (v/v) ethanol, 5 M NaCl, 3 M KCl and 1.5 M glucose. The treatment

times differed depending on the biofilm strain and the osmotic agent used, ranging from 10 min to 48 h (details in the respective section of chapter 4).

2.2.3 Diffusion of metal ions through the agar substrate of mature biofilms

Mature biofilm colonies were generated as described in section 2.2.1.2 with the difference that, here, 15 mL LB agar plates (LB medium from Fischer Scientific) were used to obtain a thinner substrate. Incubation of those *B. subtilis* NCIB 3610 on those agar plates for 24 h at 30 °C yields rose-like superhydrophobic biofilms. LBGM liquid medium was prepared and the metal ions, $CuSO_4$ or $ZnCl_2$, were added to a final concentration of 1.5 mM and 0.5 mM, respectively (as indicated in section 2.2.1.1); a fraction of LBGM was left unaltered and used as a control. Diffusion of liquid medium into the agar substrate of the biofilms was established using the set-up illustrated in Fig. 4a. The procedure was as follows: first, 7 mL of the liquid medium were pipetted into each well of a 6-well plate; then, the PTFE sample holders were tightly fitted all the way down into each well; last, ~1.5 mL of liquid media were pipetted into each well (through the holes in the surface of the sample holders) until the liquid protruded from the surface to allow for contact with the agar substrate (Fig. 4b).

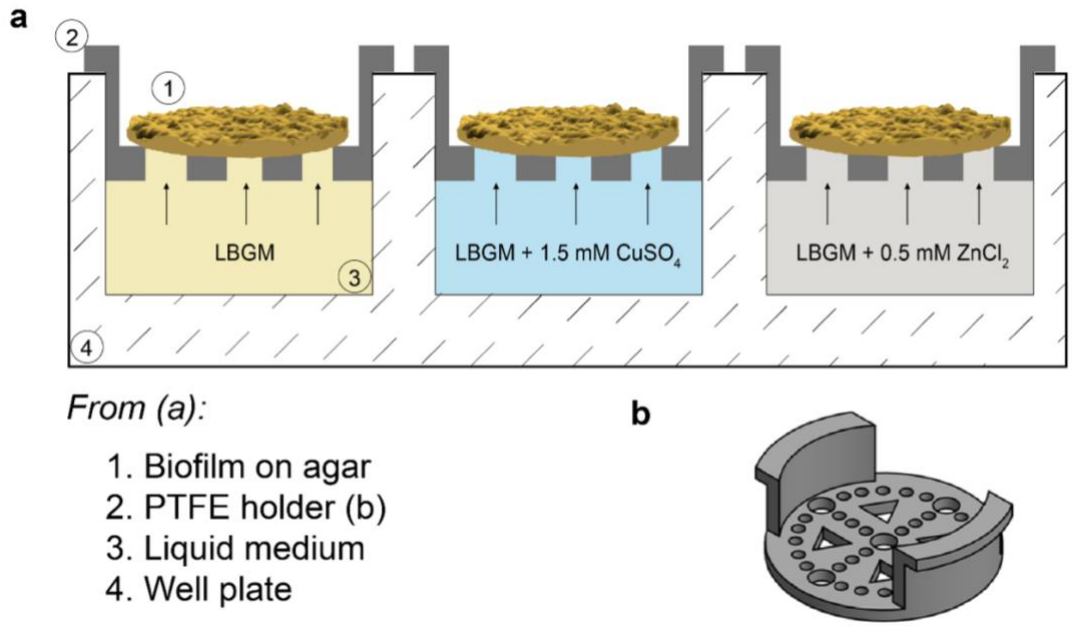

Figure 4 *Schematic depicting the set-up employed for the treatment of mature B. subtilis NCIB 3610 biofilms with LBGM liquid medium, with and without metal ions* ***(a)****, and PTFE sample holder used for the set-up* ***(b)****.*

The mature biofilm colonies and their underlying agar substrate were extracted from the petri dishes by cutting the agar around them using a cookie cutter with a diameter of 3 cm and a spatula for lifting. Then, the individual biofilm colonies were carefully placed onto the PTFE sample holders while making sure that all the holes on the surface of the sample holder were covered. To avoid abrupt changes in humidity during incubation, the well plates (covered with a lid) were placed inside a sterile plastic bag before placing them into the incubator for ~24 h at 30 °C.

2.3 Biofilm characterization techniques

2.3.1 Light profilometry

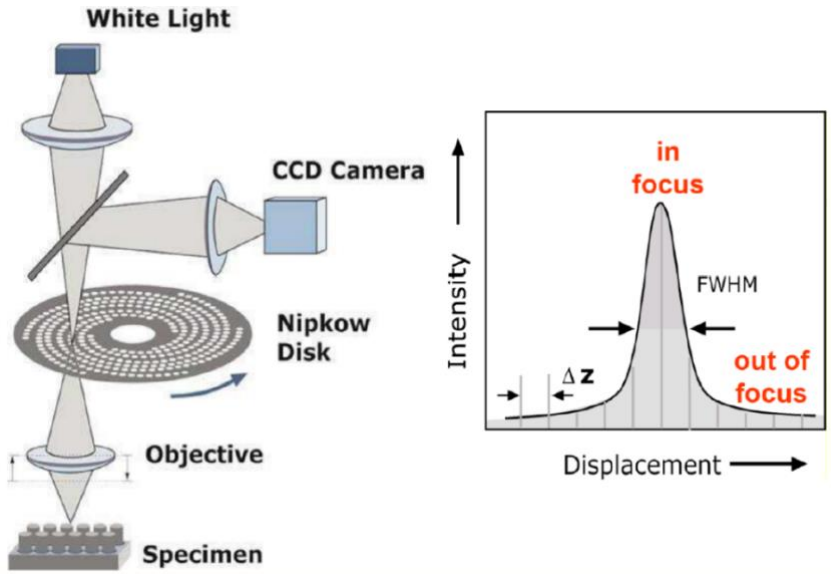

Figure 5 *Functional principle of light profilometry*. The LED source is focused through the multi-pinhole disc (MPD) and the objective lens onto the sample surface, which reflects the light. The reflected light is reduced by the pinhole of the MPD to that part which is in focus, and this falls on the CCD camera. Schematic obtained from Josef Frohn at NanoFocus [122].

Light profilometry is a variant of confocal microscopy that allows to obtain the *z*-coordinates of a surface with high accuracy. With this imaging technique, a topographical profile of a material can be obtained from which metrological parameters describing the surface can be calculated. As illustrated in Figure 5 the mechanism is as follows: for each *x/y* position, the profilometer lens is moved over a certain range in *z*-coordinates and the intensity of reflected light is measured for each of those *z*-positions. Typically, a Gaussian distribution is obtained, and the peak in reflected light intensity corresponds to the *z*-position of the surface, since here the reflected light intensity is maximal. An image from a conventional optical microscope contains both sharp and blurred details. In contrast, in the confocal image, the blurred details (unfocused) are filtered out by the operation of the multi-pinhole-disc and only light from the focal plane reaches the CCD camera (Fig. 5) [123].Therefore, a much higher resolution in the *z* direction can be obtained compared to the *x*- and *y*-direction.

For this dissertation, profilometry images were acquired using a Nanofocus µsurf profilometer (NanoFocus AG, Oberhausen, Germany). Images of bacterial colonies and pellicles were taken with 20x magnification resulting in surface images with an area of 800x772 µm. Only images with a minimum of 60% data points were considered for analysis and missing data points were interpolated. The scanned area was then evaluated with the software µsoft (Version 6.0, NanoFocus AG, Oberhausen, Germany). With this software, the parameters included in Table 3 were calculated for surface characterization of the obtained topographical profiles *z(x,y)*. All the parameters are defined in the **ISO 25178** norm [124], which specifies terms, definitions and parameters for the determination of surface texture by areal methods. The resolution of the

images is 1.56 µm in lateral direction. The step size in *z* direction is 0.22 µm; however, owing to the peak detection algorithm the profilometer uses, the resolution in *z* is better than this step size and can –under ideal conditions– be as good as 10 nm with the objective used here.

Table 3 *Surface metrological parameters*

Parameter	**Definition**
$\boldsymbol{Sq} = \sqrt{\frac{1}{A}\iint_A z^2(x,y)dxdy}$	*Root mean square surface roughness* – quantifies the standard deviation of the height distribution
$\boldsymbol{Ssk} = \frac{1}{S_q{}^3}\left[\frac{1}{A}\iint_A z^3(x,y)dxdy\right]$	*Skewness* of the height distribution
$\boldsymbol{Sku} = \frac{1}{Sq^4}\left[\frac{1}{A}\iint_A z^4(x,y)dxdy\right]$	*Kurtosis* of the height distribution
Sp	*Maximum peak height*
Sv	*Maximum pit height*
$\boldsymbol{Sz} = Sp + Sv$	*Maximum height* – quantifies the height difference between the highest peak and the deepest valley occurring in the scanned zone
$\boldsymbol{Sdr} = \frac{1}{A}\left[\iint_A \left(\sqrt{\left[1 + \left(\frac{\partial z(x,y)}{\partial x}\right)^2 + \left(\frac{\partial z(x,y)}{\partial y}\right)^2\right]} - 1\right)dxdy\right]$	*Developed interfacial area ratio* – indicates the complexity of a surface by comparing the actual surface and the projected surface
$\boldsymbol{Sdq} = \sqrt{\frac{1}{A}\iint_A \left[\left(\frac{\partial z(x,y)}{\partial x}\right)^2 + \left(\frac{\partial z(x,y)}{\partial y}\right)^2\right]dxdy}$	*Root mean square gradient* – combines both roughness and spacing information
$\boldsymbol{Sal} = \min_{tx,ty \in R} \sqrt{tx^2 + ty^2}$	*Autocorrelation length* – informs about spacing between individual roughness features. $R = \{(tx,ty): ACF(tx,ty) \leq 0.2\}$ and *ACF* denotes the autocorrelation function.

The fraction of biofilm material that the profilometer scans using the aforementioned settings corresponds to approximately 20 to 50% of the entire bulk of the material (from top to bottom). This was calculated by comparing average ***Sz*** values to the entire thickness of biofilm colonies and is consistent with previous results using the same parameter [67]. Features characterized in this fraction of the material are referred to as 'surface topography' throughout this dissertation.

2.3.1.1 Analysis of biofilm roughness over time

To investigate the roughness development of growing biofilm colonies (a-b in Fig. 6a), light profilometry images of these colonies were obtained for a period of 17 h (Fig. 6a). The

measurements were performed on two different days, resulting in 14 data curves per strain. Due to the natural development and lack of material at very early time points, the images were acquired at an edge of the biofilm colonies with a portion of the underlying agar as a reference plane (Fig. 6a). Profilometric images were taken every two hours and analyzed as described above. Except here, a correction method was applied to the measured images before calculating the surface parameter, so that the agar structure below the biofilm did not contribute to the calculated values (Fig. 6b). Essentially, at growth times later than 5 h (when a continuous biofilm layer had formed), only data from the image quadrant (a region of 400×382 µm) opposite to the agar border was analyzed (Fig. 6c-d). This procedure ensured that the edge of the biofilm colony itself did not contribute to the calculated ***Sq*** values and only roughness features of the biofilm itself were considered.

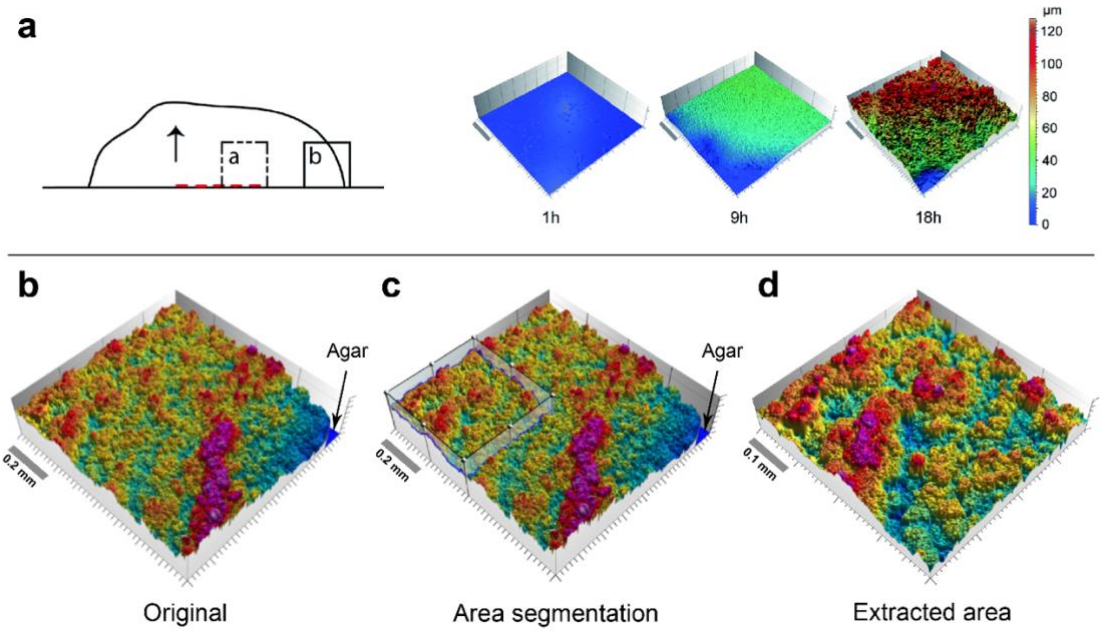

Figure 6 *Method for measuring roughness development over time.* **a)** As biofilms colonies develop from single cells to a colony that expands in area and height over time (a-b) a portion of the underlying agar is used as a reference for the measurements. **b-d)** A segmentation method **(c)** on the surface profiles **(b)**, results in an area **(c)** that contains information of biofilm roughness only.

2.3.1.2 Assessment of biofilm pellicles

To obtain a wider visualization of the pellicle surfaces, 3x3 stitched images were acquired with the profilometer. With such a method, a final area of 2.4x2.3 mm is obtained. For those images, as the water below the sample follows every movement of the profilometer stage creating ripples on the sample surface, the following image processing operator was applied: remove outliers. With this operator, isolated outliers spread over the surface, as well as outliers around the edges of the measurement area (which are very common around sharp edges) are removed. Then the resulting non-measured points were filled by interpolation using the same operator.

2.3.1.3 Assessment of topographical changes after osmotic treatment

For assessment of topographical changes after treatment with the osmotic agents, 2x2 stitched images were obtained as explained above resulting in a final area of 1.6x1.54 mm. For visualizing topographical alterations induced by ethanol, salt or glucose solutions, such locations on the biofilm surface were selected which contained distinguishable surface features; they were imaged before the treatment and their coordinates were registered. The surface of the biofilm colony was then treated as specified in section 2.2.2. Finally, a second profilometric measurement was performed at the exact same coordinates as before the treatment. The topographical changes assessed here correspond only to the upper fraction of the biofilm samples, and any (putatively additional) changes in the bulk of the material were not assessed here.

2.3.2 Determination of wetting behavior

To probe the wetting behavior of the biofilms, a 10 µL droplet of a particular liquid was placed onto the biofilm surface, and a transversal image of the liquid–solid interface was captured using a high-resolution camera (Point Gray Research, Richmond, Canada) (Fig. 7). Then, the static contact angle value was determined using the software Image J (Version 1.50b, National Institutes of Health, USA) and the "drop snake" plug-in. The following liquids were used throughout this dissertation: *dd*H_2O, 50% (v/v) aqueous solutions of 2-propanol, methanol, acetone, and ethanol (Carl Roth, Karlsruhe, Germany), as well as essential oils from cassia, clove, and thyme (Sigma-Aldrich, St Louis, USA).

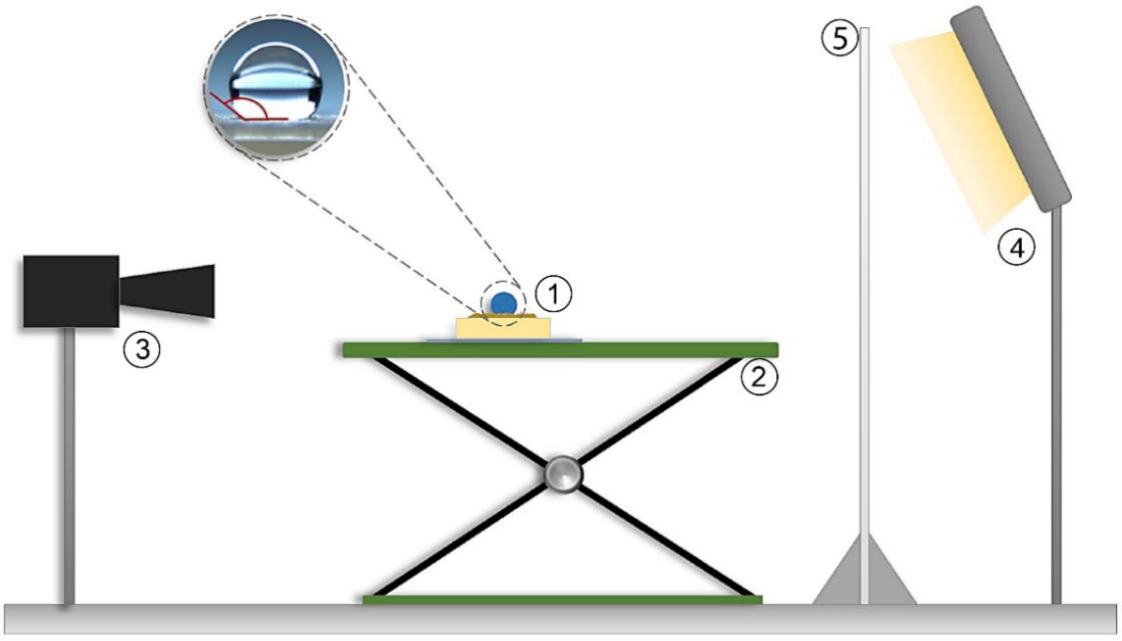

Figure 7 *Contact angle measurement.* The biofilm sample (1) is placed on a platform (2) between the camera (3) and a light source (4). The liquid droplet is illuminated by the external light, which is homogenized by a frosted glass screen (5).

2.3.2.1 Superhydrophobic surfaces

To qualitatively determine the wetting behavior of superhydrophobic biofilm samples (i.e., those with static contact angles >120°), the entire sample containing the liquid droplet on its surface was tilted, and the response of the liquid droplet was observed to distinguish between rose-like (high adhesion: droplet sticks) and lotus-like (low adhesion: droplet rolls off) superhydrophobicity. Unless specified, throughout this dissertation, samples with superhydrophobic rose-like and lotus-like characters are depicted with red and green colors, respectively. Similarly, hydrophilic samples are depicted with blue color.

2.3.2.2 Contact angle hysteresis

To determine contact angle hysteresis, the same procedure was applied as for the static contact angle measurement. However, here, the volume of a water droplet was first increased from 5 µL (in increments of 1 µL) to a final volume of 10 µL; afterwards, the volume of the same droplet was gradually decreased back to 5 µL. Transversal images were captured at each volume step and the static contact angle was determined for each of them. With this procedure, hysteresis curves can be generated, which show the advancing and receding contact angle values for a given sample in detail. Instead of curves, a degree of hysteresis can also be calculated. For this, only the final advancing (from 9 to 10 µL) and final receding (from 6 to 5 µL) contact angles were evaluated, and the difference between these two contact angle values was calculated.

2.3.3 Scanning Electron Microscopy (SEM)

For analyzing biofilm surfaces with SEM, the entire biofilm colony still attached to the underlying agar was shock-frozen with liquid nitrogen and then dried by lyophilization for at least 48 h. Light profilometry confirmed that this freezing/lyophilization process did not significantly alter the biofilm micro-topography. The lyophilized biofilm layers were carefully lifted from the dried agar and placed onto aluminum SEM sample holders, the sample was fixed to the holder *via* a conductive double sided tape. The biofilm sample was then sputtered for 40 s with Au (MED 020, BAL-TEC, Balzers, Liechtenstein). The SEM: JEOL-JSM-6060LV (Jeol, Eching, Germany), was operated at an acceleration voltage of 5 kV for imaging.

2.3.4 Mass spectrometry (MS)

To assess protein expression profiles of selected biofilm samples, proteomics analysis was performed in independent triplicates. First, the samples were resuspended in 0.9% NaCl. Then, extracellular proteins were extracted from the biofilms by subsequent vortexing and centrifugation (20 min, 12000 g, 5 °C) for three times, supernatants were pooled and intact bacteria removed by filtering with 0.45 and 0.22 µm filters (Merck Millipore, Massachusetts, USA). Absence of bacterial growth was checked by platting aliquots on LB agar. Components

smaller than 3 kDa were removed (filters: modified PES, 3 kDa, VWR) and proteins were precipitated with chloroform/methanol according to Wessel–Flügge. Proteins were solubilized in 7 M Urea / 2 M thiourea, reduced, alkylated and enzymatically digested with LysC and trypsin. Generated peptides were desalted on C18 material, lyophilized and resolved in 0.1% formic acid for MS measurement. MS analysis was performed on an Orbitrap Fusion instrument coupled online to an Ultimate 3000 Nano HPLC *via* an electrospray easy source (Thermo Fisher Scientific, Massachusetts, USA). Peptides were separated on a 50 cm C18 column (particles 2 µm, 100 A, inner diameter 75 µm, Thermo Fisher Scientific) constantly heated at 50 °C. The gradient was run from 5–32% acetonitrile, 0.1% formic acid during a 152 min method (7 min 5%, 105 min to 22%, 10 min to 32%, 10 min to 90%, 10 min wash at 90%, 10 min equilibration at 5%) at a flow rate of 300 nL/min. Most intense ions from survey scans measured in the orbitrap (*m*/*z* 300–1500) were chosen for fragmentation with high-energy collisional dissociation and spectra acquired in the ion trap (max injection time 35 ms, target value 1e4) while the instrument was operated in top speed mode. For MS/MS based peptide identification, default settings were used with the following exceptions: minimal number of unique peptides for protein identification was set to two, fast label-free quantification and match between runs options were enabled.

2.3.4.1 Comparison center vs. periphery of biofilm colonies

For assessment of protein expression, differences between the center and peripheral regions of the biofilm colonies analyzed in section 3.1.3, colonies of *B. subtilis* NCIB 3610 were grown on three different agar variants (LB, LBGM, and MSgg at 37 °C for 24 h) and the biofilm material from both regions of the colony was pooled separately. The pooled samples consisted of the following mass: 37 mg for replicate 1 and 24 mg for replicates 2 and 3. Search for MS/MS based peptide identification was performed against the *B. subtilis* 168 UniProtKB database (July 2016) using Max Quant (version 1.5.3.8) [125].

2.3.4.2 Comparison treated vs. osmotic treated biofilm colonies

For assessment of protein expression differences between the untreated and osmotic treated biofilm colonies analyzed in section 4.1.2, *P. putida* 160488 bacterial biofilms (24 mg for each sample) grown on two different agars (LBGM and MSgg at 30 °C for 24 h) were used. Search for MS/MS based peptide identification was performed against *P. putida* 160488 UniProtKB database (April 2018) using Max Quant (version 1.6.1.2) [125].

2.3.5 Bright field and fluorescence microscopy

Entire biofilm pellicles and colonies were analyzed using an Axio Zoom V16 stereomicroscope (Carl Zeiss, Jena, Germany) equipped with a Zeiss CL 9000 LED light source and an AxioCam MRm monochrome camera (Carl Zeiss). Images were captured using both bright field and

fluorescence mode; for the latter, the filer set #38 (Carl Zeiss, excitation at 470/40 nm and emission at 525/50 nm) was used to image GFP fluorescence.

For the calculation of relative fluorescence values in biofilm colonies that were grown in the presence of metal ions (section 4.2.2), the fluorescence mode of each biofilm colony was subtracted from its respective average background fluorescence mode (Fig. 8). For each growth day (N = 3), an average background fluorescence mode was calculated from a minimum of two biofilm colonies imaged with the GFP filter. Relative fluorescence mode values are referred to as "fluorescence values" for simplicity. Images were acquired using 5x magnification.

Stability of the green fluorescent protein (GFP) was tested in the presence of the metal ions used in section 4.2.2. The fluorescence of purified GFP (Merck, Darmstadt, Germany) mixed with different concentrations of $CuSO_4$ and $ZnCl_2$ solutions was analyzed both at acidic and neutral pH using a Victor^3 plate reader (Perkin Elmer, MA, United States). Neutralization was achieved by adding TRIS buffer, the purified GFP was maintained in PBS solution.

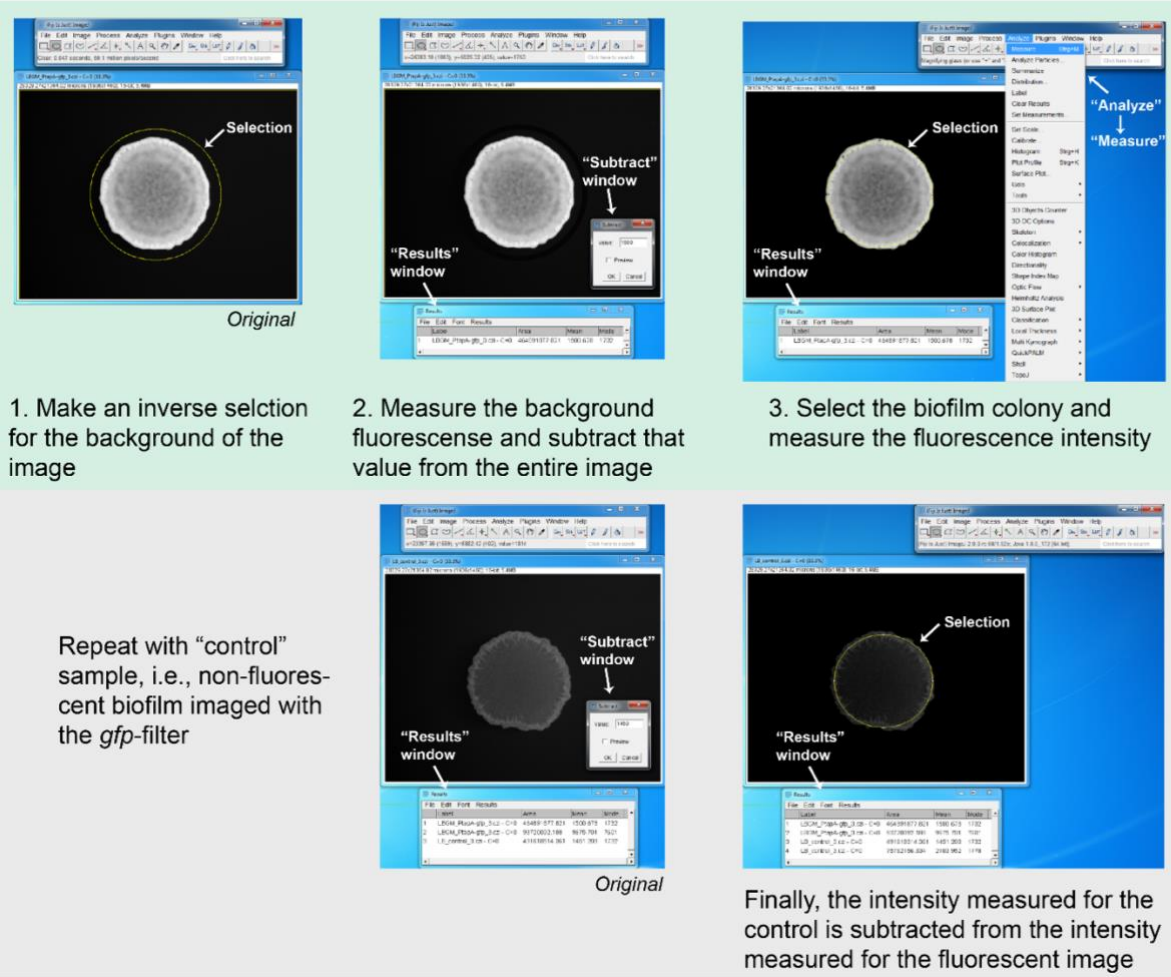

Figure 8 *Workflow for fluorescence intensity measurement of biofilm colonies.* The green background in the top section indicates fluorescent samples, the grey background in the bottom section indicates control samples.

2.3.6 Assessment of bacterial growth kinetics

Bacterial growth curves were determined with a plate reader (POLARstar OPTIMA, BMG Labtech). Overnight cultures of the desired bacteria strain were generated as described in section 2.1.2 and diluted in LB medium (0.2 mL volume) to an OD_{600} of 0.05. OD was measured at 600 nm periodically while the cultures were maintained at constant shaking at 300 rpm and 37 °C.

For assessment of metal ions effect *during* planktonic bacterial growth, the OD was followed for ~24 h and measured every ~7 min. The resulting growth curves represent the mean of all individual wells (referred to by *n*, details in the respective figure captions), from a minimum of 3 batches ($N = 3$). To assess the effect of metal ions on growth kinetics of *mature* bacteria, first, an overnight culture of the desired bacterial strain was generated, diluted, and bacterial growth was followed as described above. However, the measurement was paused after ~22 h, at which point the cultures were removed from the plate reader and challenged with the different metal ions under sterile conditions. For this, 20 µL of LBGM liquid medium was added to the control samples, amounting for 10% of the total volume. The same volume of LBGM containing either $CuSO_4$ or $ZnCl_2$ was added to the rest of the wells to obtain final concentrations of 1.5 mM and 0.5 mM, respectively. Afterwards, the growth kinetics were followed for another ~24 h. The resulting growth curves represent a mean of at least 32 wells ($n = 32$) over 3 different growth days ($N = 3$).

2.3.7 Assessment of extracellular ATP levels

The effect of metal ions on the bacterial metabolic activity was assessed for planktonic *B. subtilis NCIB 3610* when cultivated in the presence of Copper and Zinc (section 4.2.1). An ATP determination kit (Thermo Fischer, MA, United States) was used to measure concentrations of this molecule in planktonic bacteria using a Victor^3 (Perkin Elmer, MA, United States) plate reader to detect luminescence. The samples comprised overnight cultures (prepared as described in section 2.1.2) containing 1.5 mM $CuSO_4$ or 0.5 mM $ZnCl_2$ in the LB medium and standard LB-medium as a control. Extracellular ATP was measured at stationary growth phase of the cultures following the manufacturer's instructions.

2.4 Mechanical and chemical biofilm challenge

2.4.1 Erosion assays

Erosion stability tests were carried out in two modes: first, with dripping water and second, with flowing water. Both set-ups comprise a simple intravenous (IV) system equipment adapted for this particular application: the IV-bag serves as the water reservoir, the drip chamber is used as inlet or outlet, and the roller clamp (1) is used as a valve for water flow control (Fig. 9). In the dripping mode set-up (Fig. 9a), the drip chamber serves as the outlet (2),

which is located 30 cm (3) above the biofilm sample. The biofilm sample sits on a stage (4) at a 25 ° tilt angle. A high definition camera (5) is mounted onto a tripod and acquires time lapse images during the erosion experiment. The sample surface (6) contains areas of both treated and untreated biofilm, which are studied separately (the dark region in the image corresponds to treated biofilm, which becomes transparent after the treatment). The flowing mode (Fig. 9b) consists of the same elements, but is configured differently: now, the valve is completely opened (1) and the end of the tubing system serves as outlet (2) with no change in diameter from beginning to end; also, the distance (3) between the biofilm sample and the water outlet is reduced to a few millimeters. Thus, the water is guided directly from the reservoir onto the biofilm surface. Configuration items (4)-(6) remain the same as in Fig. 9a. For experiments performed in dripping mode, images were taken every 15 s, and for flowing mode this was done at different time points depending on the specific sample.

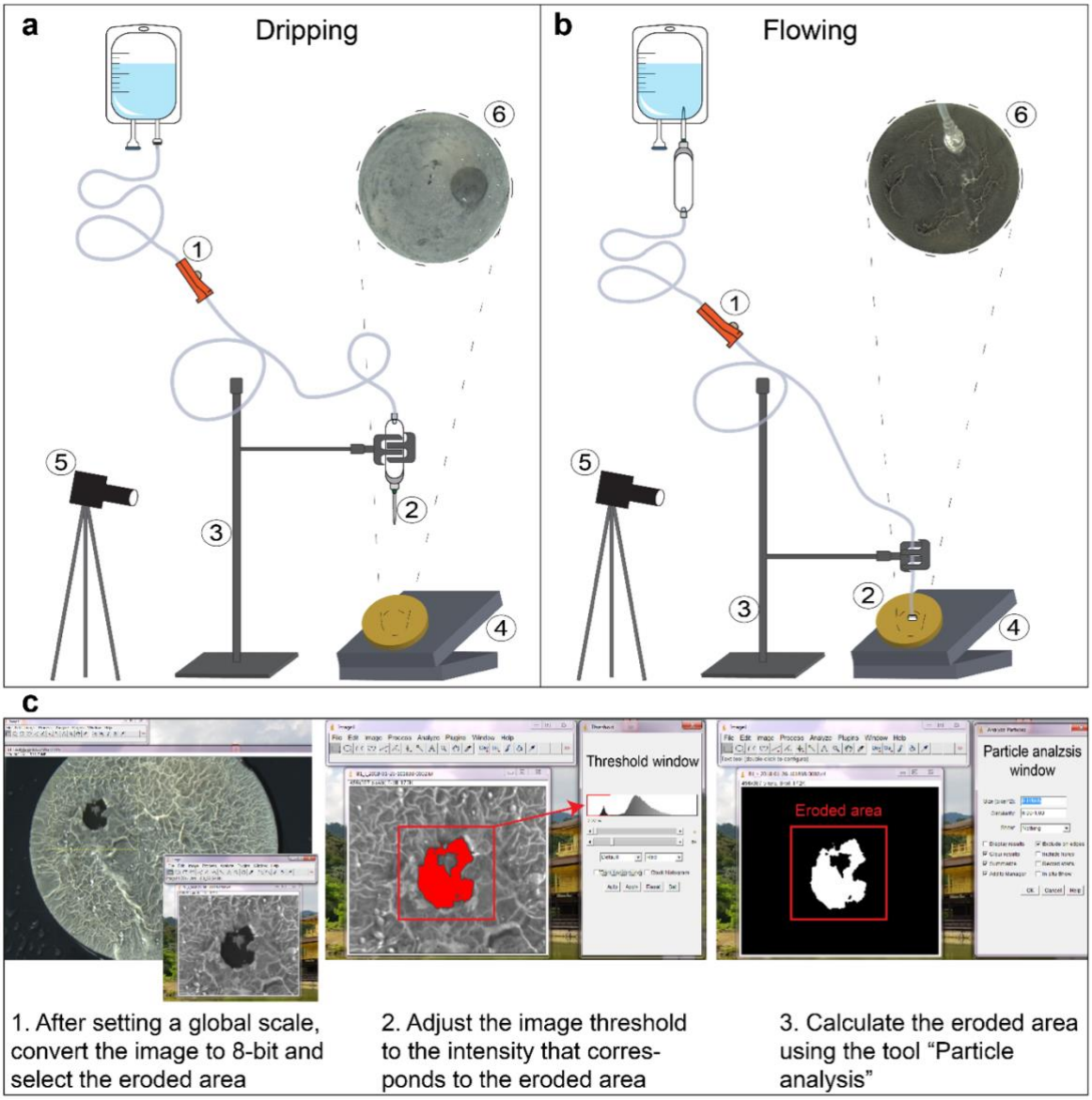

Figure 9 *Biofilm erosion set-ups.* Dripping **(a)** and flowing **(b)** configurations, elements with numbers are detailed in the main text. **c)** Workflow for the calculation of biofilm eroded area with Image J.

The biofilm samples tested here had the size of a standard petri dish (i.e., 90 mm in diameter – biofilm continuous layer). To avoid accumulation of water at the edge of the biofilm samples during the erosion experiments, the entire biofilm-covered agar layer was extracted from the petri dish and carefully placed directly onto the stage; *dd*H_2O was used as eroding agent. The treated areas were exposed to 700 µL of an 80% (v/v) ethanol aqueous solution and left undisturbed for 10 min. After incubation, the liquid was carefully removed with a pipette and the sample was left to air-dry for 2 h. Image J was used to quantitatively analyze the images obtained from the dripping experiments: a global scale was set using the known diameter of the entire biofilm sample, then each image was segmented into the area of interest and converted to 8-bit. Subsequent "particle analysis" after threshold adjustment of the image allowed for calculating the eroded area (Fig. 9c).

2.4.2 Antibiotic assays

As there are no established MICs reported for the specific combination of bacterial strains and antibiotics pertained here, the concentration of the antibiotics was determined based on published MIC_{90} values for different *Bacillus* and *Pseudomonas* strains. For antibiotic treatment of *P. putida*, biofilms, MICs reported for *P. aeruginosa* were taken as reference [126] and a concentration of 160 µg/mL of the antibiotic Piperacillin/Tazobactam (8:1) (Sigma Aldrich, St Louis, USA) was determined (this is ~20x higher than the MIC reported in the literature). For *Bacilli*, an MIC_{90} range between 0.032 and 8 µg/mL is reported for Tetracycline [126-128] and a MIC_{90} value of 8 µg/mL for Kanamycin [128]. Therefore, a concentration of 8 µg/mL was used for the treatment of *B. subtilis* NCIB 3610 planktonic bacteria with Tetracycline and a concentration of 12.6 mg/mL was determined for treatment of biofilms of the same strain with both, Tetracycline and Kanamycin (this is ~150x higher than the MIC values reported in the literature). The reason for selecting such elevated concentrations for biofilm treatment is that biofilms can be 100-1000x more resistant than planktonic bacteria [129]; therefore, antibiotic concentrations should be significantly higher for biofilms than for planktonic bacteria to avoid the risk of using insufficient levels that induce antibiotic resistance [130]. In all cases, antibiotic stock solutions were prepared according to the Clinical and Laboratory Standards Institute [131], kept frozen at −20 °C in aliquots, and thawed when needed.

2.4.2.1 LIVE/DEAD BacLight staining – after osmotic treatment

Efficiency of treatment with aqueous solutions containing antibiotics was tested after biofilm surface treatment with osmotic agents using a live/dead staining kit. Osmotic treatment of biofilm surfaces was performed as described in section 2.2.2 and such samples are referred to as "treated". To test for the effect of degradation over time, biofilms were left undisturbed for 10 min or 18 h in the presence of oxygen, and those samples are referred to as 'untreated'.

For testing *P. putida* biofilms, both treated and untreated biofilm surfaces were covered with the antibiotic solution for a duration of 2 h, or until the aqueous phase had evaporated and the antibiotic agent had precipitated on the surface (Fig. 10a). This antibiotic exposure step was

performed inside of a biosafety cabinet while keeping the lid of the petri dish slightly open under the laminar flow. Afterwards, a fragment of the antibiotic exposed biofilm surface was taken using a disposable inoculation loop and suspended in 100 µL sterile *dd*H_2O (Fig. 10a). The resulting biofilm suspension was shaken to ensure the presence of free-floating bacteria, and 50 µL of this cell suspension were extracted avoiding biofilm debris.

Viability of the antibiotic exposed biofilm cells was assessed using the LIVE/DEAD BacLight bacterial viability kit L7012 (Thermo Fischer, Massachusetts, USA). The dye was prepared following the manufacturer's instructions (1:1 ratio of propidium iodine and SYTO 9), added to the biofilm cell suspension at a concentration of 1% v/v and the samples were incubated in the dark for 15 min. The stained bacterial cells were visualized with an inverse fluorescence microscope (Leica Biosystems, Hesse, Germany) using 63× magnification; Texas red and FITC filters were used for visualization of red (propidium iodine) and green (SYTO 9) dyes, respectively. Ibidi chambers (Ibidi, Planegg, Germany) were used as sample holders. To allow for subsequent cell counting, a patch of agarose (600 µm in thickness) was placed on top of the stained biofilm cells suspension to stop the bacteria from moving. The dyes were tested for accuracy of the staining process, see section 4.1.3 for details.

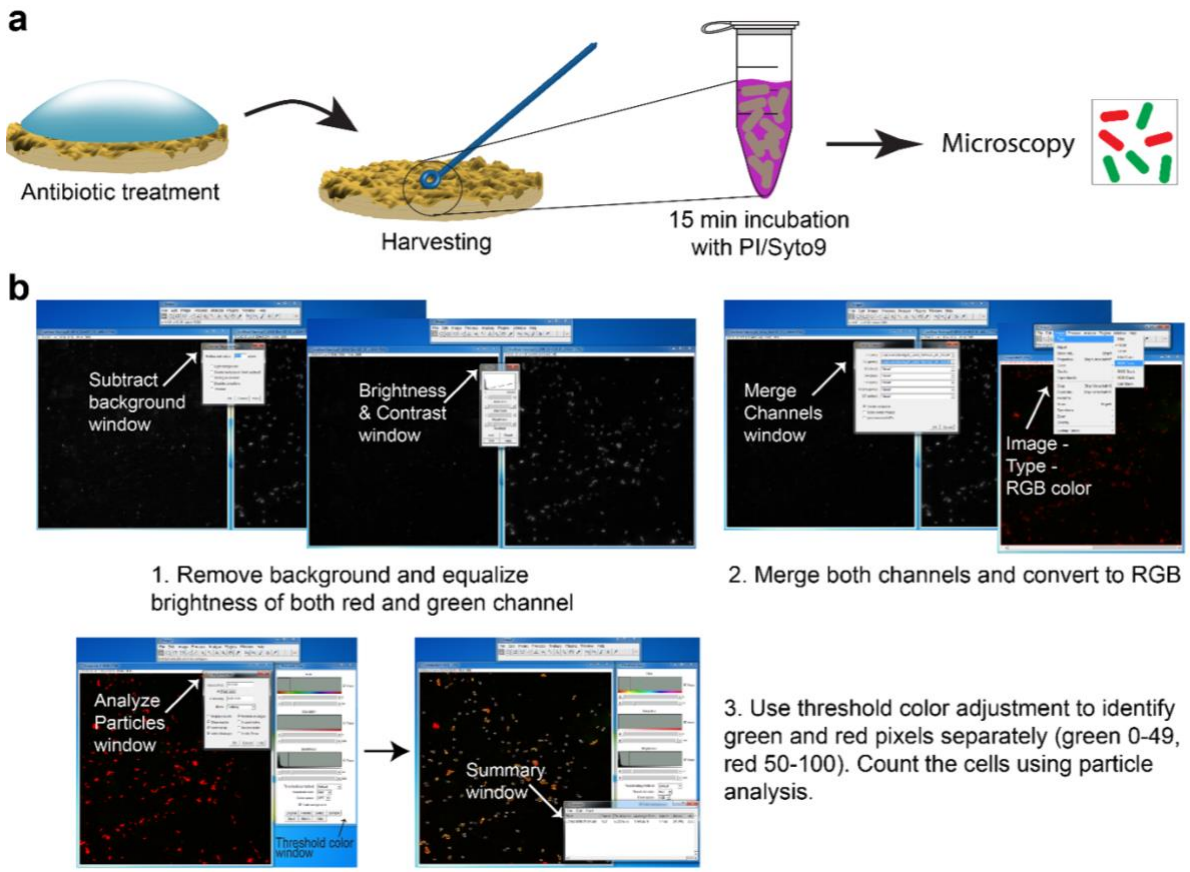

Figure 10 *Live/dead staining of antibiotic treated biofilm cells.* **a)** Treatment of biofilm surface and harvesting of cells for staining. **b)** Workflow for counting of live and dead cells using Image J.

Counting of live and dead bacterial cells was performed using Image J (Fig. 10b). First, the background was removed and the brightness intensities of the red and green channels were equalized. Then, the red and green channels were merged and the composite image was converted to RGB. Finally, red and green cells were identified separately using color threshold and counted using particle analysis.

2.4.2.2 CFU determination – after treatment with metal ions

Figure 11 shows the protocol (adapted from Martin *et al.* [79]) for testing the efficacy of both Tetracycline and Kanamycin antibiotics on biofilms formed by *B. subtilis* NCIB 3610 and treated with metal ions either during or after biofilm growth. First, entire bacterial colonies were scraped from the underlying agar, pooled, and suspended in 1 mL of an aqueous antibiotic solution. Such biofilm suspensions were left undisturbed at RT for 1 h and afterwards the biofilm-antibiotic suspension was centrifuged at 5000 rpm and 4 °C for 20 min. The pellet was washed twice (using 1 min centrifugation steps between the washing cycles) with a saline solution (prepared by dissolving 9 g of NaCl in 1 L *dd*H_2O) and resuspended in 10 mL of saline solution. To obtain a homogeneous bacterial cell suspension, a SONOPULS ultrasonic homogenizer (BANDELIN, Berlin, Germany) was used at a frequency of 20 kHz and 20% amplitude using cycles consisting of 7 pulses of 1 s duration and 1 s pause. 7 cycles were used for samples containing superhydrophobic biofilms, whereas 5 cycles were used for hydrophilic biofilms. The resulting cell suspensions were serially diluted, and 100 µL of the last dilution product was inoculated on agar plates in triplicates. Colony forming units (CFU) were assessed after incubation of the agar plates at RT for 3 days, or at 37 °C for 24 h.

Antibiotic treatment of planktonic bacteria was conducted using a modified version of the method reported by Cerca *et al.* [132]. Briefly, overnight cultures (prepared as described in section 2.1.2) were diluted to an OD_{600} of 0.05 and incubated at 37 °C and 90 rpm until an OD of 0.1 was reached. Then, the "day culture" was centrifuged at 5000 rpm and 4 °C for 5 min, the pellet was washed twice as described above and resuspended (at an OD_{600} of 0.05) in fresh LB containing the antibiotic. The resulting suspensions were further incubated at 37 °C and 90 rpm for 1 h. After antibiotic treatment, the samples were again centrifuged, washed and resuspended in saline solution to an OD_{600} of 0.05 before serial dilutions were generated and CFU plating was conducted (as described above).

CFU/mL values were obtained by multiplying the average CFU calculated from the triplicates by the dilution factor, divided by the inoculation volume. CFU/mL values reported thereafter were determined from *n* individual samples generated from at least 3 growth batches (*N = 3).*

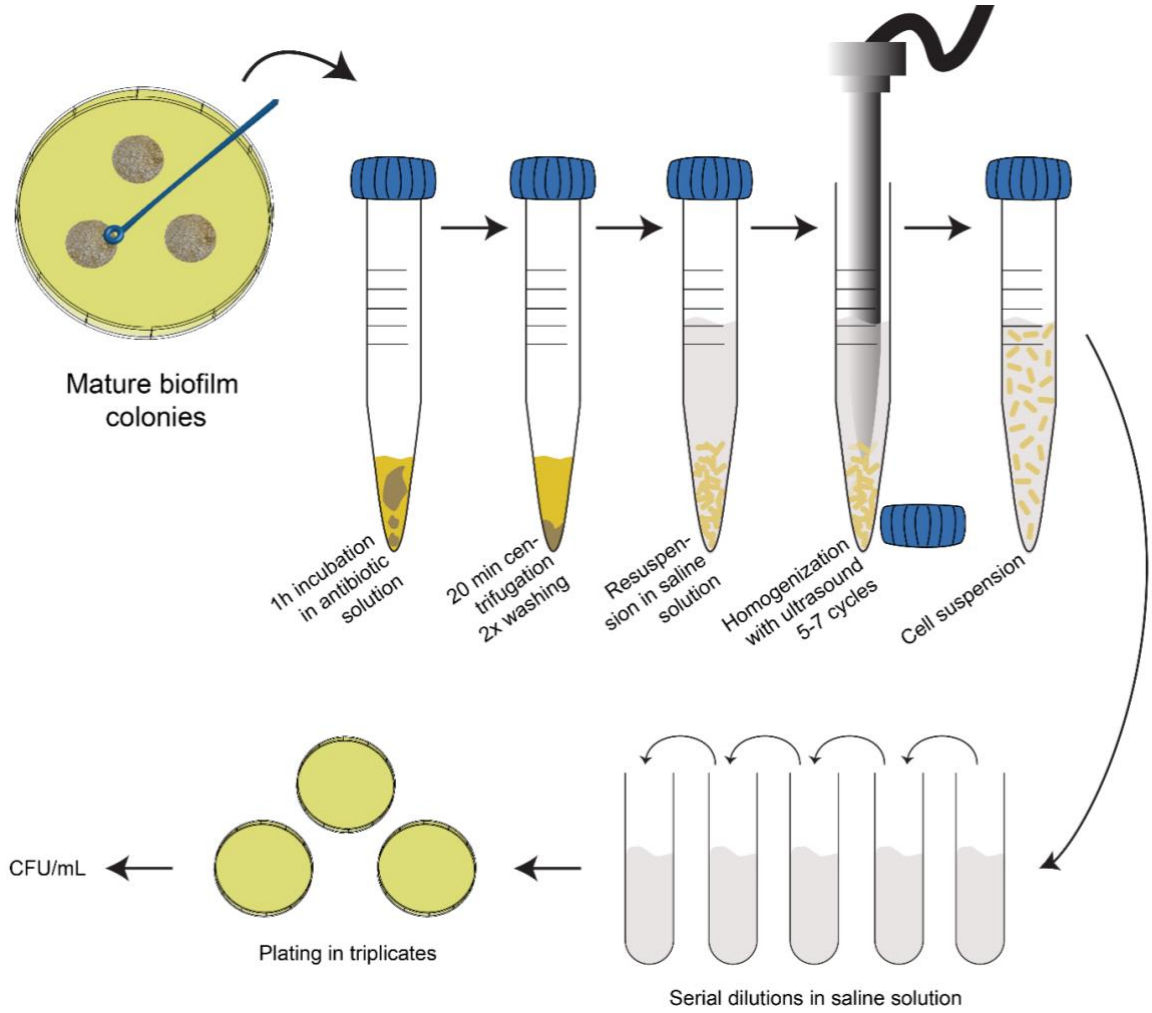

Figure 11 *Method employed for testing antibiotic efficiency on mature biofilm colonies.* CFU plating was used to account for cell viability after antibiotic exposure. Different dilution factors were used based on the type of sample.

2.5 Data Analysis

Sample sizes are described throughout as follows: for independent biological replicates the symbol '*N*' is used, whereas for technical replicates the symbol '*n*' is used.

2.5.1 Statistical data analysis

2.5.1.1 Significance tests

Significance tests were performed using the software R (Foundation for Statistical Computing, version 3.4.0) along with the user interface Rstudio. Unless specified, significant differences for all multiple comparisons (more than two groups) were detected using one-way analysis of variances (ANOVA) and Tukey post-hoc tests, a *p*-value of 0.05 was always used as cut-off for statistical significance. Assumption of normal distribution was verified using the Shapiro–Wilk test, and (less confining) by *Q-Q* plots and histograms (as large variability is expected

within biological samples). Assumption of homogeneity of variances was tested with a Levene test.

For biofilm colonies subjected to osmotic treatment (section 4.1), statistical significance was assessed pair-wise: before and after treatment. The ***Sdr***, ***Sq***, and ***Sz*** values measured on untreated and ethanol treated samples were compared by performing paired *t*-tests assuming an upper-tailed alternative hypothesis (H_1).

For biofilm samples treated with metal ions either at early or late stages of biofilm growth (section 4.2), significant differences were assessed *via* one-way ANOVAs when the populations met the assumption of homogeneity of variances, followed by a Tukey post-hoc test. A Welch ANOVA followed by Games-Howell post-hoc was used to assess samples whose datasets failed the assumption of homogeneity of variances. Here, significance was assessed for ***Sdr***, contact angle, fluorescence intensity, and CFU/mL values.

2.5.1.2 Mass spectrometry data

For statistical evaluation of the biofilm composition using mass spectrometry, volcano plots were generated from data obtained from three independent biological replicates (where $n \geq 2$ in each) to illustrate differences in protein expression between the different samples. Statistical analysis was performed in Perseus (as part of the MaxQuant environment) [133]. Only proteins that were identified based on at least 2 MS/MS counts and valid ratios in all three replicates of either of the six states were considered for data analysis in the case of center *vs*. periphery comparison. Missing values were then imputed on the basis of a normal distribution (width = 0.3, down-shift = 1.8). Volcano plots were generated on the basis of a two-sample *t*-test (both sides, FDR = 0.05, S0 = 1). Overrepresentation analysis was based on gene ontology annotations and was performed with the Bingo App in the Cytoscape environment [134]. Statistically significant regulated proteins from the volcano plot were compared to all proteins present in the plot in the category of biological process. Analysis was based on a hypergeometrical test with the multiple testing correction according to Benjamini Hochberg and a significance level of 0.05.

The reported volcano plots in sections 3.1.3 (Fig. 20) and 4.1.2 (Fig. 38) depict the following: the *y*-axis represents the *p*-value and the *x*-axis lists the binary logarithm of the *n*-fold change in protein expression levels between the different biofilm samples. The solid lines indicate a significance level of $p = 0.05$, and a required minimum fold change of 2 (s0 = 1) is used as a cut-off for significance. Red dots above the cut-off lines denote significantly differently expressed proteins.

3 Microscopic origin of the liquid repellency of bacterial biofilms

3.1 [a]Establishing the link between the surface topography and the wetting behavior of *Bacillus subtilis* NCIB 3610 biofilms

The colonization of surfaces by bacterial biofilms constitutes a huge problem in healthcare and industry. When attempting biofilm inactivation or removal, it is crucial to sufficiently wet the biofilm surface with antibacterial agents; however, certain biofilms efficiently resist wetting and the origin of this behavior remains unclear. To elucidate the mechanisms by which biofilm bacteria create liquid repellent surfaces, first, a thorough characterization of biofilms exhibiting hydrophobic surfaces is necessary. Here, it is shown that biofilms generated by the bacterium *B. subtilis* NCIB 3610 can exhibit three different modes of wetting. Depending on both the growth medium used for biofilm generation and the location on the biofilm colony, a hydrophilic and two hydrophobic biofilm variants are found, i.e., water repellent surfaces with either strong or weak water droplet adhesion. Using a combination of imaging techniques, those different wetting behaviors are correlated with structural differences of the biofilm surfaces, which are quantified with metrological parameters. It is demonstrated that the two hydrophobic biofilm variants can be described by different physical wetting regimes which are related to the lotus and rose petal effect. Lastly, a mass spectrometry analysis reveals that the distinct wetting properties of the biofilms are accompanied by alterations in proteomics levels of the biofilm matrix. The latter results inspire the study of specific matrix components previously described for NCIB 3610 biofilms in relation to their impact on a parameter affecting the biofilm wetting behavior, i.e. the surface roughness. It is revealed that both the polysaccharide and the surface layer protein BslA contribute to the development of the biofilm surface roughness. Together, these results indicate that it is a complex combination of factors including the biofilm matrix composition, surface chemistry and topography that dictate the wetting behavior of *B. subtilis* NCIB 3610 biofilm colonies.

3.1.1 Wetting behavior of NCIB 3610 biofilms grown on different agar variants

When bacteria of the strain *B. subtilis* NCIB 3610 are cultivated on standard LB agar, the formed biofilm colonies exhibit a fairly homogenous morphology with delicate vein-like structures branching out from the center to the peripheral region of the colony. In contrast, the biofilm colonies grown on LBGM agar (i.e. nutrient rich medium, Table 2) show aerial projections enclosing the center region and appear Eden-like with dense branching at the edge of the colony. Biofilms grown on MSgg agar (i.e. minimal medium, Table 2) show overall a wrinkled morphology but with a smoother texture in the center (Fig. 12a). The biofilm colony

[a] This section follows in part the publication: "*Surface topology affects wetting behavior of Bacillus subtilis biofilms*" published on 2017, in npj biofilms and microbiomes.

morphologies described here differ slightly from those described in the literature [62, 89, 115, 135, 136] as the growth temperature and growth time used here are different.

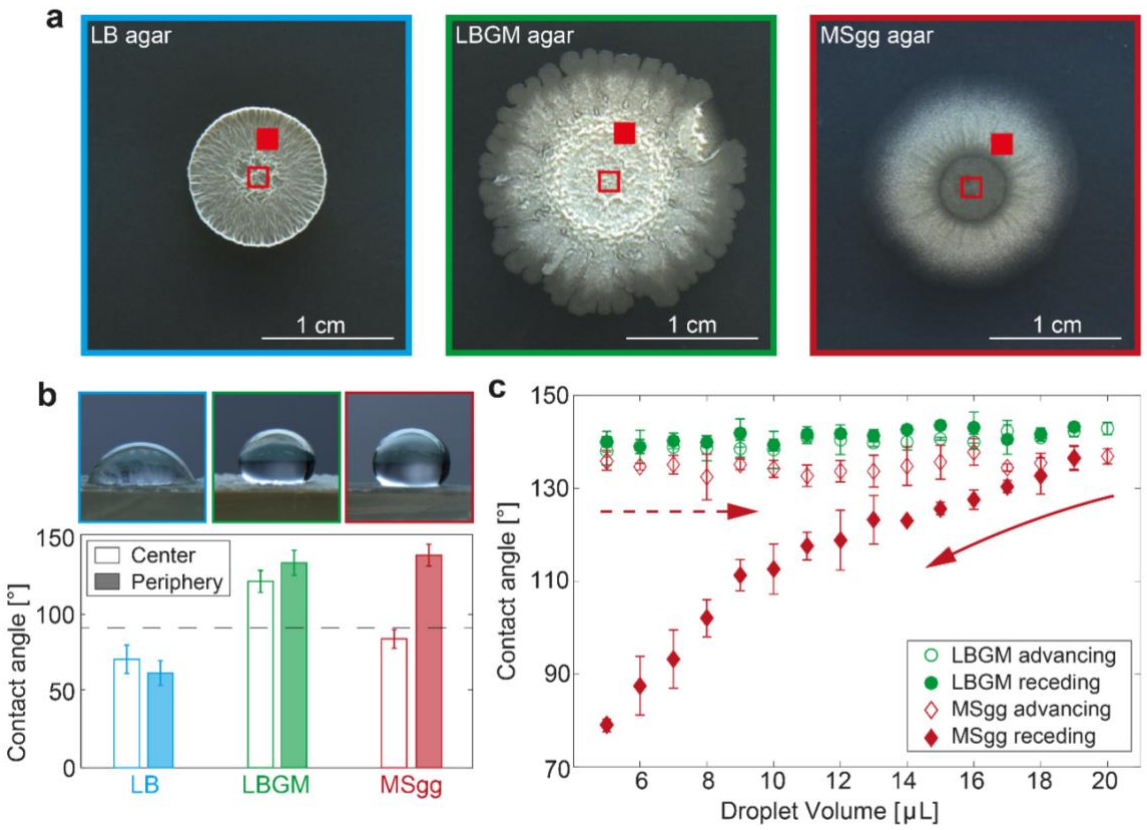

Figure 12 *B. subtilis NCIB 3610 biofilms macrocolony morphology and wetting behavior on three different media.* **a)** The regions on the biofilm surface where the wetting tests were performed are marked with a closed and open red square, respectively. **b)** Transversal image of a 10 µL water droplet on the surface periphery of the biofilm colonies. Dashed line in the contact angle diagram indicates hydrophobicity cut-off, below 90° = hydrophilic. **c)** Contact angle hysteresis diagram of the peripheral regions of LBGM and MSgg biofilms. The experimental time scale for the wetting/dewetting experiment was identical for both biofilm variants. **b-c)** Error bars denote the standard deviation as calculated from at least 9 independent samples (for data shown in **b**, $n \geq 9$; for data shown in **c**, $n = 3$; for all data: $N \geq 3$).

For probing the wetting behavior of those three biofilm variants, a 10 µL water droplet was placed onto the biofilms, and the static contact angle was determined (section 2.3.2, Fig. 7). For biofilm colonies grown on standard LB agar, a contact angle of (61 ± 8)° was obtained (Fig. 12b) which corresponds to hydrophilic behavior. Such a low wetting resistance is observed at virtually all locations of the biofilm, i.e., both in the center and the peripheral regions of the colony (Fig. 12b). In contrast, the peripheral regions of the other two biofilm variants both show hydrophobic behavior: with contact angles of (132 ± 8)° for the biofilm grown on LBGM agar and (137 ± 7)° for the biofilm grown on MSgg agar (Fig. 12b). Similarly high contact angle values were also obtained for 50/50 mixtures of water and alcohols (Fig. 13a), which is consistent with previous findings for *B. subtilis* biofilms grown on MSgg agar [26]. Although the peripheral regions of both the LBGM and the MSgg biofilm show hydrophobic properties, the wetting behavior of the central regions of those two biofilm variants differs: in the center of the MSgg grown biofilm, a rather hydrophilic behavior is observed (Fig. 13b)

with a contact angle of only (83 ± 6)°. In some cases it appears that the water droplet slips below the central area of the MSgg biofilm and detaches the biofilm from the agar layer. In contrast, in the central region of the LBGM grown biofilm, a contact angle of (120 ± 7)° is observed, which clearly indicates a hydrophobic surface (Fig. 12b).

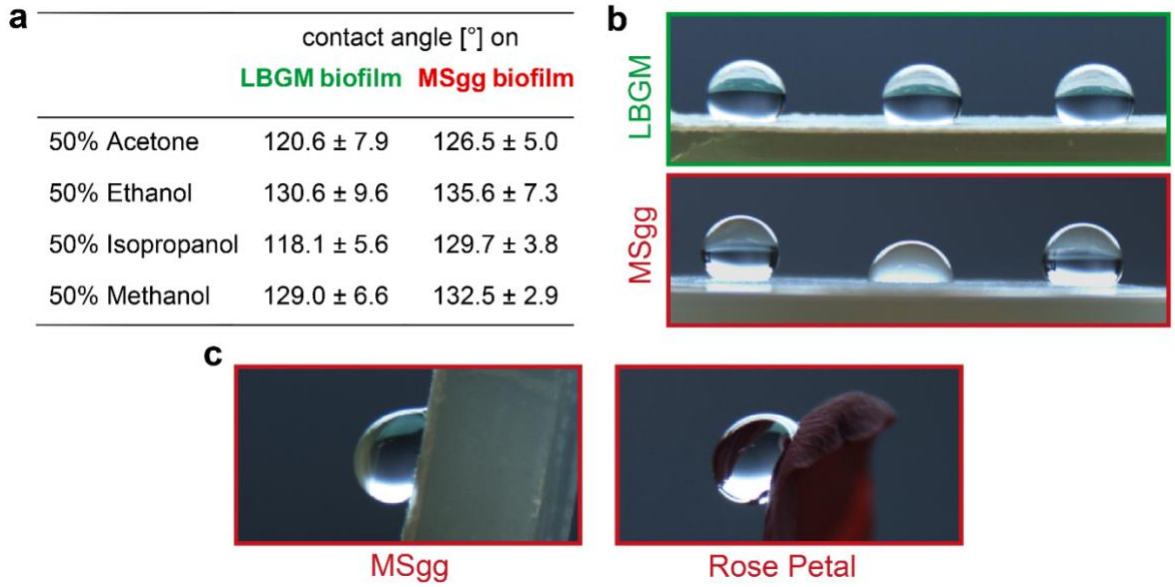

Figure 13 *The different liquid behaviors found on B. subtilis NCIB 3610 biofilms*. **a)** Wetting resistance of the peripheral regions of LBGM and MSgg biofilms to solvents. Errors denote the standard deviation as calculated from at least 3 individual samples ($n \geq 3$). **b)** Transversal images of bacterial colonies wetted with water droplets. **c)** Hanging water droplet on a vertically tilted biofilm grown on MSgg agar (left) and on the surface of a rose petal (right).

A strong wetting resistance is observed on a broad range of natural as well as artificial materials and can be further classified into lotus-like and rose-like behavior [3, 137]. On a lotus leaf, very high contact angles up to 150° are observed, and water droplets easily roll off the surface when the leaf is slightly tilted [15]. In contrast, a hydrophobic surface which exhibits strong adhesion forces towards a water droplet is, for example, found on rose petals [138]. Here, these strong adhesion forces prevent a small water droplet from rolling off the surface of the rose petal – even if the petal surface is tilted or turned upside down (Fig. 13c –right). At the same time, such rose petal surfaces show a hysteresis in the contact angle, i.e. a constant contact angle when the volume of a wetting water droplet is increased, but a decreasing contact angle when the volume of this droplet is reduced again. Thus, in a next step, the wetting behavior of the two hydrophobic biofilm variants were further characterized. First, a small water droplet was placed onto the biofilms and then the volume of the water droplet was gradually increased from 5 µL to 20 µL (Fig. 12c). Afterwards, the volume of the water droplet was step by step decreased back to 5 µL. For the LBGM biofilm variant, the contact angle of the droplet remains virtually constant during this process (Fig. 12c –green symbols). Furthermore, when the surface of the LBGM grown biofilm is tilted, the water droplet easily rolls off the biofilm surface. These results motivate that the wetting behavior of NCIB 3610 biofilms grown on LBGM is related to that of lotus leaves, i.e. hydrophobic without any perceivable contact angle hysteresis.

The very same bacteria, however, are able to form biofilms with rose-like wetting behavior when grown on MSgg agar: the MSgg biofilm sample can be tilted vertically and the water droplet stays attached to the surface (Fig. 13c –left). Also, a pronounced contact angle hysteresis was found for the MSgg biofilm: the contact angle remains constant when the volume of the water droplet is increased (advancing contact angle), but the contact angle continuously decreases when the water droplet volume is lowered again (receding contact angle) (Fig. 12c –red symbols).

3.1.2 NCIB 3610 biofilm surface topography and physical wetting regimes

Although the detailed wetting behavior of rose petals and lotus leaves is different, they both constitute strong hydrophobic biosurfaces. A structural feature the two biosurfaces share is that they both exhibit a rough surface topography on the micro- as well as on the nanoscale. Thus, in a next step, the roughness of the peripheries of the two hydrophobic biofilm variants were tested against that of the hydrophilic biofilm variant to show whether the former exhibit stronger features. A suitable technique to characterize the surface topography of a material on the microscale is light profilometry (section 2.3.1, Fig. 5). Indeed, when the surfaces of the three biofilm variants were analyzed with this technique, the obtained surface profiles revealed different topographies (Fig. 14a).

The peripheral region of biofilms grown on LB agar exhibits relatively smooth height features with peaks in the range of ~80 µm. In contrast, the peripheral surface of the hydrophobic LBGM biofilm appears to be much rougher: indeed, here the maximal height difference in the surface structures is on the order of ~290 µm. Finally, the MSgg biofilms show peripheral surface features of ~160 µm in height but with narrower spacing than those observed for LB biofilm. To confirm these differences in the surface topography of the three biofilm variants, SEM images of the biofilm samples were acquired (Fig. 14b). At low magnification, SEM probes a similar length scale as light profilometry, and indeed the visual impression obtained from the profilometry images was confirmed by the SEM pictures: the peripheral regions of the hydrophilic biofilms appear to be smoother than those of the hydrophobic biofilm variants which, in turn, both show a multitude of roughness features (Fig. 14). At higher magnification, the topographical differences between the hydrophilic and the hydrophobic biofilm variants are even more pronounced (Fig. 14c). In the periphery, the surface structure of the hydrophilic biofilm is highly porous. In contrast, in the peripheral surface of the hydrophobic biofilm variants, the bacteria are tightly packed and the surface shows little to no pores (Fig. 14c).

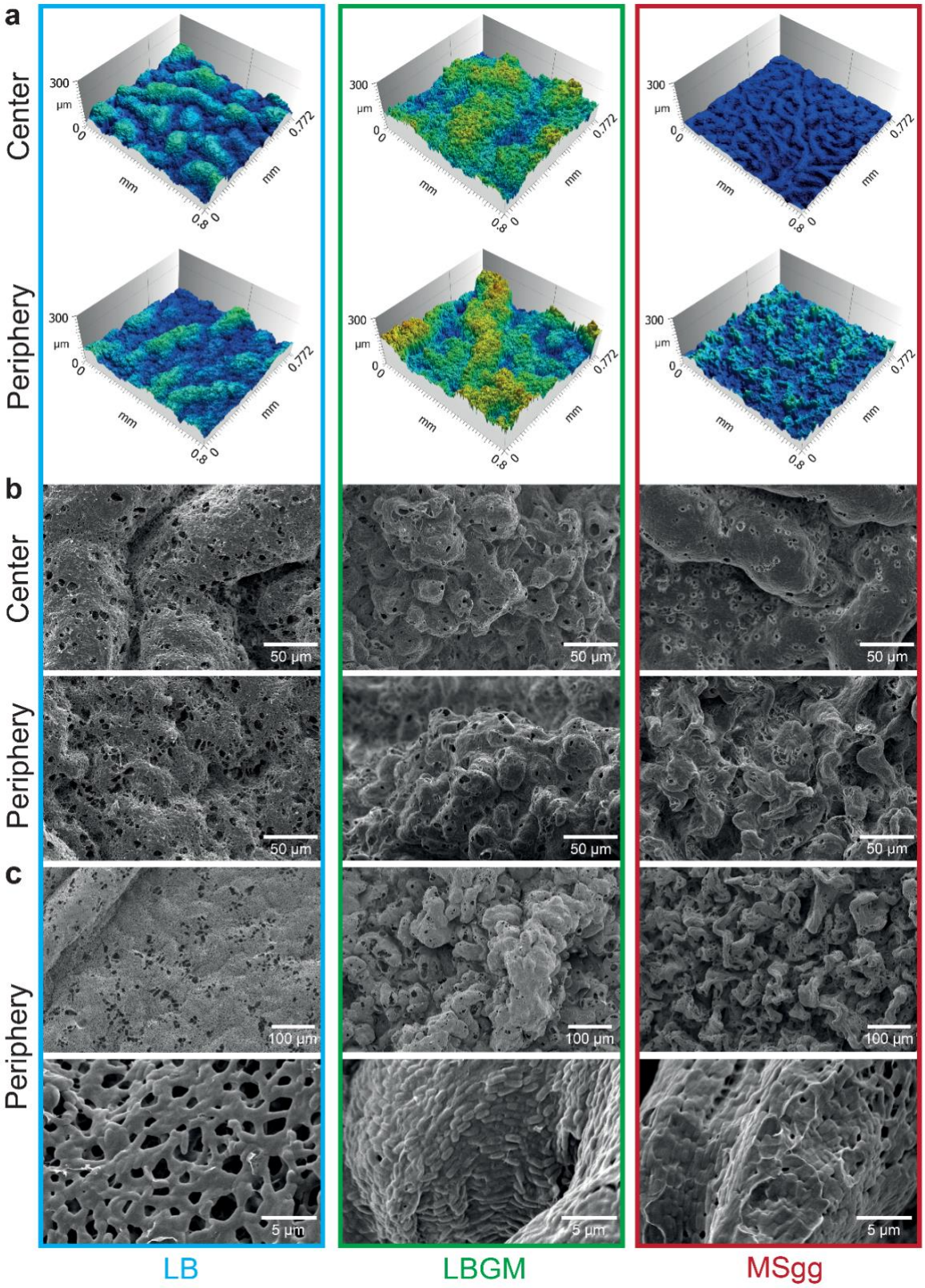

Figure 14 *Surface topography of B. subtilis NCIB 3610 biofilms.* **a)** Light profilometry images of biofilms formed on the three different agar variants at 20x magnification. **b)** SEM images taken at a similar magnification than light profilometry. **c)** SEM images of the periphery at 200x (top) and 5000x (bottom) magnification.

In addition to those pronounced structural differences in the periphery of hydrophilic and hydrophobic biofilms, respectively, it appears that also the two hydrophobic biofilm variants differ from each other in terms of their surface topography. Both the profilometry as well as the SEM images suggest that the spacing between the larger surface-features found in the periphery (wavy structures) of the LBGM biofilm is larger than for the MSgg biofilm. Thus, in a next step, the profilometry images were analyzed in more detail. The idea was to calculate quantitative metrological parameters (section 2.3.1, Table 3) from the surface periphery of the biofilm colonies that either verify or falsify the visual impression discussed so far. The root mean squared roughness, ***Sq***, is widely used to characterize the surface topography of materials. However, neither ***Sq*** nor higher order powers of the surface height, such as skewness ***Ssk*** or kurtosis ***Sku*** can sufficiently distinguish between the three biofilm variants (Fig. 15a). On the other hand, absolute height parameters such as the maximal peak height, ***Sp***, the deepest valley depth, ***Sv***, and the maximum height, ***Sz***, show significant ($p < 0.05$) differences among all three biofilm surfaces. With each of those three parameters, the smallest feature size is observed for the LB grown biofilms, intermediate values for MSgg biofilms, and the largest features for LBGM grown biofilms (Fig. 15a) – in full agreement with the visual impression discussed before. To quantify the spacing between the most pronounced roughness features, the length of the fastest decay of the autocorrelation function, ***Sal***, was calculated. The widest spacing is shown by LBGM biofilms where $\boldsymbol{Sal}_{\mathrm{LBGM}} = (119 \pm 27)$ µm is found. This value also shows significant ($p < 0.05$) differences among all biofilm variants (Fig. 15a). Furthermore, two parameters combining both roughness and spacing information were considered: the root mean square surface slope, ***Sdq***, and the developed interfacial area ratio, ***Sdr***. The ***Sdq*** parameter shows significant differences ($p < 0.05$) among the three biofilm variants (Fig. 15a). Since the relative increase in the total surface area is directly related to the wetting energy [139], it was expected that the ***Sdr*** parameter –which indicates the complexity of a surface by comparing the actual surface and the projected surface, would also be able to distinguish among the three biofilm variants. Indeed, the calculated ***Sdr*** values are significantly ($p < 0.05$) different for the three biofilm variants; the LB biofilms show the smallest increase in the surface area, whereas the largest value of ***Sdr*** is observed for the LBGM biofilms (Fig. 15a).

Although a number of metrological surface parameters which can successfully distinguish between the peripheries of the three biofilm types have been found, not all surface texture parameters listed in ISO norms returned significant differences. Thus, in a next step, a more general mathematical analysis of the surface topography was tested, instead of calculating a whole list of individual metrological parameter values. A discrete Fourier analysis is commonly used to analyze complex signals and to quantitatively determine the contribution of sub-signals with different wavelengths [140]. In such an approach, the 2D surface of the biofilm is approximated by a sum of sinusoidal waves. Then, the average power spectral density lists the amplitudes of those waves as a function of the corresponding wavelengths. As depicted in Fig. 15b, this Fourier analysis can differentiate between the peripheral regions of the three biofilm variants: at small wavelengths, the hydrophilic biofilms (LB) clearly stand out, as here the amplitudes are almost one order of magnitude smaller than for the other two biofilm types (LBGM, MSgg). This regime, e.g., wavelengths in the range of tens of micrometers, is normally referred to when a surface roughness is determined. Consistently, the smallest ***Sq***

value was found for the periphery of the hydrophilic LB biofilms. However, higher wavelengths contribute to the surface topography as well, and constitute a surface feature which is typically referred to as waviness. At those larger wavelengths, i.e., in the range of 100 µm and above, the LBGM biofilms have peripheral surface features with amplitudes that are approximately one order of magnitude larger than those of both the hydrophilic (LB) and the rose-like (MSgg) biofilms. This result agrees very well with both the SEM images for the peripheral biofilm areas shown in (Fig. 14b) (in which the spacing between the most pronounced individual surface features appears to be smaller for the MSgg grown biofilm than for the LBGM variant), and the ***Sal*** values discussed before.

a

	Sq [µm]	***Ssk***	***Sku***
LB	10.2 +/- 2.9	0.45 +/- 0.53	4.26 +/- 1.85
LBGM	51.5 +/- 13.5	0.61 +/- 0.46	3.12 +/- 0.83
MSgg	19.9 +/- 1.6	0.08 +/- 0.13	3.41 +/- 0.23

	Sp [µm]	***Sv*** [µm]	***Sz*** [µm]	***Sal*** [µm]	***Sdq***	***Sdr*** [%]
LB	43 +/- 13	37 +/- 11	80 +/- 20	56 +/- 12	1.8 +/- 0.4	70 +/- 20
LBGM	156 +/- 35	130 +/- 27	286 +/- 51	119 +/- 27	10.6 +/- 2.8	522 +/- 132
MSgg	83 +/- 10	77 +/- 9	160 +/- 17	34 +/- 4	4.5 +/- 0.6	228 +/- 36

b

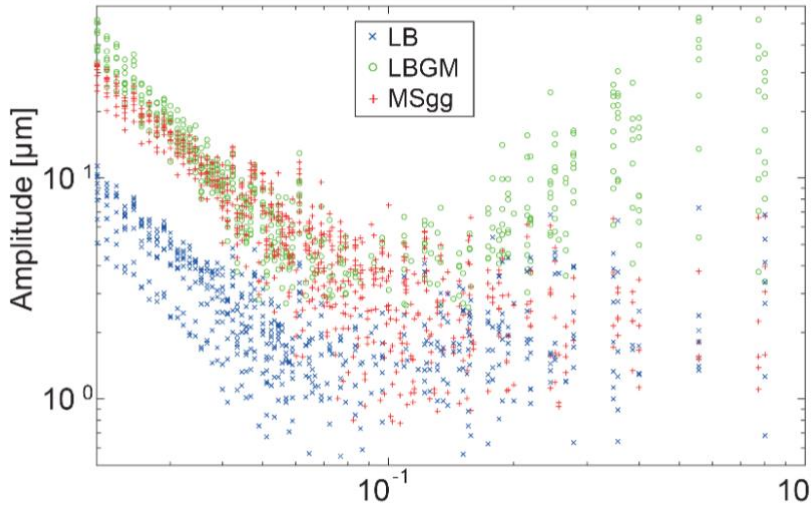

Figure 15 *Characterization of the surface profiles obtained from the periphery of the different B. subtilis NCIB 3610 biofilms.* **a)** Individual surface parameters defined in the ISO norm, boxed values indicate significant differences, where $p = 0.05$ (section 2.3.1, Table 3) and error values denote the standard deviation. **b)** The average power spectral density was calculated using a fast Fourier transformation of the surface profiles. For the interpretation of the obtained data, it is crucial to recall that the spatial resolution of the profilometry images, i.e. the pixel width of the scanning process, limits the spectrum of wavelengths. As the pixel size in the analyzed profilometry images is 1.566 µm and errors for remodeling the edges of the surface are especially high for low wavelengths, wavelengths smaller than 20 µm were disregarded in the calculated power spectrum.

To further challenge the hypothesis that the wetting behavior of biofilms is linked to differences in their surface topography, the metrological analysis was extended to study the spatial heterogeneity of the biofilm surfaces. When the central and peripheral regions of a given bacterial biofilm colony were compared, a similar relationship between the surface topography and the wetting resistance of those biofilm regions was observed (Fig. 16), as discussed before

when the peripheral regions of the three biofilm variants were compared (Fig. 15a). For instance, the central (hydrophilic) area of the MSgg biofilm displays a smoother surface than its (hydrophobic) periphery (Fig. 14). Quantitatively, this is reflected in the significantly ($p < 0.05$) lower ***Sz*** and ***Sdr*** values calculated for the biofilm center (Fig. 16 –open boxes). In contrast, the central and peripheral regions of LBGM grown biofilms both exhibit hydrophobic properties. Consistently, higher ***Sz*** and ***Sdr*** values were obtained from the local surface profiles at both locations of these biofilms than for the MSgg or LB biofilms (Fig. 16). Finally, the central and the peripheral regions of LB biofilm colonies show similar hydrophilic wetting behavior and ***Sz*** and ***Sdr*** values mostly lower than those obtained in hydrophobic biofilm areas (Fig. 16). This extended analysis confirms the notion that the surface topography of the biofilms and their wetting behavior are directly related.

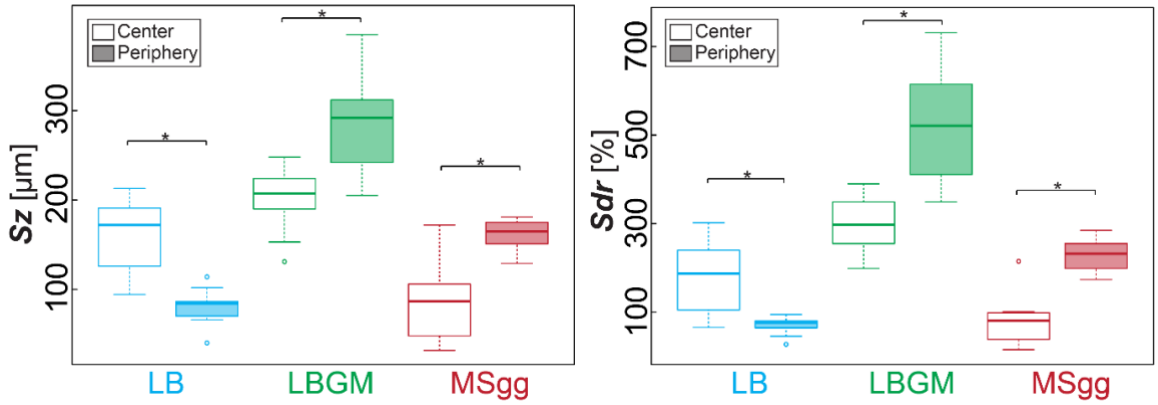

Figure 16 *Spatial heterogeneity of B. subtilis NCIB 3610 biofilm colonies.* A subset of metrological parameters, the ***Sz*** and the ***Sdr*** values, confirm the notion that the surface topography is related to the wetting behavior of biofilms even when the surfaces features are spatially heterogeneous. Stars indicate statistically significant differences, where $p = 0.05$. Boxes represent Q1-Q3, bold lines represent the median, and bars span from max. to min. ***Sz*** and ***Sdr*** values were obtained from at least 9 independent samples ($n \geq 3$, $N \geq 3$).

So far, the differences in the surface structure of *B. subtilis* NCIB 3610 biofilms have been correlated with the observed differences in their wetting behavior. Quantitative metrological parameters calculated from the surface topography of the biofilms support this idea. Moreover, the two hydrophobic biofilm variants show significantly different surface topographies as well. Wetting experiments revealed a lotus-like wetting resistance for LBGM biofilms and a rose-like wetting resistance for the periphery of MSgg biofilms. Thus, next, this analogy was further tested, i.e., if similar physical wetting mechanisms as described for the corresponding leaf/petal surfaces are also responsible for the wetting resistance of the hydrophobic biofilms. For instance, trapped air bubbles are reported to locally separate the microscopic surface features of a lotus leaf and a water droplet [15]. This mechanism is referred to as a Cassie/Baxter state, a three-phase wetting interface comprising a solid, a liquid, and an air component [16]. In contrast, for rose petals an impregnated Cassie regime is reported, i.e., the microstructures of the rose petal surface are in contact with the wetting fluid [3]. High adhesion forces towards a water droplet and a pronounced contact angle hysteresis –as also observed for the MSgg biofilm– are a direct consequence of this impregnated wetting state.

To test whether the two hydrophobic biofilm variants can be described by a Cassie/Baxter and an impregnated Cassie wetting state, respectively, the surface-liquid interface for the three biofilm variants was evaluated next. In a first step, the biofilms were brought in contact with an aqueous staining solution and then the biofilm surfaces were imaged using fluorescence microscopy. *Z*-projections of confocal image stacks (Fig. 17a) show differences in the staining behavior of the biofilms, which are consistent with the differences in the surface topographies and the different wetting regimes discussed before: biofilms grown on LB agar are stained uniformly as expected for a hydrophilic surface. Biofilms grown on LBGM agar are mainly stained at the peak areas of the surface structures, which suggests that the aqueous staining solution does not get in contact with the valleys of the biofilm surface. In contrast, MSgg biofilms seem to be stained much more efficiently than the LBGM biofilms, as only thin non-fluorescent valleys are found separating the well-stained surface roughness features. Apparently, the MSgg biofilm variant –although showing hydrophobic behavior in its periphery– allows most of its surface to be wetted by the staining solution. In contrast, LBGM biofilm surfaces seem to partially avoid contact with water.

Profilometry images acquired before, during and after wetting of the biofilm colonies with a dye-free water droplet (Fig. 17b) support the results obtained from biofilm staining. For imaging the biofilm/water droplet interface, vertical scanning was performed through the sample starting at the upper surface of the water droplet. While moving the focus plane downwards, a second interface appeared, this is the interface shown in Fig. 17b, “during wetting”. A fair amount of valid data points can be acquired at the biofilm/air interface. However, for the solid/liquid (biofilm/water) interface, only a small amount of valid data points could be acquired. The latter may be caused by the high water content of bacterial biofilms which renders the biofilm/water interface difficult to image with light profilometry (Fig. 17b, LB sample). For LBGM biofilms, areas with a large flat interface appeared during wetting. When the water droplet was removed with compressed air, these flat interfacial areas disappeared again, and the identical biofilm surface topography was found as it was present before wetting. This result suggests that the flat interfaces observed during the wetting process are established by trapped air bubbles separating the rough biofilm surface and the bottom of the water droplet. In contrast, for the peripheral region of the biofilms grown on MSgg agar, the surface topography of the biofilm/water interface appears to be similar to the biofilm/air interface imaged before wetting (Fig. 17b). Here, planar interfacial areas as observed for the lotus-like LBGM biofilm did not occur. However, after the water droplet was removed with pressurized air, small interfacial areas with a flat topography were detected. Those flat interfaces are established at higher *z*-coordinates than the biofilm contour. Thus, they likely represent the upper surface of micro-cavities filled with water. This interpretation would also be consistent with the idea that –due to the presence of an impregnated Cassie state– the MSgg biofilm exhibits strong adhesion forces towards water droplets. Of course, also the LB biofilm surface exhibits residual water after the wetting process, but here this finding is not surprising considering that a Wenzel wetting state [28] is expected for a hydrophilic material.

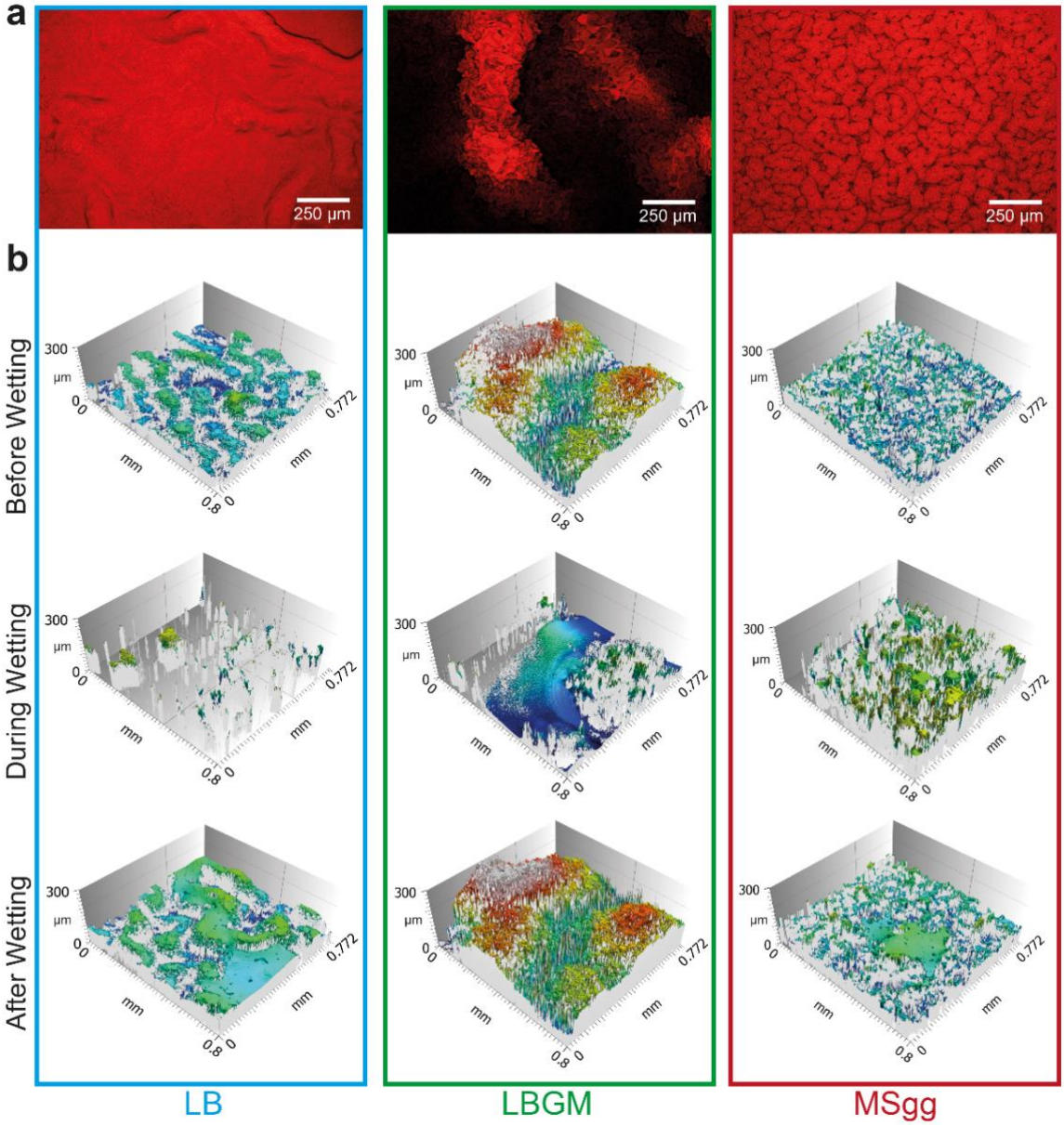

Figure 17 *Surface analysis of the peripheral regions of B. subtilis NCIB 3610 biofilms before, during, and after wetting.* **a)** Confocal fluorescence images, scale bar denotes 250 µm. **b)** Light profilometry images taken with a 20x objective.

The results discussed so far imply that a link between surface topography and wetting behavior exists for three bio-surfaces of different origins, i.e. NCIB 3610 biofilms, rose petals and lotus leaves. Next, a second bacterial strain was characterized the same way as done for the NCIB 3610 strain to test if the observations obtained before are exclusive of biofilms formed by the latter. Interestingly, the identical trend found for NCIB 3610 biofilms, i.e. hydrophilic behavior on LB agar, hydrophobic (lotus-like) behavior on LBGM agar and hydrophobic (rose-like) behavior on MSgg agar, is observed for the peripheral regions of *B. subtilis natto* biofilms. Also, the observed wetting behaviors correlate with similar differences in the biofilm topographies (Fig. 18). Furthermore, the ***Sdr*** values obtained for the peripheral region of the MSgg biofilm variants of both *B. subtilis* NCIB 3610 and *B. subtilis natto* showing rose-like wetting resistance agree very well with the values obtained for actual rose petals (Fig. 19a).

This further underscores the analogy drawn between the wetting resistance of rose petals and that of hydrophobic MSgg biofilms.

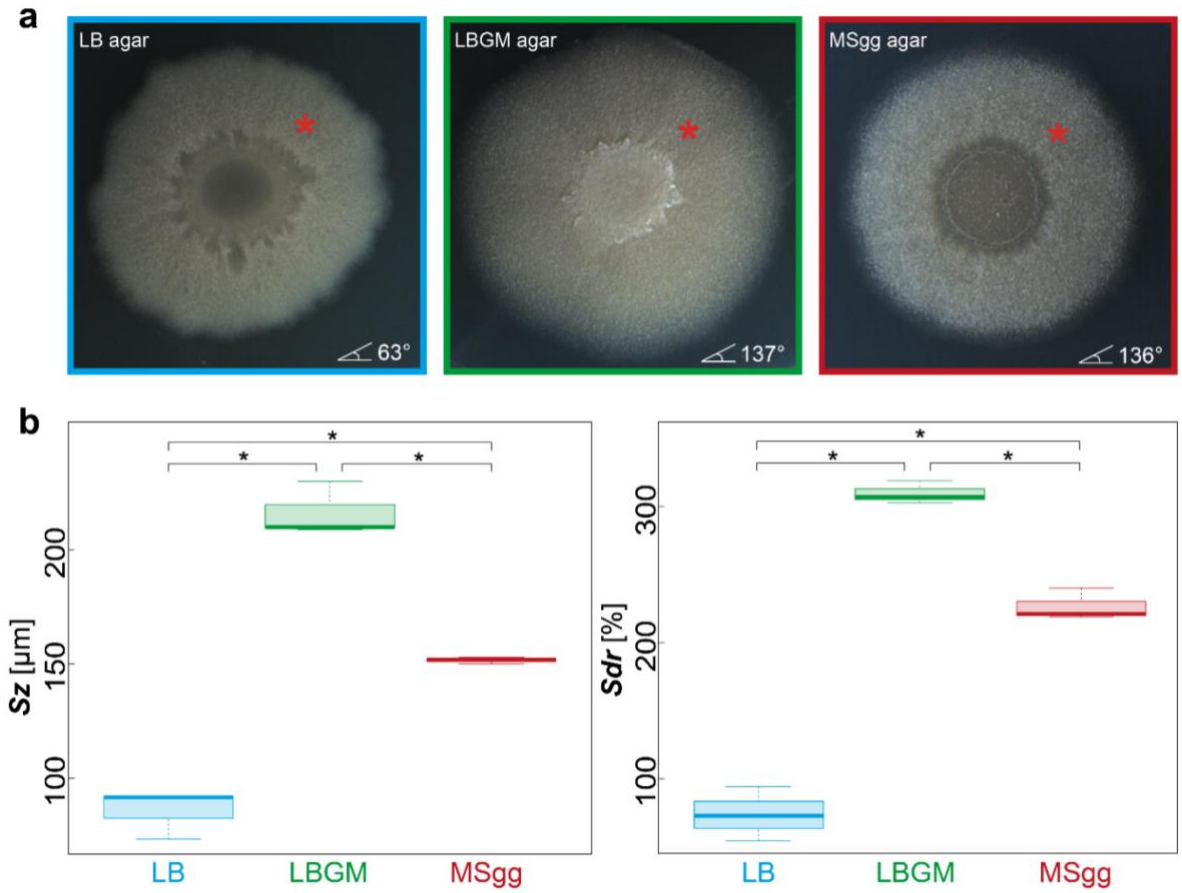

Figure 18 *Characterization of the peripheral regions of biofilm colonies formed by B. subtilis natto grown on three agar variants*. **a)** The region of the biofilm colonies where the wetting tests were performed are marked with a star. Values in the lower right corner represent the contact angle. **b)** Metrological parameters as calculated from the surface profiles of 3 individual samples (n = 3) obtained with light profilometry (section 2.3.1, Table 3). Boxes represent Q1-Q3, bold lines represent the median, and bars span from max. to min. Stars denote significant differences, where $p = 0.05$.

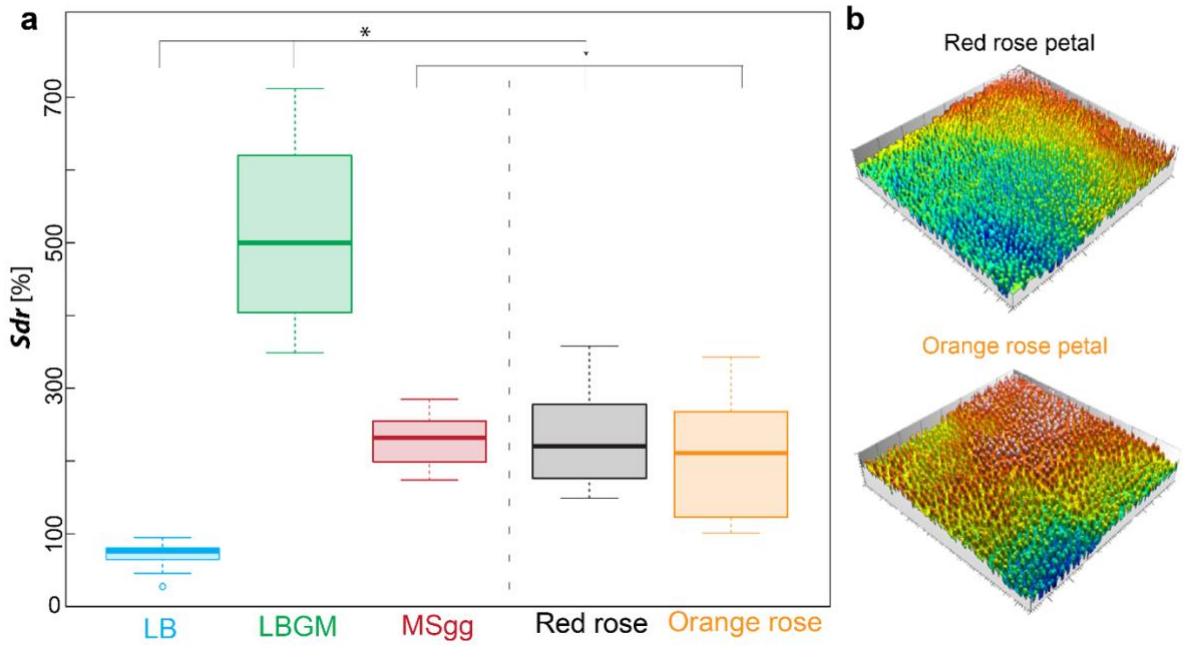

Figure 19 *Topographical characterization of rose petals as performed with light profilometry.* **a)** The ***Sdr*** values of the peripheries of NCIB 3610 biofilms (same as Fig. 16) are compared to those obtained from selected red and orange rose petal surfaces. Similar to MSgg biofilms, the petals of red and orange roses show hydrophobic properties with high droplet adhesion. For rose petal samples, the ***Sdr*** values were obtained from 14 individual surface profiles (n = 14) performed on a minimum of 4 rose petals. Boxes represent Q1-Q3, bold lines represent the median, and bars span from max. to min. Stars denote statistical significance, where p = 0.05. **b)** Surface topography of rose petals as obtained with light profilometry with 20x magnification. A soft correction method was applied when needed, i.e. to remove isolated outliers, outliers around the edges, and measurement noise. The removed outliers were replaced by a smooth shape calculated from the neighbors, resulting in a more accurate surface image.

3.1.3 Biochemical composition of the different variants of NCIB 3610 biofilms

Having demonstrated that the three NCIB 3610 biofilm variants indeed exhibit different physical wetting mechanisms, in a last step it was tested whether the observed differences in biofilm wetting and topography are accompanied by differences in the biofilm composition. This assumption is reasonable considering that a nutrient rich medium such as LB agar and a minimal growth medium such as MSgg agar are likely to give rise to different proteomic expression profiles of the bacteria. To test this, a mass spectrometry analysis was performed on the different biofilm variants and between the center and periphery of each biofilm variant (Fig. 20). For statistical evaluation of the biofilm composition, volcano plots were generated from data of three different experimental replicates, Fig. 20 illustrates the differences in protein expression. The y-axis represents the p-value and the x-axis lists the binary logarithm of the n-fold change in protein expression levels between the two regions or the two biofilm variants. The solid lines indicate a significance level of p = 0.05 and a minimum fold change of 2 ($s0$ = 1) which was used as a cut-off for significance. The grey dots below the cut off lines correspond to proteins expressed in both compared samples without significant differences. The red dots above the cut off lines represent proteins which are expressed at significantly higher or lower levels in each of the compared samples. Indeed, such analysis of extracellular proteins of the

peripheral regions of LB, LBGM and MSgg biofilms revealed significant differences in protein expression (Fig. 20a).

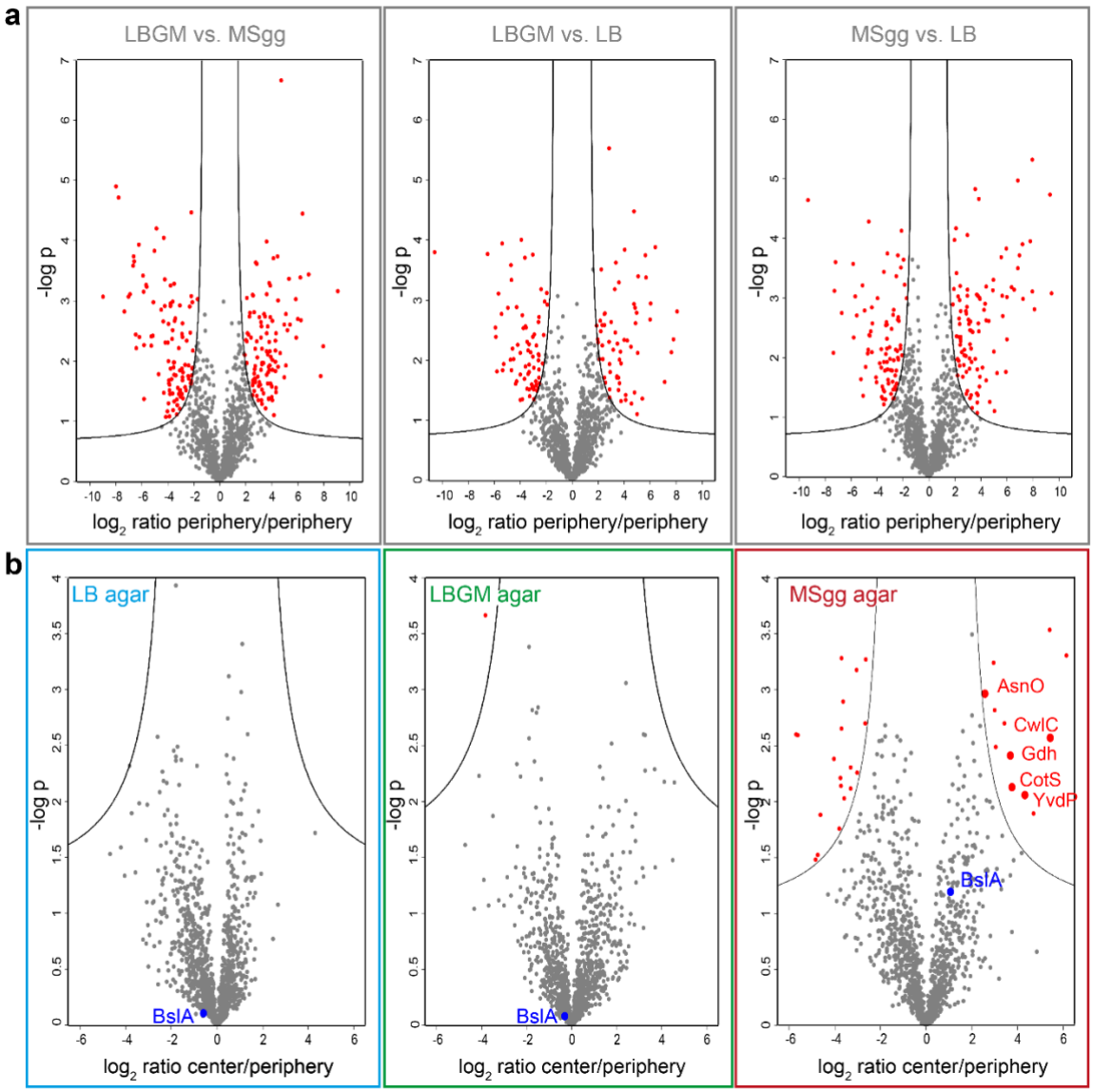

Figure 20 *Proteomics analysis of B. subtilis NCIB 3610 biofilms grown on three different media.* **a)** Comparison among the peripheries of biofilms grown on LB, LBGM, and MSgg agar. **b)** Comparison between center and periphery of biofilm samples grown on one agar variant at a time. See section For details on how the volcano plots were generated, see section 2.5.1.2.

Significant alterations in the expression level of proteins was also detected between the central and peripheral regions of MSgg biofilm colonies, but not when comparing the center and peripheries of LB or LBGM biofilm colonies, respectively (Fig. 20b). This finding is especially interesting as only the MSgg biofilm variant showed spatially heterogeneous wetting behavior. Moreover, among those proteins expressed at higher levels in the central region of these MSgg biofilms, mostly such proteins which are related to spore formation, are overrepresented (Table 4). When analyzing cells extracted from the center and peripheral regions of biofilms grown on MSgg agar with phase contrast microscopy, indeed, a large number of bacterial spores were

found in samples corresponding to the center, but not in the periphery (Fig. 21). The occurrence of spores is consistent with the limited amount of nutrients present in the MSgg agar.

Table 4 *Biological function of the overrepresented proteins involved in sporulation that were identified in Fig. 20b.*

Protein	Name	Function
AsnO	Asparagine synthase (glutamine-hydrolyzing) 3	Asparagine synthase involved in a subpathway that synthesizes L-asparagine from L-aspartate; expressed late in sporulation [141]; strains lacking AsnO fail to sporulate
BslA (YuaB)	biofilm surface layer protein A	Inhibitor of KinA autophosphorylation, required for complex colony architecture [142], one component that facilitates assembly of biofilm formation [136] and is proposed to contribute to their surface repellency [62, 66]
CotS	Spore coat protein S	Spore coat protein localized to the inner coat and/or on the outside of the cortex of the mature spore [143]
CotQ (YvdP)	Spore coat protein Q	Spore coat protein with oxidoreductase activity
CwlC	Sporulation-specific N-acetylmuramoyl-L-alanine amidase	Amidase that lyzes the mother cell wall at the end of sporulation by hydrolyzing the link between N-acetyl-muramoyl residues and L-amino acid residues in certain cell-wall glycopeptides [144, 145]
Gdh	Glucose 1-dehydrogenase	Oxidoreductase involved in sporulation; catalytic activity: D-glucose + NAD(P)+ = D-glucono-1,5-lactone + NAD(P)H

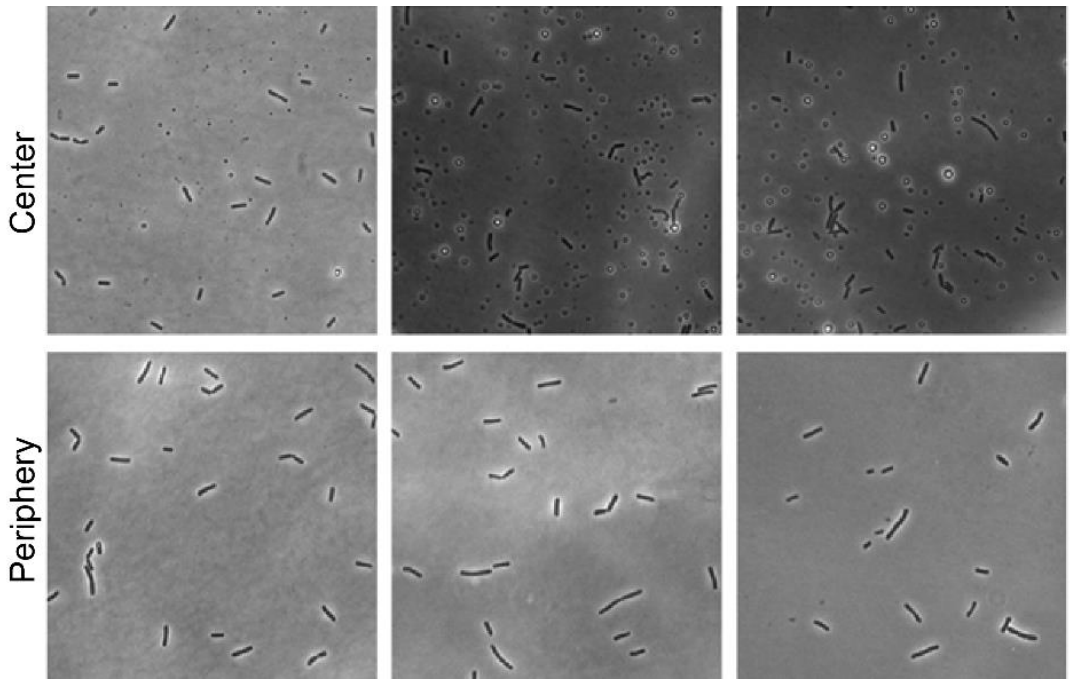

Figure 21*. Phase contrast microscopy of cells/spores extracted from the central and peripheral regions of B. subtilis NCIB 3610 biofilm colonies generated on MSgg agar.* Images were acquired with a 100x lens.

Interestingly, the surface layer protein BslA (= YuaB) which has been suggested to be the main factor contributing to the hydrophobic properties of *B. subtilis* NCIB 3610 biofilms [62, 89] is not detected at significantly different levels in either regions of the MSgg biofilm (Fig. 20b). When the wetting behavior of a biofilm colony generated by a *B. subtilis* mutant strain that is unable

to produce BslA [62] was analyzed, strongly hydrophilic colonies on all agar variants were observed (Fig. 22a). Consistently, all those colonies formed by the mutant strain show smooth surface topographies with ***Sdr*** values comparable to (or even lower than) those obtained for hydrophilic wild-type colonies (Fig. 22b). Moreover, in a previous study performed by Kobayashi *et al*. [62], it was reported that a *B. subtilis* mutant strain unable to produce the fiber forming protein TasA generates hydrophilic biofilm colonies, although BslA should be present in the matrix. Together, those findings underscore that the wetting behavior of *B. subtilis* biofilms is also strongly influenced by the topography of the biofilm and not only by the presence or absence of certain hydrophobic surface layers formed by proteins or other secreted biomolecules. Of course, a proteomics analysis does not test for other classes of biomolecules beyond polypeptides (such as lipids, DNA or metabolic byproducts), yet the presence or absence of such other biofilm macromolecules may also have an impact on the topography of the biofilm colony. Because of that, it is not trivial to disentangle the contribution of a specific biofilm matrix component on the chemical properties of a biofilm surface and its topography.

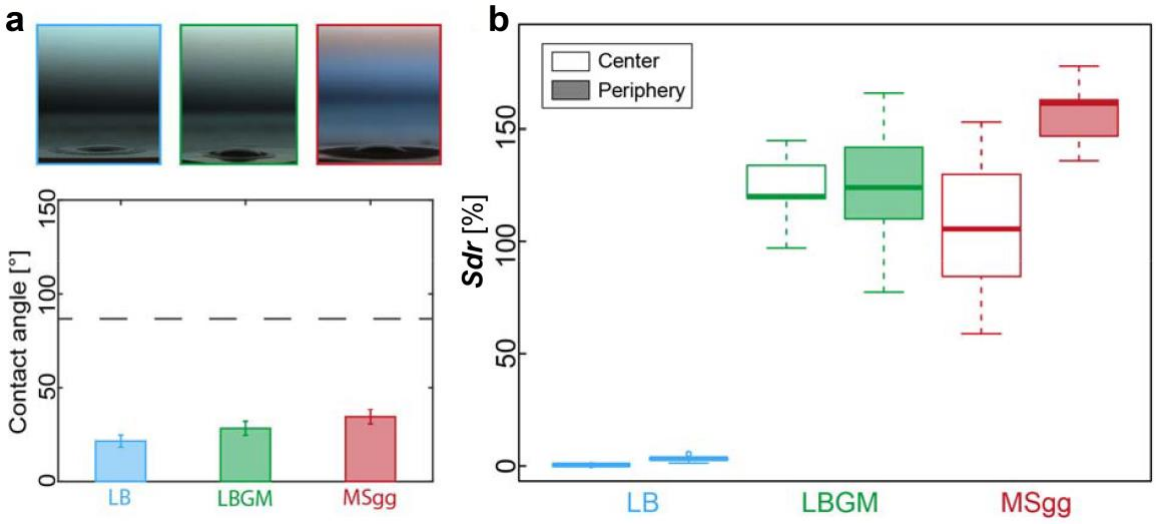

Figure 22 *Surface topography and wetting behavior of biofilms formed by a B. subtilis NCIB 3610 mutant strain unable to produce BslA.* **a)** Transversal images of a 10 µL water droplet on biofilms colonies generated by the strain N24 (Table 1) on the three agar variants: LB, LBGM, and MSgg. Dashed line in the contact angle diagram indicates hydrophobicity cut-off, below 90° = hydrophilic. Error bars denote the standard deviation as calculated from at least 5 individual samples ($n \geq 5$). **b)** Values of ***Sdr*** calculated from profilometry images acquired with 20x magnification ($n \geq 5$). Boxes represent Q1-Q3, bold lines represent the median, and bars span from max. to min.

3.1.4 [b]Effect of the individual matrix components on the final NCIB 3610 biofilm surface roughness

Inspired by the previous findings and given that several main matrix components of biofilms formed by *Bacillus subtilis* have already been determined [61, 62], the individual contributions of the main matrix components of NCIB 3610 biofilms on the final surface roughness were

[b] This section follows in part the publication: "*Matrix composition determines the dimensions of Bacillus subtilis NCIB 3610 biofilm colonies grown on LB agar*" published on 2017, in RSC Advances.

explored next. Using light profilometry (as described in section 2.3.1, Fig. 5) the development of biofilms formed by two wild-type strains (B-1 and NCIB 3610) which differ in their matrix composition, and three NCIB 3610 mutant strains lacking the ability to produce specific EPS components, was followed over time, and the changes in the surface roughness were measured. Here, biofilms were grown on standard LB agar for simplicity, and the widely used ***Sq*** parameter was selected to describe the changes in surface roughness over time.

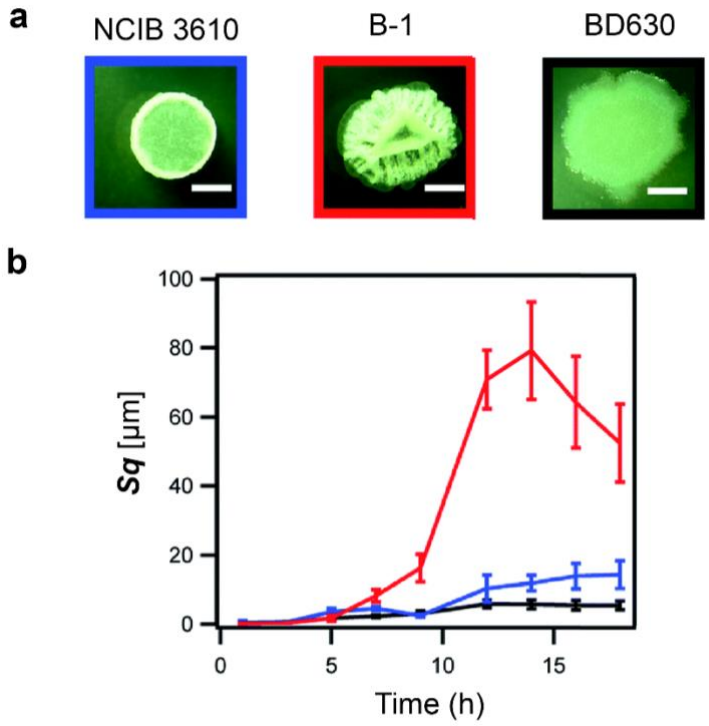

Figure 23 *Biofilm colony morphology and microscopic surface roughness values for the WT strains B. subtilis NCIB 3610 (blue) and B-1 (red) in comparison to the non-biofilm forming strain BD630 (black).* **a)** Images of biofilm colonies taken after 18 h of growth, the scale bar represents 2 mm. **b)** The ***Sq*** parameter (Table 3) denotes the increase in surface roughness over time. The error bars denote the 95% confidence intervals.

First, the two biofilm-forming *Bacillus subtilis* wild type strains (B-1 [69] and NCIB 3610 [115]) were analyzed (Table 1). Whereas the biofilm matrix of NCIB 3610 is described to be mainly composed of two proteins (BslA and TasA) and an exopolysaccharide [61-63]; the biofilm matrix of strain B-1 is described to be mainly composed of γ-polyglutamate [69]. Then, those results were compared to data obtained for a *B. subtilis* strain (BD630 [117], Table 1) that is unable to form a biofilm (Fig. 23a). Over a course of 17 h it was observed that B-1 biofilm colonies exhibit the strongest increase in surface roughness, followed by strain NCIB 3610 (Fig. 23b). In contrast, BD630 exhibits a smooth colony surface at all times (Fig. 23). The final surface roughness values at 17 h obtained for biofilm colonies formed by strains B-1 and NCIB 3610 agree with previous investigations [146] and correlate well with the rough biofilm colony morphology seen in microscopy images (Fig. 23a). Interestingly, strain B-1 exhibits a reduction in biofilm colony surface roughness at later time-points. It is believed, that the strong formation of wrinkles observed for strain B-1 (Fig. 23a) (a feature that is less pronounced for biofilm

colonies generated by strain NCIB 3610 and fully absent for colonies generated by strain BD630) leads to an increase in the experimental error for data obtained with the profilometer at time-points later than 12 h. After 12 h, the local area that is imaged with the profilometer to obtain the ***Sq*** values (section 2.3.1, Table 3) differs at each time-point. Hence, for biofilm colonies generated by strain B-1, the profilometric images might have been obtained either on top of a wrinkle or within a valley, which increased the error at later time-points.

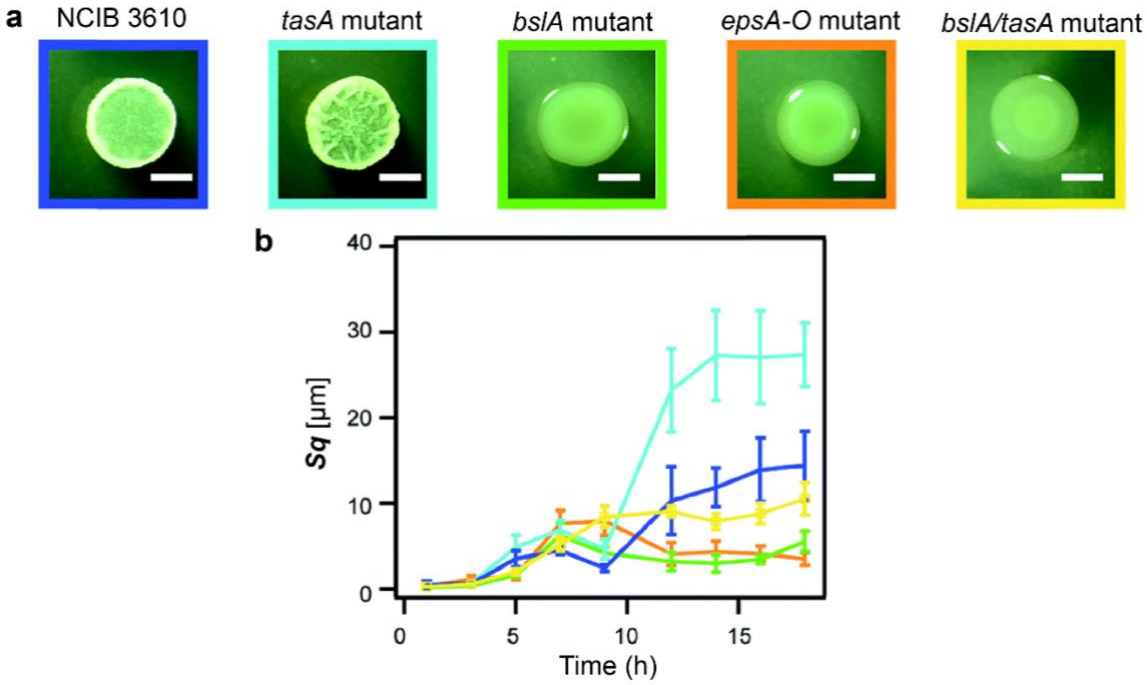

Figure 24 *Biofilm colony morphology and microscopic surface roughness values for the NCIB 3610 strain (blue) and its deletion mutants: tasA (turquoise), bslA (green), epsA-O (orange) and bslA/tasA (yellow).* **a)** Images of biofilm colonies after 18 h growth, the scale bar represents 2 mm. **b)** The ***Sq*** parameter (Table 3) denotes the increase of surface roughness over time. The error bars denote the 95% confidence intervals.

The differences found in surface roughness development for the three different WT strains indicate that the matrix produced by the biofilm forming strains (B-1 and NCIB 3610) could affect this growth parameter. Thus, analyzing biofilms formed by the NCIB 3610 strain, for which matrix components are known, could lead to an understanding of the individual contribution of the matrix biomolecules on the final biofilm surface roughness. The matrix of these biofilms is mainly composed of an exopolysaccharide produced by the gene products of the *epsA-O* operon [61] and an amyloid fiber-forming protein, TasA [63, 68]. A second biofilm matrix protein has been identified, BslA, which is a self-assembling hydrophobin primarily found on the surface of *B. subtilis* NCIB 3610 biofilms [62, 66]. To quantify the influence of those three matrix biomolecules on the final surface roughness, the temporal evolution of the ***Sq*** parameter was analyzed for three different mutants of strain NCIB 3610 lacking the ability to produce a particular matrix component (Table 1). The data obtained for biofilm colonies formed by these mutant strains was then compared to the roughness values obtained for the NCIB 3610 wild-type. The biofilm colonies formed by the mutant strain unable to produce the TasA protein are observed to have the roughest final biofilm surface, followed by the surface of NCIB 3610

wild-type biofilms. In contrast, biofilm colonies formed by the *epsA-O* mutant and the *bslA* mutant show smooth surfaces and very low ***Sq*** values (Fig. 24). The latter finding indicates that biofilm formation by these strains is heavily impaired and this observation also agrees with both, the colony morphology seen in microscopy images and previous findings for the *bslA* mutant strain (Fig. 24a and 22). This suggests that both the exopolysaccharide and the BslA protein are mainly responsible for the development of the roughness features in these biofilm surfaces.

As it has been shown that the expression of the polysaccharide is required in order for the BslA protein to localize to the biofilm matrix [62], it is challenging to disentangle their individual contribution to the final surface roughness. A mutant lacking expression of the polysaccharide could be (as a result) lacking the deposition of the hydrophobin protein into the matrix as well, so the effects observed so far for the *epsA-O* mutant could be affected by this. Therefore, a *bslA/tasA* double mutant strain was also tested, one that can express the exopolysaccharide *only* (Table 1). This way, the contribution of the polysaccharide itself was assessed on the final biofilm surface roughness. Indeed, the microscopy images reveal very smooth biofilm colonies for this strain, and the ***Sq*** values are lower than those measured for NCIB 3610 wild-type colonies (Fig. 24). This finding confirms that –although bslA has the greatest effect– it is a combination of both matrix components, the exopolysaccharide and BslA that determine the final biofilm surface roughness.

3.1.5 Why do bacteria form biofilms with different wetting properties?

In summary, with the metrological approach introduced here, a correlation between the topography of bacterial biofilms formed by *B. subtilis* NCIB 3610 with the wetting behavior of those bio-surfaces was established. The differences in surface topographies were observed not only for biofilms grown on different agar variants, but also within a given biofilm colony grown under limited nutrient conditions. In all cases where differences in the biofilm wetting behavior were found, those differences were accompanied both with significant topographical differences as well as alterations in the protein composition of the biofilm matrix. Furthermore, the final surface roughness developed by those biofilm colonies when grown on LB agar was shown to be a result of the contribution of two main matrix components: the exopolysaccharide and the BslA protein.

From a biological point of view, the existence of three different wetting regimes for *B. subtilis* biofilms is curious. Whereas a hydrophilic biofilm surface might not be ideal as prolonged contact with water will facilitate biofilm dissolution and erosion over time [147], it is less obvious why biofilms would exhibit two variants of hydrophobic behavior. At this point, it might be important to recall that an impregnated Cassie state (i.e., rose-like wetting) was observed for biofilms grown during limited nutrient supply (i.e., on MSgg agar). Here, in contrast to the lotus-like state, where air bubbles separate the biofilm surface and the water phase, the biofilm surface is partially in contact with water but still behaves hydrophobic. Probably, this particular wetting state could be helpful for two reasons: first, the impregnated hydrophobic surface may

help avoid biofilm erosion while maintaining a moist biofilm surface which, in turn, would prevent the biofilm from drying. At the same time, small water droplets on the biofilm surface could create a microenvironment which allows the biofilm bacteria to spread by swimming or flagellum-independent migration [59]; thus, enabling them to explore neighboring areas in search of additional nutrients [148]. When the nutrient supply becomes limiting, the presence of dead cells in the biofilm could be one possible factor contributing to the occurrence of a rough biofilm topography [149], which –as demonstrated here– alters the wetting behavior of the biofilm. It appears reasonable that the growth of biofilms both in nutrient-rich and nutrient-poor environments leads to the development of different wetting properties of biofilm colonies which are adapted to the particular environmental conditions.

A spatially heterogeneous wetting behavior as observed on MSgg grown biofilms has already been reported for certain plants [150, 151] and animals [152, 153], where it is thought to promote water collection. For instance, arid climate plants such as *Lupin regalis* possess leaves with hydrophobic tips, but –at the same time– a highly hydrophilic inner region [150]. This enables the plant to 'catch' water droplets from rain or dew on their leaves until they are big enough to roll into the center and then down to the stem and the roots. Such a natural water guidance mechanism based on surface polarity has inspired the design of artificial structures that manipulate water flux [154-156]. A similar mechanism may aid biofilms growing in limiting nutrient conditions (as they are also present in MSgg agar) to guide water towards the center of the colony –potentially to gather more nutrients from the surroundings, or to cause osmotic spreading [148] of the bacteria and thus reach a larger area of nutrient availability.

Although there is an increasing amount of work relating biofilm surface hydrophobicity to one specific matrix component: the BslA protein. It is clear that the intricate wetting mechanisms exhibited by biofilms are not a result of only one element. Here, it was shown that both BslA and the exopolysaccharide –the latter, not only by promoting localization of this protein to the biofilm matrix, but by its own contribution– are responsible for the final surface roughness of NCIB 3610 biofilm colonies grown on LB agar. This underlines the previous observations that it is not the contribution of one factor but a combination of surface roughness (provided by more than one matrix biomolecule) and surface chemistry that allow biofilms to form non-wetting surfaces. This complex protection allows biofilms to exist almost impervious to environmental stresses, and in such settings where they are undesirable, it represents a great problem. Together, the latter results clearly demonstrate the need to better understand why bacteria generate different biofilm topographies on different surfaces and how to exert control over this process.

3.2 [c]The link between surface topography and wetting is *not* strain-specific and also expands to other biofilm forms: i.e. *pellicles*

As reported in the previous section, a clear link exists between the wetting behavior of biofilms generated by *B. subtilis* NCIB 3610 and *B. subtilis natto*, and their microscopic surface topography. Furthermore, hydrophobic biofilms formed by these strains employ similar mechanisms as described for lotus-leaves and rose-petals to resist wetting [88, 157]. Such a correlation is of great significance not only to increase our understanding of biofilm protection mechanisms, but it might also represent a key element to fight biofilms when undesirable. Biofilms with liquid repellent surfaces possess increased protection towards antibiotic solutions [65] and erosion [158], hence, surfaces with hydrophilic properties would be desired. By developing strategies to target the surface topography of biofilms, one could indirectly affect their wetting resistance. However, for these strategies to be effective, the link between surface topography and wetting behavior should not be strain-specific and should be robust to different environmental conditions.

In this section, the previously proposed relation between the surface topography and the wetting behavior is challenged and extended to biofilm colonies formed by several bacterial strains in different environments. It is demonstrated that, regardless of the growth conditions and the origin of the bacteria, the surfaces of biofilm colonies and their entailing roughness features can still be subdivided in: hydrophilic -lowest complexity, hydrophobic rose-like -intermediate complexity, and hydrophobic lotus-like -highest complexity. Furthermore, the link stands even when biofilms formed at the liquid-air interface, i.e. *pellicles* (that show smoother surfaces) are analyzed.

3.2.1 Analysis of biofilm colonies created by other bacterial strains

To test if the relation between the microscopic surface roughness and the wetting behavior can be extended to other biofilm colony variants, i.e. as formed by other bacterial species, the surfaces of three *Bacillus* strains were compared to those generated by two other bacterial species. Surface characterization was performed using the same techniques as before: light profilometry and contact angle measurements. First, the relation between the surface topography and the wetting behavior was challenged for the *Bacillus* strains by changing the growth conditions at which the biofilms were cultivated. When *B. subtilis* NCIB 3610 and *natto* are cultivated at different humidity levels, for different growth times, and on different nutrient media, the formed biofilm colonies still exhibit the three distinct types of wetting behavior reported before: hydrophilic and two variants of hydrophobic: rose-like and lotus-like (Figs. 25 and 26). Also, for another biofilm-forming *Bacillus*, *B. subtilis* B-1, the biofilm surfaces could be subdivided into rose-like and lotus-like hydrophobic (Figs. 25 and 26). Second, two other bacterial species were introduced: *Pseudomonas putida* and *Bhurkolderia*

[c] This section follows in part the publication: "*Topographical alterations render bacterial biofilms susceptible to chemical and mechanical stress*" published on 2018, in Biomaterials Science.

thailandensis. Interestingly, such species are also able to form biofilms with water repellent surfaces that can be related to those formed by rose petals and lotus leaves, even when cultivated at various growth conditions (Figs. 25 and 27). This demonstrates that the occurrence of lotus-like and rose-like hydrophobicity is not limited to *Bacillus subtilis* biofilms but is a more generic feature.

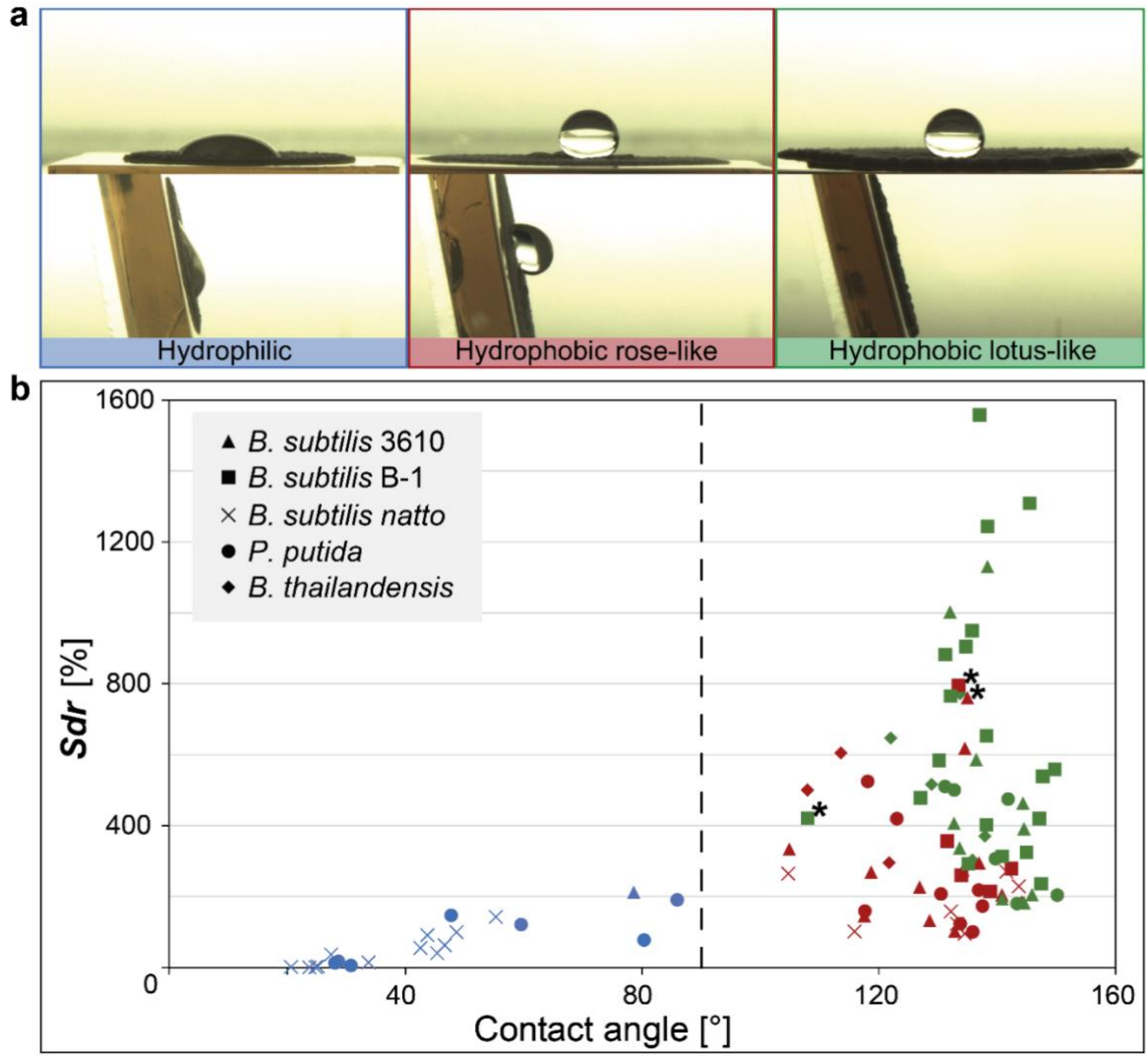

Figure 25 *Relationship between the wetting behavior and the surface topography for different biofilm variants.* **a)** Images of a droplet of *dd*H_2O on different biofilm surfaces before (upper row) and after tilt (lower row) illustrating the different wetting behaviors found in **b**. **b)** Data points represent the average of three replicates from a specific growth condition (Fig. 26 and 27). The vertical line separates hydrophilic (blue) from hydrophobic samples (green, red). Green symbols denote lotus-like hydrophobic biofilms, whereas red symbols represent rose petal-like. Samples marked with a star might be a result of technical measurement errors (Fig. 28)

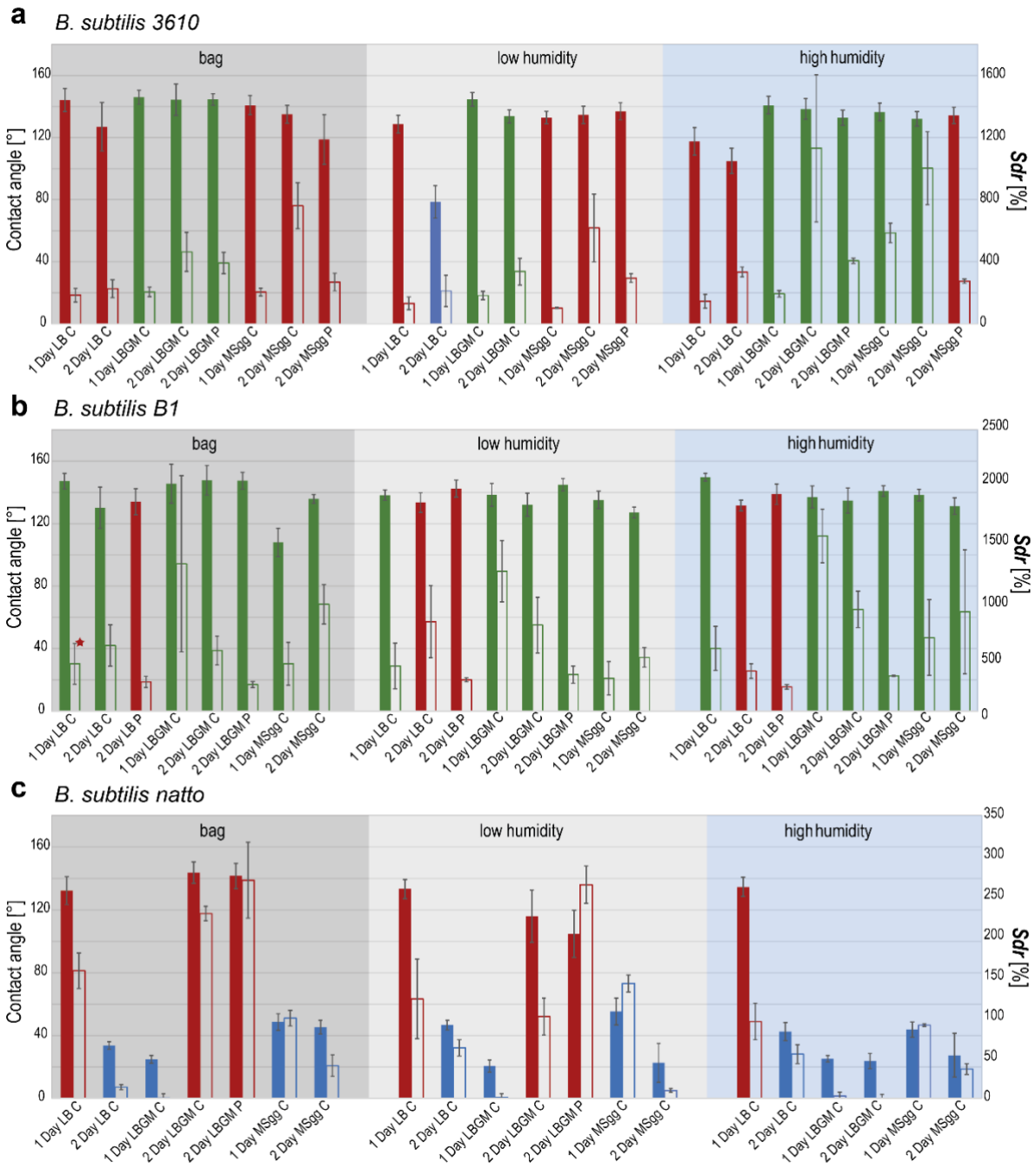

Figure 26 *Contact angle and* ***Sdr*** *values obtained for biofilm colonies generated by different Bacillus subtilis strains*. Data is shown for the *B. subtilis* strains NCIB 3610 **(a)**, B-1 **(b)** and *natto* **(c)** and represents the individual data that is summarized in the phase diagram of Fig. 25. Error bars denote the standard deviation as obtained from at least three different biofilm colonies ($n \geq 3$, $N \geq 1$). Filled bars correspond to CA, open bars to ***Sdr*** values. Bars colored in blue indicate hydrophilic behavior, whereas green and red bars indicate the two variants of hydrophobic behavior, i.e. lotus-like (green) and rose-like (red). The colonies were either grown on LB, LBGM or MSgg agar (Table 2) at different humidity and growth times (i.e., 1 or 2 days) (section 2.2.1.2). If the area was large enough, measurements were performed at both, the center (C) and the periphery (P) of the biofilm colony. The sample marked with a red star (B. subtilis B-1 grown in a bag) was difficult to classify as some replicates showed lotus-like and some showed rose-like hydrophobicity. Thus, two symbols (one marked in red and one marked in green) are present in the phase diagram of Fig. 25 to represent this particular set of growth conditions.

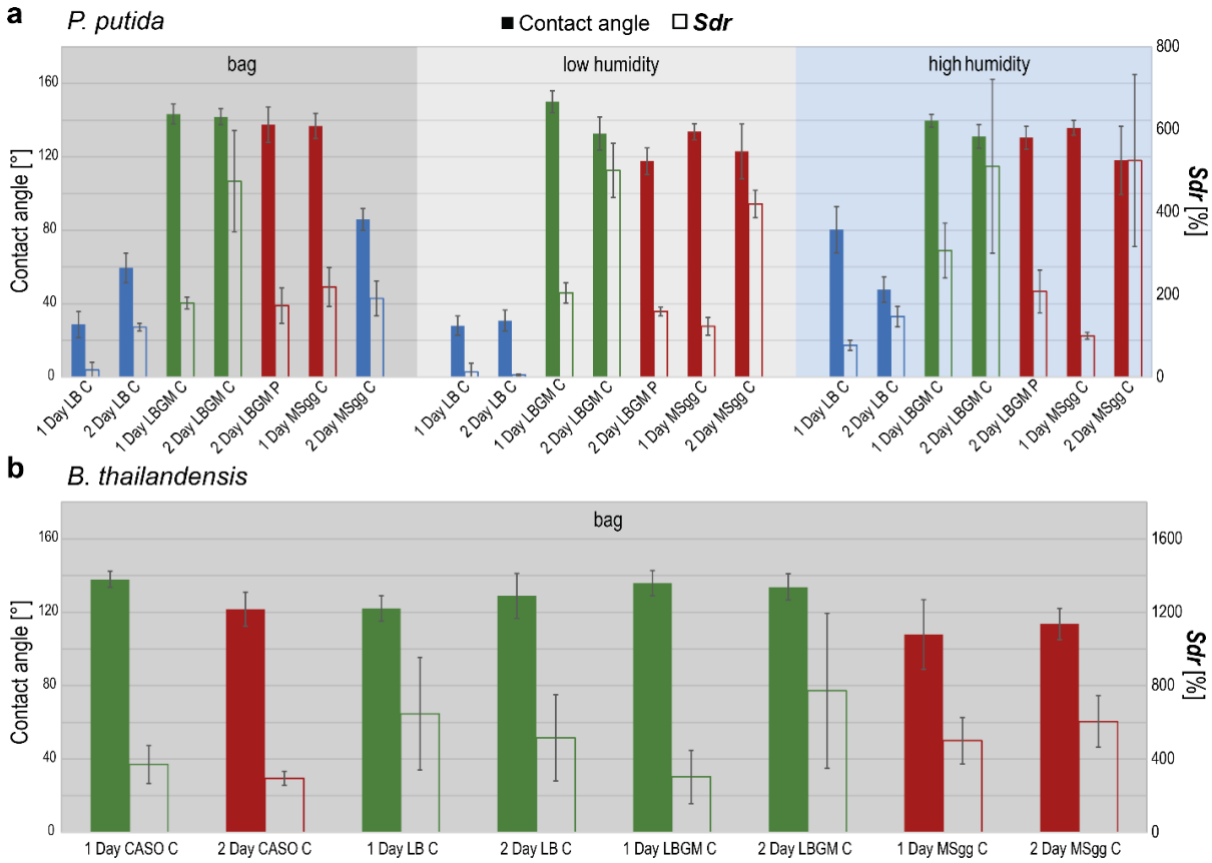

Figure 27 *Contact angle and* ***Sdr*** *values for biofilm colonies generated by Pseudomonas putida and Burkholderia thailandensis bacteria.* The data shown for *P. putida* **(a)** and *B. thailandensis* **(b)** represents the individual data that is summarized in the phase diagram shown in Fig. 25. Error bars denote the standard deviation as obtained from at least three different biofilm colonies ($n \geq 3$, $N \geq 1$). Filled bars correspond to CA, open bars to ***Sdr*** values. Bars colored in blue indicate hydrophilic colony behavior whereas green and red bars indicate the two variants of hydrophobic behavior, i.e. lotus-like (green) and rose-like (red). The colonies were either grown on LB, CASO, LBGM, or MSgg agar (Table 2) at different humidity and growth times (i.e., 1 or 2 days) (section 2.2.1.2). If the colony size was large enough, measurements were performed at both, the center (C) and the periphery (P) of the biofilm colony.

Next, the microscopic surface features of biofilms formed by *B. sutbilis* NCIB 3610, B-1, and *natto*, as well as the species *P. putida* and *B. thailandensis*, were characterized by the ***Sdr*** metrological parameter (Table 3). As reported in section 3.1.2, this parameter is more efficient –compared to ***Sq*** or other exclusively height parameters, in describing surfaces with complex features; it can successfully differentiate between biofilm topographies with hydrophilic (***Sdr*** < 100%), rose-like (***Sdr*** ~ 200%) and lotus-like (***Sdr*** > 400%) wetting properties [88]. Actually, this relation appears to be more generic as, here as well, three distinct populations can be observed in the contact angle/***Sdr*** phase diagram depicted in Fig. 25. For almost all biofilm variants investigated here, a similar relation between their wettability (as quantified by the contact angle) and their surface topography was found: the lowest ***Sdr*** values occur for hydrophilic biofilm colonies and the highest ***Sdr*** values for biofilms with lotus-like wetting resistance.

As can be observed in Figures 25 and 26, some data points are marked with stars. Of course, when performing such a comprehensive characterization of a biomaterial, problems arise from

different possible measurement error sources. Indeed, two typical error sources occur while characterizing the biofilm surfaces of the five different bacterial strains cultivated at the various growth conditions used here. One is related to the contact angle measurements and the second to the topographical characterization with light profilometry, and those errors sources expand to the four marked biofilm colonies. For the first sample, relatively low CA values (in the range of 110°) were measured even though the biofilms show lotus-like behavior. In panel **(a)** of Fig. 28, a lateral image of such a *B. subtilis* B-1 biofilm sample is shown; here, a pronounced rim around the colony is present. Such a rim makes the interface between the water droplet and the biofilm surface difficult to visualize and leads to an underestimation of CA. To avoid this artefact, typically the outer layer of the biofilm colony is removed with a scalpel before measuring the CA (as shown in panel **(b)** of Fig. 28 for a different sample) but in the particular case shown in panel **(a)**, the colony size was too small to do this. Nevertheless, the surface texture of the sample clearly shows roughness features on several length scales as depicted in panel **(c)**; and this is consistent with both the high ***Sdr*** value measured in this sample, as well as with the observed lotus-like wetting resistance (Fig. 28). The other three samples represent biofilms with rose-like hydrophobicity but unusually high ***Sdr*** values. Panel **(d)** of Fig. 28 shows a *B. subtilis* B-1 biofilm surface with a complex topography. However, the right quadrant of this picture suffers from a considerable amount of noise. Such noise sensitively affects the ***Sdr*** value calculated from this region even though the local topography in this area is relatively smooth; hence, the high ***Sdr*** value calculated for this particular sample is artificially high. Panels **(e)** and **(f)**, show two examples of *B. subtilis* 3610 biofilm surfaces where unusually high ***Sdr*** values were also calculated even though the biofilms show rose-like hydrophobicity (Fig. 28). For both samples, mesoscopic worm-like structures can be observed on the surface (which is characteristic for *B. subtilis* 3610 biofilms grown on MSgg agar [115]). Here, the large variations between the *z*-coordinates, i.e. between the top of the wormy hills and the pits of the valleys separating the wormy structures, lead to large ***Sdr*** values. It is unclear, whether or not this mesoscopic contribution to the ***Sdr*** value is physically meaningful. It was shown that, for artificial surfaces with multi-scale roughness features, a larger separation distance between the roughness features allows for adhesion of water droplets and thus entails rose-like hydrophobicity [3], which would be consistent with the observations reported here.

Although the phase diagram graphically depicting the relation between surface topography and wetting behavior shows some overlap in the hydrophobic quadrant, it is still very clear that three clusters are formed (Fig. 25). The technical errors discussed before, which are introduced by the characterization techniques, the examiner, or the biological variations in the samples, could be responsible for the overlap of data in the hydrophobic clusters. However, this extended analysis indicates that the biofilm surface topography is linked to the biofilm wetting behavior, and that this relation is relatively independent from the detailed growth conditions used to cultivate those biofilms, i.e. on semi-solid substrates exposed to air.

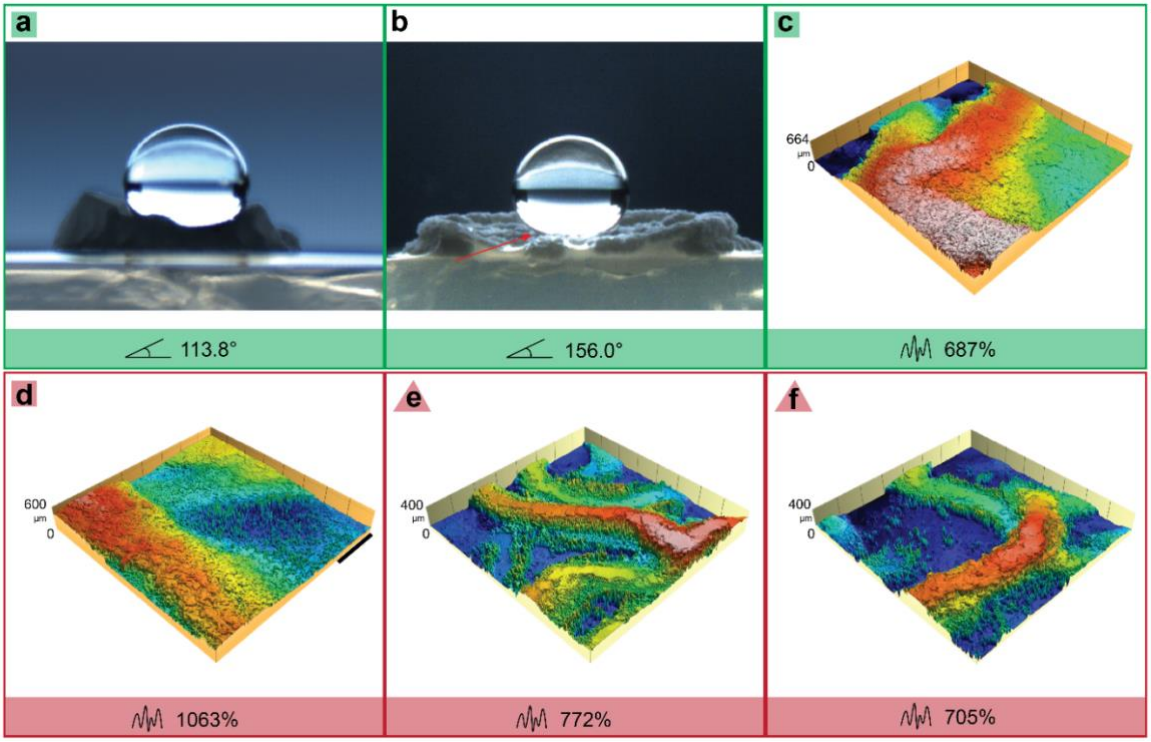

Figure 28 *Discussion of selected samples from the phase diagram shown in Figure 25.* The three points marked with an asterisk in Fig. 25 correspond to four different samples. The lateral scale bar in **(d)** represents 200 µm and applies to the x- and y-axes of all profilometric images shown in this figure. Values below images in **a-b** denote CA, and those in **c-f** denote ***Sdr***.

3.2.2 Analysis of biofilm pellicles

Since the correlation between surface topography and wetting behavior showed to be robust for several biofilm colony variants and for different environmental conditions. Next, a different type of bacterial biofilm was assessed. Biofilms that are not attached to solid surfaces, but instead form at the liquid-air interface, are called *pellicles*. Here, wild type *B. subtilis* NCIB 3610 and three derivative strains are used for pellicle formation (see Appendix 1: List of strains for details): *e+t*, a strain product of complementation between a strain unable to produce the exopolysaccharide and another strain unable to produce TasA; *e4A+t4B*, an evolved strain of the *e+t* variant; and *wt6C*, an evolved strain of the wild-type [77]. By testing strains with such different matrix compositions, the relation between surface topography and wetting behavior was further challenged. Once it was established that the different strains are able to form pellicles when cultivated in static liquid nutrient (Appendix 1: Methods for pellicle formation), their surfaces were analyzed using light profilometry and wetting tests (in the same way as done for biofilm colonies).

The first observation is that, even on liquid, *B. subtilis* bacteria are able to form hydrophobic surfaces, but also, that the topographical features of biofilm pellicles are less pronounced than the ones observed on biofilm colonies at the same magnification (Fig. 29a-b). The reason for such topographical differences could be that the analyzed biofilm pellicles have very different sizes compared to colonies: whereas the reported biofilm colonies have a diameter of ~1-2 cm,

the pellicle samples described here have a lager diameter confined only by the space they grow on (six well-plates, where each well is ~3.5 cm). Visualization of surface features on these larger samples could be limited by the small measurement area provided by a magnification originally selected for analyzing the smaller biofilm colonies. To tackle this possible problem, a wider measurement area was selected, to obtain a more extensive visualization of the surface roughness features of these biomaterials. For this, a stitching method was used with the light profilometer to obtain images with an area of 2.4x2.3 mm that corresponds to 3x3 images at a 20x magnification (section 2.3.1.2, Fig. 29a).

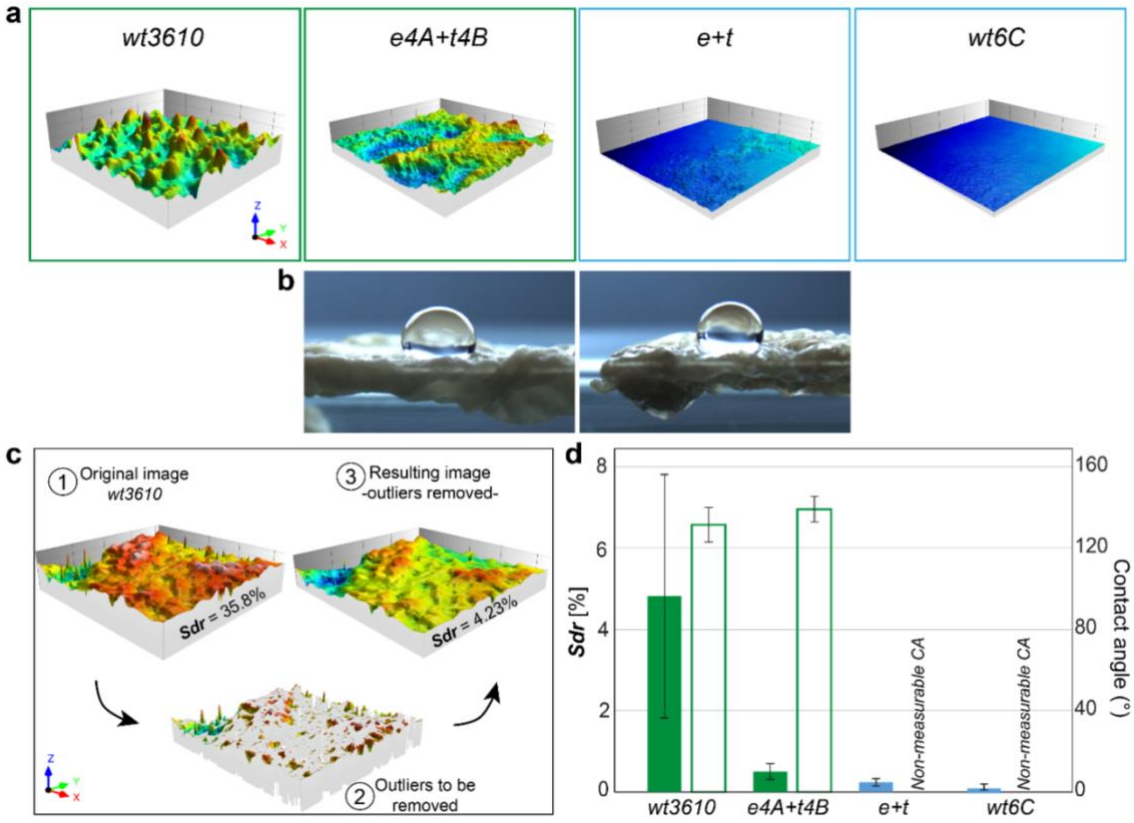

Figure 29 *Analysis of surface topography and wetting properties of biofilm pellicles.* **a)** Profilometric images acquired with a 20x objective using the stitching method and resulting in 3x3 images, where the x-axis represents 2.4 mm and the y-axis 2.3 mm. The absolute height of the images is 84 µm for the wt3610 sample, whereas half of that value represents the z-axis of the rest of the samples. **b)** Transversal images of a 10 µL droplet of *dd*H_2O on the surface of pellicles formed by *wt3610* (left) and *e4A+t4B* strains when grown on LBGM liquid medium. **c)** Operator for removing outliers is applied on a stitched 3x3 image of wt3610 (1) where unusual peaks are removed (2) resulting in an interpolated smoother and more realistic surface image (3) (section 2.3.1.2). **d)** Values of ***Sdr*** (closed bars –left) and contact angles (open bars –right) for pellicle biofilms. ***Sdr*** is obtained from single profilometric images. Contact angles of the strains *e+t* and *wt6C* are not included as the material's surface is porous and both droplet images and numeric values could not be obtained. The error bars denote the standard deviation as obtained from at least 7 individual measurements ($n \geq 6$).

Although a larger visualization of the pellicle surface was obtained with the stitching method, other challenges emerged here during characterization as a large amount of technical errors are produced when such method is used on biofilm pellicles. Essentially, while the profilometer stage (with the sample on top during this *in-situ* measurement) moves in the *x*- and *y*-direction during stitching, the liquid medium below the pellicle moves with it, and that body of liquid provokes movement of the sample surface (Fig. 29c). These movements affect the

measurement as the information of the surface (in the form of reflected light) is continuously changing. The resulting measurement errors, in the form of peaks or holes that protrude/pierce the visible surface, are not observed when the same method is used on biofilm colonies grown on agar (Section 4.1). Interestingly, after processing those images that contain errors by removing outliers (section 2.3.1.2, Fig. 29c), those 3x3 images return similar ***Sdr*** values as single images of the same samples (with an area of 800x772 µm) taken with the same magnification (Fig. 29c-d). This finding shows, that the ***Sdr*** parameter is reliable in describing the complexity of the microscopic surface, regardless of the final sample size or the macroscopic features outside of the scope of the measurement area. As in some cases the stitched images exhibit outliers that are too large to be corrected by the same processing method, the values reported hereafter correspond to single images.

In confirmation of the initial observations, the ***Sdr*** values measured for biofilm pellicles differ greatly from the ones reported previously for biofilm colonies (Figs. 25b and 29d). Whereas a range between 100-400% in the ***Sdr*** values was observed for biofilm colonies, a range between 0-8% is observed for the pellicles examined here (Fig. 29d). However, contact angle measurements reveal that, also for pellicles, a hydrophobic lotus-like behavior can be observed for the WT strain and the evolved complemented strain *e4A+t4B;* whereas the strains *e+t* and *wt6C* exhibit porous surfaces and their contact angles could not be measured (Fig. 29). The former finding agrees with previous observations that when *B. subtilis* NCIB 3610 is cultivated on LBGM agar (Table 2), hydrophobic lotus-like biofilms are formed (sections 3.1.1 and 3.2.1). Furthermore, the relation between surface topography and wetting behavior is further strengthened by these results, as also for pellicles, the hydrophobic samples are the ones showing the highest ***Sdr*** values and rougher surface features (Fig. 29a and c) –when compared to hydrophilic/porous samples, yet, at overall lower roughness values. Although the ***Sdr*** parameter is not able to sensitively distinguish between the surfaces formed by the strains *e4A+t4B* and *e+t,* which exhibit different wetting behavior, it is clear from the surface topography images (Fig. 29a) that the hydrophobic samples exhibit a more complex surface than the hydrophilic ones.

The reason why bacteria grown on liquid substrates form larger biofilms, and in turn, smoother surfaces, could be that, in liquid bacteria can swim in search for nutrients and is only confined by the size of the container. Whereas for biofilm colonies –those formed on solid substrates, most bacteria become immotile after attachment to the substrate and expands by stacking-up and creating ripples, thus creating rougher surfaces. The finding that bacteria can produce pellicles with hydrophobic surfaces is surprising as the environment, where they develop, is saturated with liquid. Permeability to liquids (i.e. the medium they grow on) is expected to provide them with the necessary nutrients to grow. However, for the case of the WT and *e4A+t4B* pellicles that show hydrophobic lotus-like wetting behavior, such permeability is probably only present, and necessary, at the liquid-solid (pellicle) interface for nutrient supply. The porosity found in pellicles formed by the strains *e+t* and *wt6C* could be due to a combination of their extremely smooth surfaces (***Sdr*** values close to zero) and an altered matrix composition, as the former strain is a combination of two deficient bacteria types and the latter a product of evolution. Although the adaptive and evolutionary reasons for bacteria to produce

pellicle surfaces with different properties are beyond the scope of this section. It seems that, regardless of the type of substrates (agar or liquid medium), when sufficient nutrients are available, bacteria can produce biofilms with hydrophobic surfaces and an increased protection from environmental stressors.

3.2.3 Summary of section 3.2 and implications for biofilm control

It has been shown that biofilm formation on agar substrates is greatly affected by environmental conditions such as nutrient availability, temperature, incubation times, and humidity [67, 88]. Here, nine different bacterial strains were cultivated at different environmental settings that directly affect their morphological features. In all cases, a link between the biofilm surface topography and the wetting behavior as proposed in the previous section could be confirmed. Light profilometry and wetting experiments allowed to create a phase diagram depicting the resulting surface complexity *vs*. the corresponding contact angle values measured for all those bio-surfaces. In such a representation, three clusters of data can be distinguished, and each cluster represents a biofilm type: hydrophilic – low surface complexity; hydrophobic rose-like – intermediate complexity; and hydrophobic lotus-like – highest complexity. This finding was obtained regardless of the bacterial origin, or the growth conditions at which these biofilm colonies were generated (when grown on agar substrates). Although at lower scales, a brief characterization of biofilm pellicles (biofilms formed on liquid) resulted in a similar trend as well: the highest surface complexity corresponded to hydrophobic samples, whereas the smoothest surfaces exhibited hydrophilic or porous behavior. Due to the strong differences in the absolute ***Sdr*** values obtained for pellicles compared to biofilm colonies, these results could not be included in the aforementioned phase diagram. However, it is clear that the analogy presented before is not limited to biofilm colonies formed by *B. subtilis* NCIB 3610 bacteria, but extends to bio-surfaces generated in extremely different environments and by several different bacterial strains.

Of course, when dealing with biofilms growing in pipes or on catheters, their hydrophobic surface properties constitute a serious issue: only when an aqueous solution containing anti-bacterial agents is in contact with the biofilm surface, the bactericidal molecules will have a chance to enter the biofilm. Therefore, finding a method to convert the wetting resistance of biofilms from lotus-like to rose petal-like, or even hydrophilic, could be an important stepping stone in fighting those biofilms. Together with the development of dedicated anti-fouling surfaces which prevent bacterial adhesion and therefore the initiation of biofilm formation [159-161], improving the accessibility of biofilm surfaces to liquids is an important goal. Success in this particular area will also allow for more efficient weakening of the mechanical properties of biofilms, e.g., by targeting the bacterial adhesion machinery [162, 163] thus facilitating biofilm removal. Now, that the analogy between surface topography and wetting behavior has been validated, its potential use for biofilm control can be explored. Although several challenges will arise by the fact that biofilms are highly hydrated materials, developing a physical approach that targets the material's surface roughness could be a step in that direction. Such strategies are presented in chapter 4.

3.3 [d]Surface topography and wetting can be used to trace evolutionary processes in bacterial biofilms

So far, it was made clear that bacterial biofilms possess intricate mechanisms that protect them from environmental stresses. However, biofilms can be viewed from different angles: whereas the focus has been on their protection from the exterior, now it is shifted to evolutionary processes happening within the biomaterial. For this, the same techniques used before for characterizing surface hydrophobicity are borrowed from materials science and transferred to the study of experimental evolution in microbes; specifically, the process of diversification. Evolutionary diversification is a very common process in bacterial biofilms as they offer structured environments with alternative niches varying in nutrient and oxygen content. The distinct variants are often called morphotypes as they are identified based on distinct colony morphologies. Hence, the aim here is to use light profilometry and wetting experiments, to assess whether the products of diversification of *B. subtilis* NCIB 3610 can be clearly distinguished based on their physical properties. For this, four morphotypes obtained from evolutionary diversification in pellicle biofilms are isolated and grown on agar substrates to form biofilm colonies. It is demonstrated that the surfaces of the morphotypes can be quantitatively differentiated using metrological parameters, and that their surface complexity can be –in most cases– related to levels in expression of matrix components and different wetting behaviors. The quantitative analysis introduced here, is a powerful tool for supporting the observations obtained with traditional methods in the area of microbial ecology where physical characterization techniques are not commonly used tools.

3.3.1 Diversification in *Bacillus subtilis* biofilms

First, to examine whether evolutionary diversification can be observed in *B. subtilis* NCBI 3610 pellicle biofilms, six populations were allowed to evolve in parallel for over ca. 200 generations (Appendix 2: Methods). Pellicles were visually accessed after each subsequent transfer, and their productivities (total cell number/mL) were assessed every 5th transfer. All pellicles appeared robust throughout the experiment preserving a thick and wrinkly structure similar to the ancestral strain. In all six populations, four distinct colony types –morphotypes– were detected in the CFU assay. A representative example from each morphotype was isolated from population 1 and stored as a pure culture stock for further studies. To better assess differences between the morphotypes, a colony spotting assay was performed (Appendix 2: Methods) on two alternative media types: minimal biofilm-promoting MSgg medium [115] (Fig. 30), and LB medium (Fig. 31). Inspired by the striking differences in the appearance of the morphotypes on LB medium, the following names are introduced: Wrinkly—displaying an increased complexity in the colony center; Rough—similar to the ancestor; Spreader—showing dramatically increased colony expansion and Smooth—exhibiting a very flat surface similar to

[d] This section follows in part the publication: "*Evolution of exploitative interactions during diversification in Bacillus subtilis biofilms*" published on 2018, in FEMS Microbiology Ecology.

certain biofilm mutants [68] (Fig. 31a). Hence, the morphotypes are referred to by those names hereafter.

3.3.2 Quantification of physical differences among the products of diversification

Next, light profilometry was performed on all morphotypes and the ancestor, both on LB and MSgg medium, to examine their microscopic surface profiles and quantitatively describe differences between the diversification products (Figs. 30 and 31, a-b). Although the results were affected by the media type, certain pronounced differences between the morphotypes were media independent. The Smooth variant shows a lack of surface complexity on both media types that is reflected by an ***Sdr*** value close to zero. On MSgg medium, the Ancestor and Wrinkly morphotypes show the highest surface complexity that is about 4-fold higher as compared to the colonies of the Rough and Spreader variants (Fig. 30a-b). On LB medium, all morphotypes depict lower surface complexity as compared to the ancestor, with higher ***Sdr*** values for the Wrinkly and Rough derivatives (Fig. 31b).

Interestingly, all the biofilm colonies (except for the smooth morphotype) exhibit different surface features at the center and periphery, and it was reported that those differences can result in heterogeneous surface properties [88] (section 3.1.2). Thus, the surface profiles of expanding colony edges were also analyzed. It was observed that, when cultivated on MSgg medium, only the Spreader variant exhibits lower surface complexity at the edge of the colony when compared to the ancestor. In contrast, on LB, all strains show lower ***Sdr*** values at the edge of the colony when compared to the ancestor (Fig. 32).

After the metrological characterization, wetting studies were performed on all four morphotypes and the results were compared to those obtained for the ancestor strain. These tests revealed that the Smooth variant lacks the typical biofilm hydrophobicity and behaves completely hydrophilic on both, MSgg and LB media (Figs. 30 and 31, a and c). The latter is not surprising as those surfaces show the lowest ***Sdr*** values on both media. When grown on Msgg medium, the Wrinkly morphotype shows a non-wetting behavior similar to the ancestor, but not on LB –where its surface complexity is lower (Figs. 30 and 31). Both, the Ancestor and Wrinkly strains, when grown on MSgg, exhibit rose-like hydrophobic behavior and ***Sdr*** values of ~200%, which is typical for biofilms formed by NCIB 3610 on MSgg agar [88]. The Rough and Spreader variants show hydrophilic properties in both media consistent with their lower surface complexities when compared to the ancestor strain. Interestingly, when grown on LB, the expanding edge of the spreader variant shows hydrophobic rose-like properties (Fig. 31a and c); however, this is again not surprising as the ***Sdr*** values in the periphery of those samples is also in the range of 200% (Fig. 32b) [88]. Except for the Spreader morphotype, it was not possible to assess the wetting behavior for the rest of the biofilm colonies at their peripheries due to their smaller colony size. However, it is expected that all sections of the biofilm colonies would behave correspondingly to their surface complexity: roughest surfaces – hydrophobic, smoothest surfaces –hydrophilic.

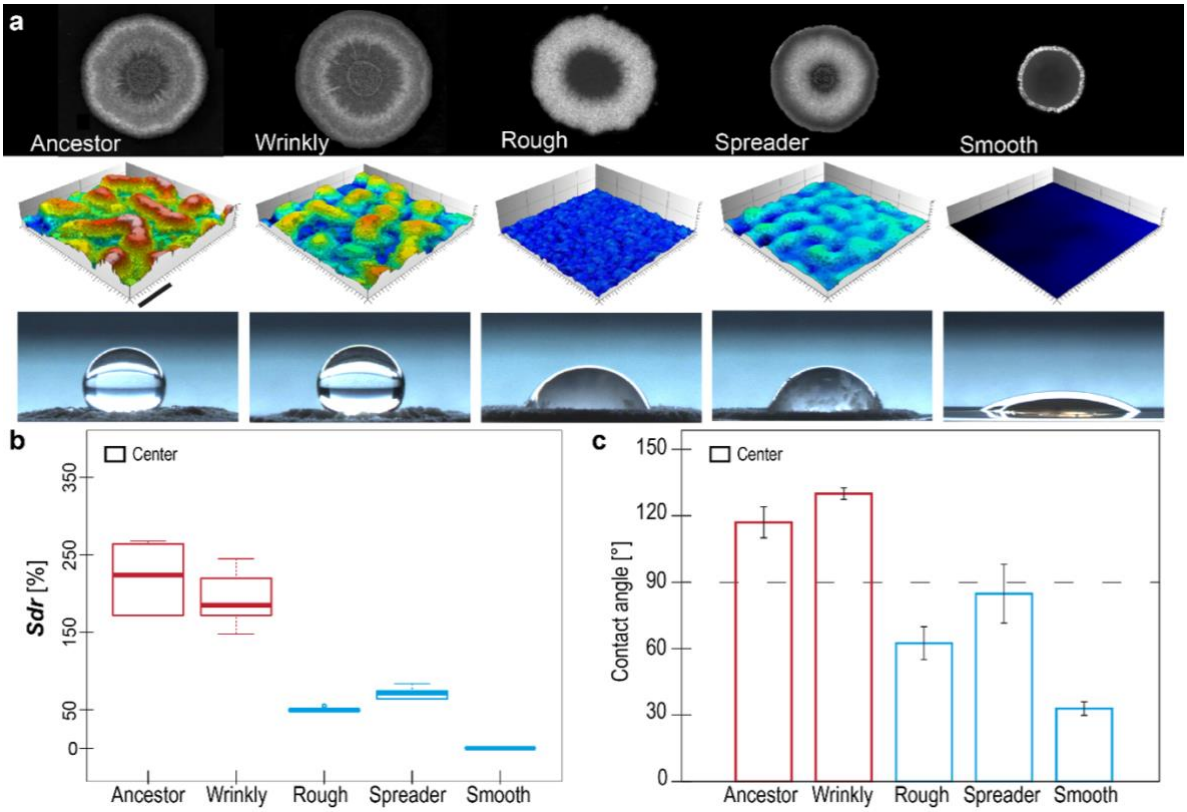

Figure 30 *Morphotype morphology and quantitative characterization of their colony features displayed on MSgg agar*. **a)** Top: colony morphologies of the ancestor and four distinct morphotypes. Middle: surface topographies of the colony center of the ancestor and evolved morphotypes as acquired with light profilometry. The color scale depicts heights, where dark blue represents the lowest and white represents the highest features. Colonies were grown for 48 h at 30 °C. Scale bar in black represents 200 µm. Bottom: transversal image of a 10 µL droplet of *dd*H_2O on the center of each biofilm colony. **b)** Values of ***Sdr*** calculated for the center of at least 5 individual colonies ($n \geq 5$). Boxes represent Q1-Q3, bold lines represent the median, and bars span from max. to min. **c)** Contact angle values calculated at the colony center. Error bars denote the standard deviation as calculated from 3 individual samples ($n = 3$). The dashed line represents the contractual hydrophobicity cutoff, separating the hydrophilic (below the line) from hydrophobic (above) surfaces. **b-c)** The colors correspond to the sample's wetting behavior: red = rose-like hydrophobic, blue = hydrophilic.

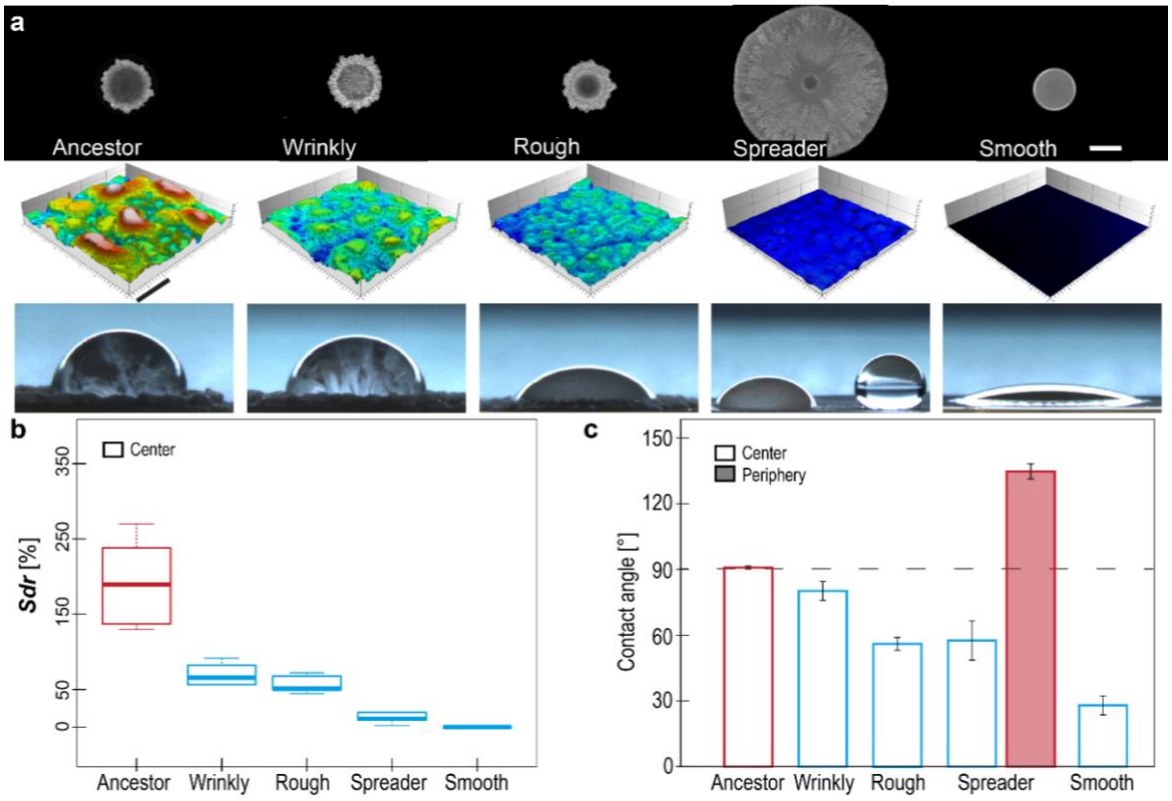

Figure 31 *Morphotype morphology and quantitate characterization of their colony features displayed on LB agar*. **a)** Top: colony morphologies of the ancestor and four distinct morphotypes. Scale bar in white represents 5 mm. Middle: surface topography of the colony center as acquired with light profilometry. The color scale depicts heights, where dark blue represents the lowest and white represents the highest features. Colonies were grown for 48h at 30°C. Scale bar in black represents 200 µm. Bottom: transversal image of a 10 µL droplet of *dd*H_2O on the surface center, or periphery (in the case of the Spreader morphotype). **b)** Values of ***Sdr*** calculated for the center of at least 5 individual colonies ($n \geq 5$). Boxes represent Q1-Q3, bold lines represent the median, and bars span from max. to min. **c)** Contact angle values calculated at the colony center and periphery (in the case of the Spreader morphotype). Error bars denote the standard deviation as calculated from 3 individual samples ($n = 3$). The dashed line represents the contractual hydrophobicity cut-off, separating the hydrophilic (below the line) from hydrophobic (above) surfaces. **b-c)** The colors correspond to the sample's wetting behavior: red = rose-like hydrophobic, blue = hydrophilic.

Inspired by this, and due to the fact that the observed structural differences between the the morphotypes are quite dramatic, it was further hypothesized that these differences could be linked to different levels of EPS production by the morphotypes [62, 67]. As previously shown in section 3.1.4, biofilm surface roughness is greatly influenced by the individual components of the matrix. Perhaps, a higher production of EPS could lead to enhanced surface roughness and wetting resistance (as observed for the Wrinkly morphotype) and a lower production could lead to the opposite effect (as observed for the Smooth morphotype). In order to test this, the matrix-gene reporters P_{tapA}-*gfp* and P_{eps}-*gfp* (Appendix 2: List of strains) were introduced into the four morphotypes and the ancestor strain, and changes in matrix genes expression were determined. Fluorescence images of colonies developed by P_{tapA}-*gfp* and P_{eps}-*gfp* labeled strains on MSgg agar suggest that the lowest expression of both matrix genes occurs in the Smooth variant, moderate expression (comparable to the ancestor) in the Spreader variant, and increased expression in the Wrinkly and Rough variants (Appendix Figs. 1 and 2). These observations suggest that the trend observed from surface complexity is –to a certain extent– consistent with the observed expression of matrix components.

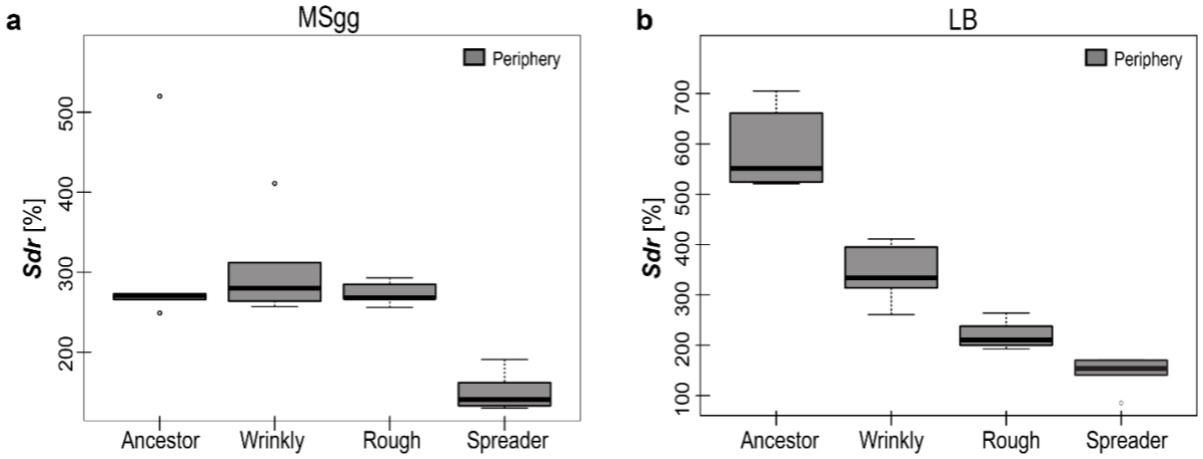

Figure 32 *Characterization of the periphery of the biofilm colonies depicted in Figs. 30 and 31*. **a)** Values of ***Sdr*** calculated for the periphery of colonies developed on MSgg agar. **b)** Values of ***Sdr*** calculated for the periphery of colonies developed on LB agar. **a-b)** The ***Sdr*** values were obtained from at least 5 individual samples ($n \geq 5$). Boxes represent Q1-Q3, bold lines represent the median, and bars span from max. to min. The color black indicates that those samples were not characterized in terms of wetting behavior.

3.3.3 Evolutionary diversification leads to quantitative differences in biofilm surface characteristics

Here, a novel quantitative approach was employed to describe four evolved morphotypes and to confirm that they are different from each other and from their common ancestor. Surface profilometry combined with wetting studies are especially helpful in the case of early morphotypes (Wrinkly or Rough): whereas they still resembled the ancestral colony in terms of macro-scale morphology, remarkable differences in microstructure and hydrophobicity are revealed. The latter is of great importance as it has been previously indicated that subtle differences in colony microstructure could be of profound importance for the wetting behavior of biofilm colonies [65, 88] and, consequently, for their resistance to antimicrobials [65].

Some recent findings show that a complex surface topography is not sufficient to establish non-wetting behavior in *B. subtilis* colonies [65]. This is not surprising as the biofilm surface topography cannot be easily disentangled from the surface chemistry, and small changes in the matrix composition can affect both chemistry and topography (as previously discussed in section 3.1.4). Here, it was observed that the measured surface complexity is positively correlated with the levels of matrix genes expression, at least to a certain extent. Of course, this correlation is not perfect: for the Rough variant, an increased expression of both the *tapA* and *eps* operons was observed and yet, decreased surface complexity and hydrophobicity were measured –compared to the ancestor. However, overexpression of the matrix elements tested here does not necessarily lead to an enhanced surface complexity/hydrophobicity. The function of one of those elements: TasA, is not even associated with enhancing (physically or chemically) those surface properties. In fact, the overexpression of matrix components in the Rough and Wrinkly morphotypes is accompanied by a subtle increase in colony area, whereas the Smooth morphotype shows a decreased colony area and lower EPS expression. In line with this observation and as reported by Kesel *et al*., the polysaccharide has been shown to be the main factor (together with BslA) influencing both biofilm surface roughness and colony area in *B. subtilis* NCIB 3610 biofilms [67]. Perhaps, in some cases, the overproduced matrix elements are not necessarily enhancing roughness features but, instead, are allowing for biofilm colony expansion.

Furthermore, in another study involving the evolution of *B. subtilis* NCIB 3610 pellicles, it was shown that a defective strain unable to produce the exopolysaccharide can evolve autonomy to colonize the liquid-air interface by altering the remaining component, TasA [77]. The latter is achieved through substitutions of certain residues in the TasA protein to cysteine. The evolved TasA fibers revealed a thicker structure thought to provide the polysaccharide-deficient matrix with a more robust architecture. However, when both cysteines found in the evolved TasA were substituted into the WT *B. subtilis* background, in which the exopolysaccharide component was still present, the formed pellicles showed extreme hydrophilic and porous behavior. In contrast, the ancestor and WT strains formed pellicles with superhydrophobic surfaces. This finding underscores the importance of the matrix elements for the final chemical and physical characteristics of the biofilm surface, and that these factors are interdependent in terms of hydrophobicity.

Although more tests would be required to address specific details arising from such a convoluted study involving several disciplines, these studies revealed that evolutionary diversification can lead to clear and measurable differences in the colony surface characteristics with correspondingly different wetting properties. Moreover, those alterations in the surface properties generated by evolutionary processes still follow the line of argumentation presented before: biofilm surface topography is related to the wetting behavior (Fig. 33). Together, these results underline the potential of approaching different areas, such as microbial evolution, with multidisciplinary quantitative characterization techniques.

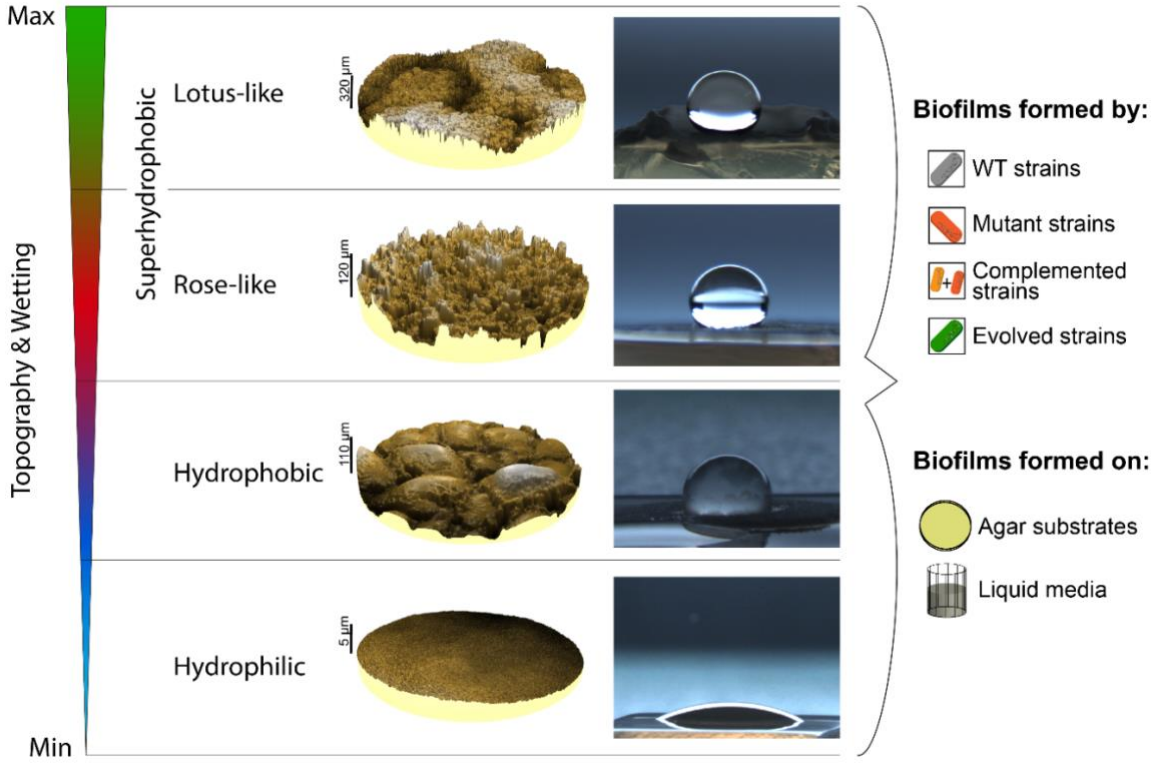

Figure 33 *Summary of chapter 3.* The relation between the biofilm surface topography and the wetting behavior was observed across a wide range of conditions for biofilms formed by bacteria from different origins. In general, the highest surface complexity corresponded to superhydrophobic lotus-like biofilms, intermediate complexity to superhydrophobic rose-like or hydrophobic biofilms, and the lowest complexity to hydrophilic biofilms.

4 Strategies to weaken the superhydrophobicity of bacterial biofilms: a physical route to biofilm control

4.1 [c]Osmotic deflation of biofilm colony surfaces

For the inactivation or removal of bacterial biofilms via chemical or physical processes, it is crucial to sufficiently wet the biofilm surface. However, as discussed in chapter 3, many bacterial biofilms efficiently resist wetting by water, oil or even organic solvents, and part of the reason for this resistance is the high surface roughness of the biofilm. Here, it is demonstrated how exposing the surface of mature biofilm colonies to concentrated ethanol, saline or glucose solutions results in topographical changes that increase their wettability. With this approach, even omniphobic biofilm colonies become wettable towards aqueous solutions and oils. As a result of this reduced liquid repellency, the biofilms become susceptible to erosion by water which allows for their removal from the substrate they have been grown on. Moreover, bacteria within pre-treated biofilms can now be inactivated with antibiotic solutions. Thus, the biofilm treatment strategy presented here presents a new stepping stone for fighting biofilms in either industrial or medical settings.

4.1.1 Short treatment with concentrated ethanol solutions renders biofilms wettable

Previously, a clear link between surface topography and wetting behavior was established on biofilm surfaces formed by different bacterial strains and in several environmental conditions (sections 3.1 and 3.2). These observations motivated the following hypothesis: if the roughness features of a highly complex biofilm surface could be smoothened, such a biofilm surface should lose its strongly hydrophobic character. It has been shown earlier that the surface roughness of certain *B. subtilis* biofilms can be decreased by exposing the entire colonies to 80% ethanol for 60 min [146]. The observed topographical changes were suggested to arise from a dehydration of the biofilm colonies after ethanol exposure. This notion is consistent with the use of such solvent as part of the biological sample preparation procedure for scanning electron microscopy, where biofilm shrinkage has been reported [164]. Indeed, the exposure of a hydrated sample to concentrated organic solvents such as ethanol leads to diffusion driven mass transfer, i.e. water will leave the sample and alcohol will enter it until an equilibrium concentration is reached [165, 166]. Thus, here, it was tested if ethanol-induced biofilm dehydration and the ensuing alterations in the biofilm topography would render hydrophobic biofilms wettable.

To test this hypothesis, ethanol solutions were applied to the surfaces of those biofilm colonies which showed the most complex topographies (i.e., lotus-like *B. subtilis* B-1 biofilms with very high ***Sdr*** values, section 3.2, Fig. 25) and the effect of different exposure times was tested. For a 60 min exposure of B-1 biofilm surfaces to 80% ethanol, similarly strong topographical

[c] This section follows in part the publication: "*Topographical alterations render bacterial biofilms susceptible to chemical and mechanical stress*" published on 2018, in Biomaterials Science.

alterations as reported before were found [146] and the biofilms were rendered hydrophilic (Fig. 34). Interestingly, also short exposure times as low as 10 min caused similar effects: treated B-1 biofilm samples lost their hydrophobic character and showed both contact angles towards water on the order of ~40° (Fig. 34b) and a clear reduction in ***Sdr*** values of ~50% (Fig. 34a).

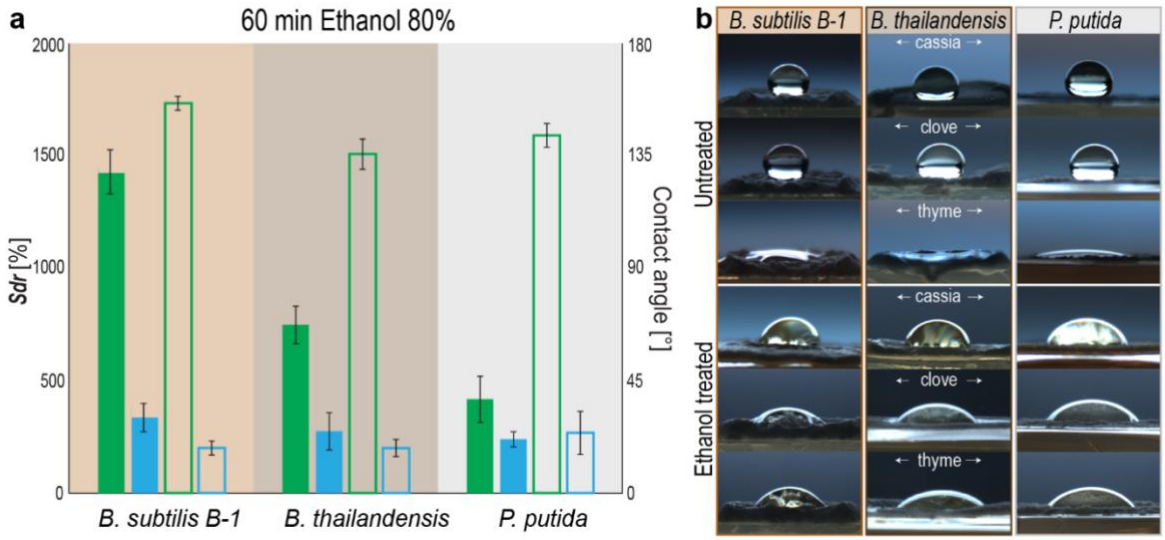

Figure 34 *Influence of long and short exposures of different biofilms to 80% ethanol solutions.* **a)** Values of ***Sdr*** (filled bars, left axis) and contact angle data (open bars, right axis) as obtained from biofilm colonies generated by *B. subtilis* B-1, *B. thailandensis* and *P. putida* when grown on LBGM agar. Green bars correspond to samples tested before ethanol treatment and blue bars to samples tested after treatment. In all cases, the treatment converted lotus-like hydrophobic samples (green) into hydrophilic samples (blue). Error bars denote the standard deviation as calculated from at least 2 individual samples ($n \geq 2$). **b)** Images showing lateral views of 10 µL droplets of essential oils placed onto different biofilm colonies before ('untreated'), and after ('treated') a 10 min ethanol treatment.

It is important to note that, without the application of such an ethanol treatment, those *B. subtilis* B-1 biofilms not only repel water but also organic solvents and oils, i.e. they behave omniphobic (Table 5 and Fig. 34b). In terms of biofilm treatment, this oil-repellency is a problematic property as selected essential oils from plants or fruits possess strong anti-bacterial properties [167, 168]. However, the benefits of such essential oils are difficult to harness if the biofilm surface repels them. Indeed, lotus-like B-1 biofilms were found initially to repel essential oils from both cassia and clove; yet, after an ethanol-induced topographical 'smoothening' (Fig. 35c), these biofilms became wettable towards these oils (Fig. 35b and 34b). This finding underscores the efficiency of the topographical alteration and suggests that the ethanol exposure primarily affects the topographical properties of the biofilm surface rather than its chemical properties.

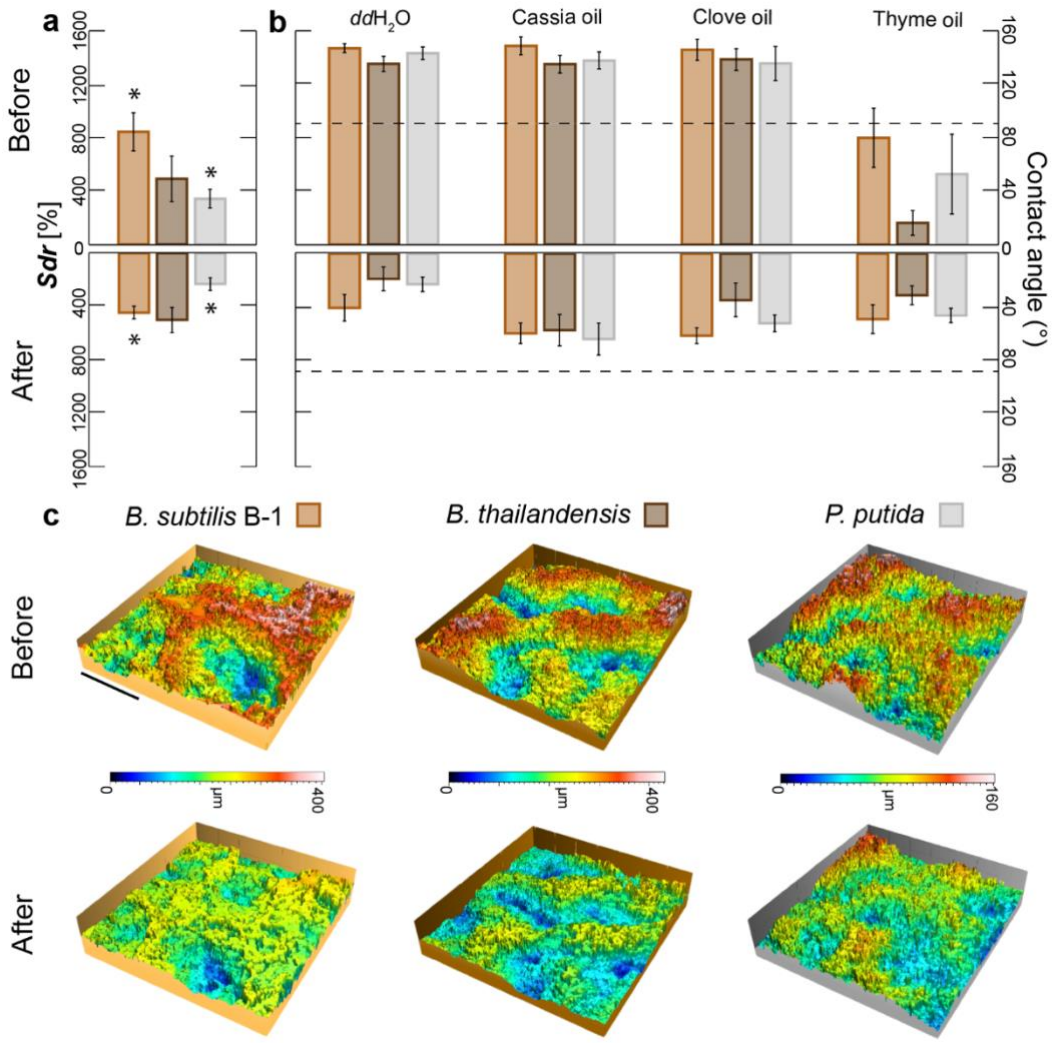

Figure 35 *Topographical and wetting alterations after a short ethanol treatment of biofilm surfaces formed by three different bacterial species. B. subtilis* B-1 biofilms originally show a highly developed surface with ***Sdr*** values in the range of 1000% **(a)** and lotus-like wetting behavior with very high CA **(b)**. After treatment with 80% ethanol for 10 min, the surface roughness is reduced **(a, c)** and the biofilms become wettable towards water and essential oils **(b)**. A similar trend is observed for *B. thailandensis* and *P. putida* biofilm colonies **(a, b, c)**. Error bars denote the standard deviation as calculated from at least 6 independent samples ($N = 3$, $n \geq 2$). Stars denote significant differences between untreated and treated biofilm colonies, where $p = 0.05$. The scale bar in **(c)** denotes 500 µm in *x*- and *y*-coordinates. The color code represents the *z* axis.

Table 5 *Contact angles of B. subtilis B-1 biofilms grown on LBGM agar for different liquids with low surface tension.* Surface tension values for all liquids were taken from the literature as indicated in the references. The error values denote the standard deviation as calculated from 3 individual samples ($n = 3$).

		***B. subtilis* B-1 biofilms grown on LBGM agar**	
Solution	**Concentration (v/v)**	**Surface tension (mN/m) at 25 °C**	**Contact angle (°)**
Isopropanol	50%	24.26 [169]	143.56 ± 12.24
Methanol	50%	32.86 [169]	143.54 ± 4.80
Acetone	50%	28.60 [170]	145.71 ± 2.85

Of course, as described in section 3.2.1, the occurrence of lotus-like surfaces is not limited to biofilms formed by the *Bacillus subtilis* species. Hence, two other species capable of forming biofilms with lotus-like surfaces were tested: *Pseudomonas putida* and *Burkholderia thailandensis*. Similarly, when the surface of biofilm colonies generated by *P. putida* were exposed to ethanol in the same way as described before for *B. subtilis* B-1 biofilms, a clear deflation of their surface structures was also observed (Fig. 35c). As a consequence of a 10 min exposure to ethanol, the ***Sdr*** values obtained from the treated biofilms show a decrease of ~30% (Fig. 35a) and the biofilms are rendered wettable (Fig. 35b). Also biofilms generated from *B. thailandensis* lost their omniphobic properties after the ethanol treatment (Fig. 35b); however, here, a measurable decrease in ***Sdr*** values is only detected for longer treatment times (Fig. 34a). Maybe, a short exposure to ethanol causes topographical alterations which are sufficient to alter the biofilm wetting properties but too small to lead to measurable changes in the ***Sdr*** parameter as determined by optical profilometry. However, significant differences before and after ethanol treatment are observed on two additional parameters that characterize the biofilm surface topography: the root mean square surface roughness, ***Sq***; and the maximum height difference of the surface features, ***Sz***; on all biofilms types (Table 3, Fig. 36).

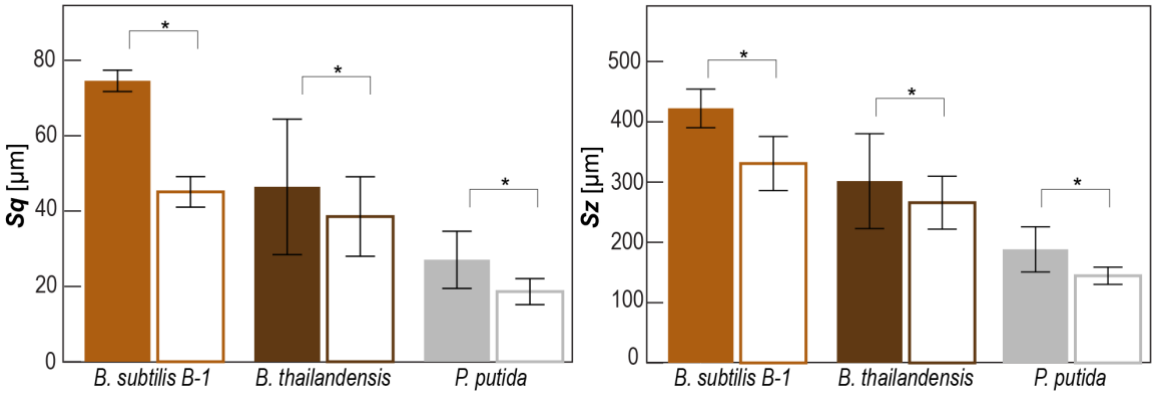

Figure 36 *Surface roughness and maximum height of biofilms treated for 10 min with an 80% ethanol solution.* ***Sq*** and ***Sz*** values (Table 3) obtained from the surface of the same biofilm samples shown in Fig. 35a before (closed bars) and after (open bars) treatment with ethanol for 10 min. Error bars denote the standard deviation as calculated from at least 6 independent samples ($N = 3$, $n \geq 2$). Stars denote significant differences between untreated and treated biofilm colonies, where $p = 0.05$.

In general, ethanol contact with the biofilm could cause conformational changes in one or more of the matrix components (e.g., protein denaturation) even at such short exposure times. This could affect the chemical composition of the biofilm surface and, in turn, its surface tension. Thus, affecting the wetting behavior as quantified by the reported contact angle values. In the case of *B. subtilis* biofilms, the surface layer hydrophobin BslA, e.g., loses its function as a hydrophobic coat when this protein is present in its monomeric form; also, it does not assemble on the biofilm surface when internal disulfide bonds are formed incorrectly [65]. It is possible that some of the treatments conducted here affect the conformation and thus activity of this *B. subtilis* surface layer protein as well as other biofilm matrix components, which could affect biofilm wetting behavior without causing measurable changes in the biofilm surface roughness.

4.1.2 Concentrated salt and sugar solutions require longer treatment times

Although the efficiency of the ethanol treatment is remarkable, using concentrated ethanol solutions for altering the surface topography of biofilms could cause negative side effects on the surfaces the biofilm grows on –at least in certain medical or industrial settings. Thus, in a next step, it was explored if the same effect could be obtained by using less aggressive chemicals. When looking for alternative biofilm treatments that could induce a similar topographical 'smoothening', it was hypothesized that an osmotic pressure acting on the biofilm surface might be responsible for the observed effects. Indeed, osmotic dehydration is a typical fruit and vegetable preservation method in the food industry, where water is partially removed from compartments with lower solute concentration and transported into compartments of higher solute concentration [165, 171]. Different osmotic agents including salts and sugars are currently used in this process, and typical exposure times range from a few hours to days [171]. Inspired by this food preservation process, here, inducement of osmotic dehydration of biofilms was attempted by applying concentrated solutions of salts and sugar on the surfaces of these biomaterials (section 2.2.2).

Biofilm surface treatment with the concentrated osmotic agents 5 M NaCl, 3 M KCl and 1.5 M glucose was performed in the same way as previously described for ethanol solutions, and putative topographical changes were assessed by imaging the surface of each biofilm sample *in situ* before and after treatment with the osmotic solutions (section 2.3.1.3). First, short incubation times of 1 h or 2 h were tested on the roughest samples, i.e. lotus-like *B. subtilis* B-1 biofilms. However, with those exposure times, no visible alteration of the biofilm surface was detected by profilometry (denoted by the ***Sdr*** values before and after treatment) nor a change in hydrophobicity was reported by the measured CA (Fig. 37a). Thus, longer exposure times of 18 h or 48 h were then tested. Here, a clear reduction of the surface features was observed; however, owing to the long duration of this exposure step, partial evaporation or absorption of the osmotic solution by the biofilm surface was observed in some cases (Fig. 37b). Thus, to achieve comparable conditions, only those combinations of biofilm colony surfaces and osmotic solutions, where the treating droplet maintained a stable shape and size throughout the experiment, were analyzed (shaded conditions in Fig. 37b).

a

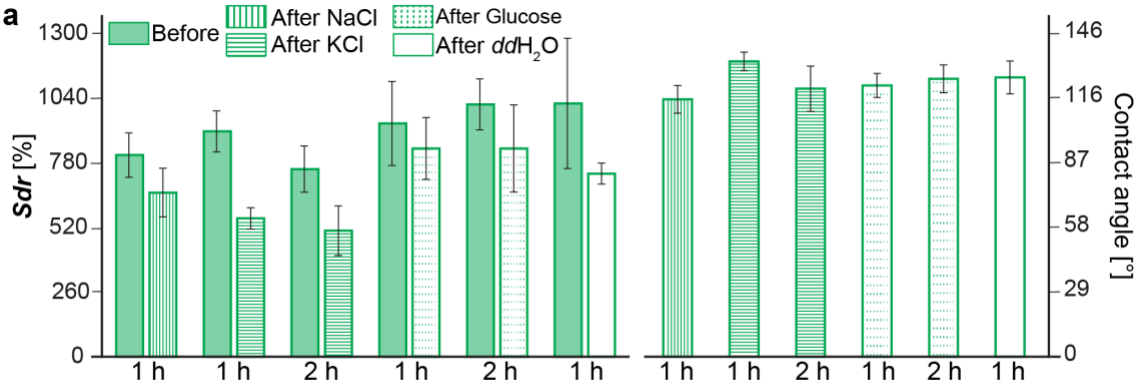

b

	All strains	*B. subtilis* B-1	*P. putida*	*B. thailandensis*
Osmotic agent	t = 0	t = 18 h	t = 18 h	t = 48 h
Glucose	+++	+++	++	+++
NaCl	+++	-	+++	+++
KCl	+++	-	-	++
*dd*H₂O	+++	++	+	++

(+++) initial maximum volume, (-) final volume equal or close to zero.

Figure 37 *Influence of a short exposure of B. subtilis B-1 biofilms towards osmotic solutions and final relative volumes of the different osmotic agents after long exposure times on all three biofilm variants.* **a)** Contact angle (right) and ***Sdr*** values (left) before and after treatment with osmotic agents for 1 or 2 h on lotus-like hydrophobic biofilms formed by *B. subtilis* B-1 on LB agar. The maximum value of the *y*-axis (CA = 146°) represents the average CA value obtained for untreated biofilms, and the values represented by the bars denote the average CA after treatment. Error bars denote the standard deviation as calculated from at least 3 individual samples ($n \geq 3$). **b)** Long-term stability of a water droplet (containing an osmotic agent) on different biofilm samples which all initially show lotus-like wetting behavior. As explained in the example pictures below, the symbols "+++", "++", "+" and "-" indicate the relative volume of a droplet after long treatment times in comparison to its initial volume.

Results obtained from samples, that allowed a stable treatment, show that osmotic dehydration of lotus-like *P. putida* biofilms with NaCl solutions produces the strongest topographical alterations. Here, the ***Sdr*** value calculated from the treated biofilm samples shows a reduction of up to 46% (Fig. 38a). As a consequence of this NaCl treatment and the ensuing strong topographical changes, the surface of these lotus-like biofilm colonies became highly adhesive towards water, i.e. it acquired rose-like behavior as demonstrated by contact angle hysteresis measurements (Fig. 38a).

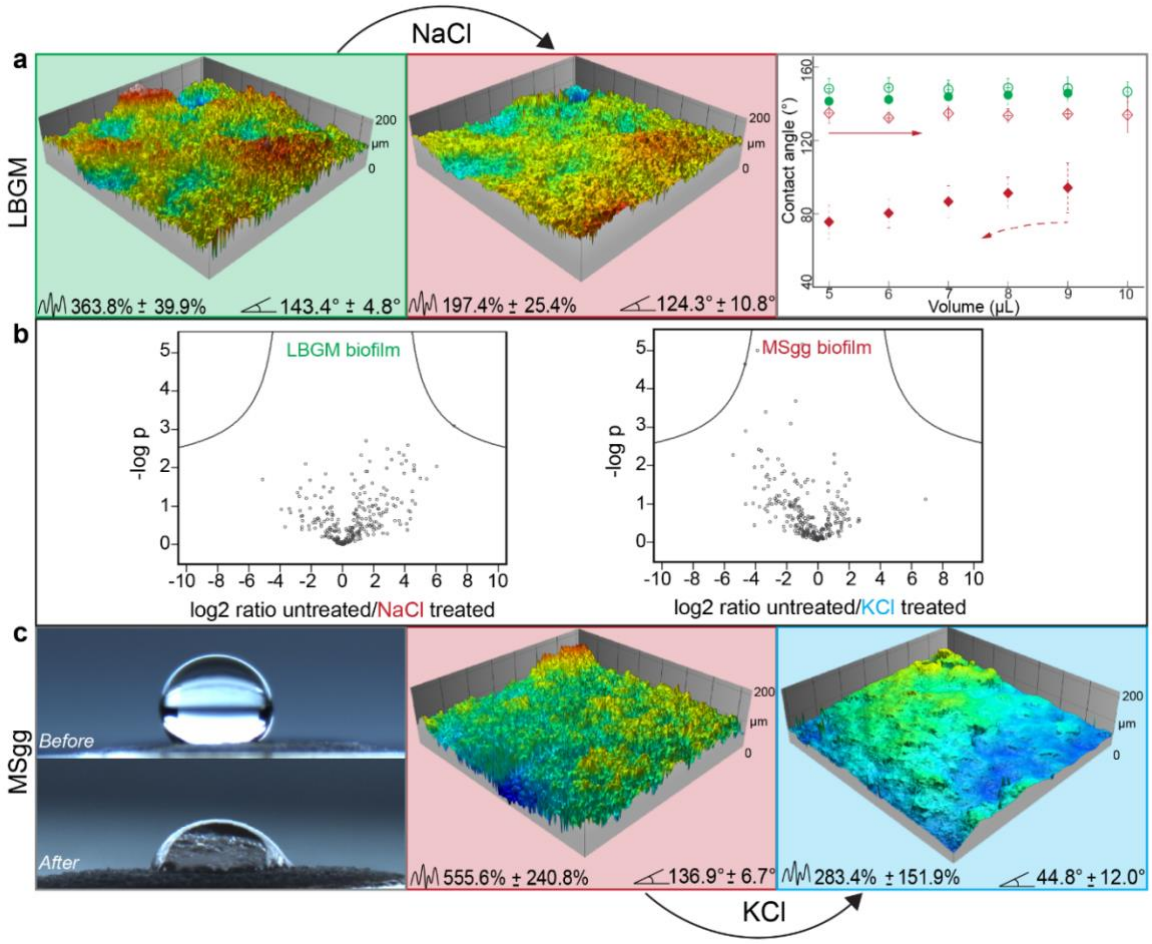

Figure 38 *Topographical, wetting, and proteomic changes in treated P. putida biofilms with NaCl and KCl solutions*. **a)** Profilometric images of a *P. putida* biofilm grown on LBGM agar before and after NaCl treatment. CA hysteresis measurements (right panel) of untreated (circles) and osmotically treated samples (diamonds); empty symbols denote advancing CA, filled symbols denote receding CA. **b)** Volcano plots showing differences in protein expression of untreated *vs.* osmotically treated *P. putida* biofilms. Grey circles represent proteins which do not exhibit significant expression change (p = 0.05, see section 2.5.1.2 for details). **c)** Transversal and profilometric images of a *P. putida* biofilm grown on MSgg agar before and after KCl treatment. **(a-c)** The numbers at the bottom of the images denote average ***Sdr*** and CA values, respectively. Error values and bars denote the standard deviation as calculated from at least 6 independent samples (N = 3, $n \geq 2$). The colors of background and symbols represent the biofilm wetting behavior: green – hydrophobic lotus; red – hydrophobic rose; blue – hydrophilic.

For lotus-like biofilm samples generated by *B. subtilis* B-1 or *B. thailandensis*, similar results were obtained when those biofilm samples were treated with a glucose solution for 18 h and 48 h, respectively. Due to the initially higher surface complexity of both of these biofilms –as compared to *P. Putida*, the deflation effects can be easily observed on the profilometric images taken after the treatment. As a consequence of these topographical alterations, a switch from lotus- to rose-like wetting behavior was measured in both cases, as denoted by higher CA hysteresis after glucose exposure (Fig. 39).

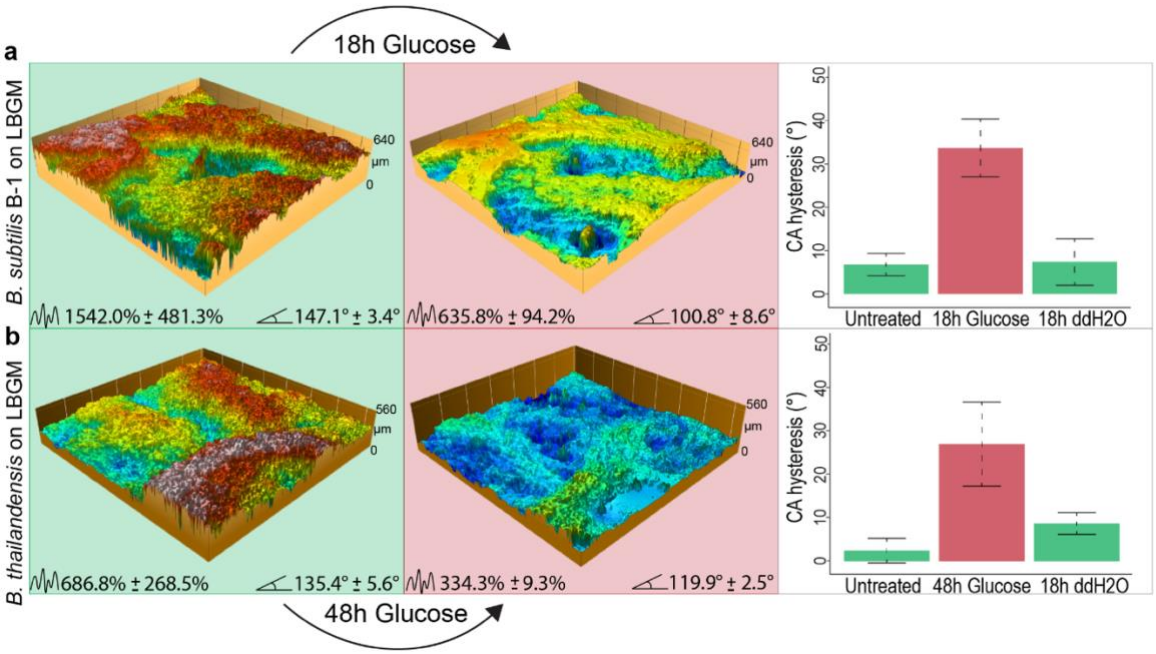

Figure 39 *Topographical and wetting alterations of biofilms formed by B. subtilis B-1 and B. thailandensis bacteria after long exposure to glucose solutions.* **a)** Profilometric images of a *B. subtilis* B-1 biofilm grown on LBGM agar before and after Glucose treatment. CA hysteresis values for untreated and both osmotically and water treated samples are shown in the far right. CA hysteresis values were calculated as the difference between the advancing CA and receding CA of a water droplet on the biofilm surface when a droplet volume was first increased from 5 µL to 10 µL and then reduced again to 5 µL (in steps of 1 µL each). **b)** Profilometric images and CA hysteresis values before and after treatment of *B. thailandensis* biofilms with a glucose solution. **(a-b)** The numbers at the bottom of the images denote average ***Sdr*** and CA values, respectively. Error values and bars denote the standard deviation as calculated from at least 3 individual samples ($N \geq 1$, $n \geq 3$). The colors of background and symbols represent the biofilm wetting behavior: green – hydrophobic lotus, red – hydrophobic rose.

So far, using concentrated salts and sugar solutions, a change from the highest surface complexity to intermediate complexity was achieved; next, it was explored if a similar treatment could yield a hydrophilic biofilm when a hydrophobic rose-like biofilm surface (with intermediate complexity) is chosen. To test this, biofilm colonies generated by *P. putida* grown on MSgg agar (which exhibit rose-like surfaces) were selected and treated with all osmotic solutions described before. Here, the strongest effect was obtained by exposing the biofilm surfaces to a KCl solution: a decrease in ***Sdr*** of ~50% and a final contact angle of ~45° was measured (Fig. 38c). Control experiments were also performed with *dd*H_2O on both, lotus-like and rose-like *putida* biofilms (Fig. 40) as well as on lotus-like B-1 and *thailandensis* biofilms (Fig. 39). In all control cases, the samples retained their initial hydrophobic character, demonstrating that the effects described above indeed result from the high concentrations of osmotic agents in the aqueous solutions. Either hysteresis curves or simple CA measurements confirmed these results; for instance, in the case of the rose-like *P. putida* biofilms, after removing the "treating" water volume, residual water remained trapped in the micro-roughness features of the biofilm surface (as indicated by the locally flat areas in the profilometric image in Fig. 40), which is typical for rose-like hydrophobic surfaces after water exposure [88]. Furthermore, a proteomics analysis of osmotically treated *P. putida* biofilm samples revealed no significant differences in protein expression compared to untreated biofilms (Fig. 38b).

These results suggest that the topographical "smoothening" effect achieved with the osmotic solutions might be a physical mechanism, which is relatively independent of the type of bacteria or the cultivation conditions.

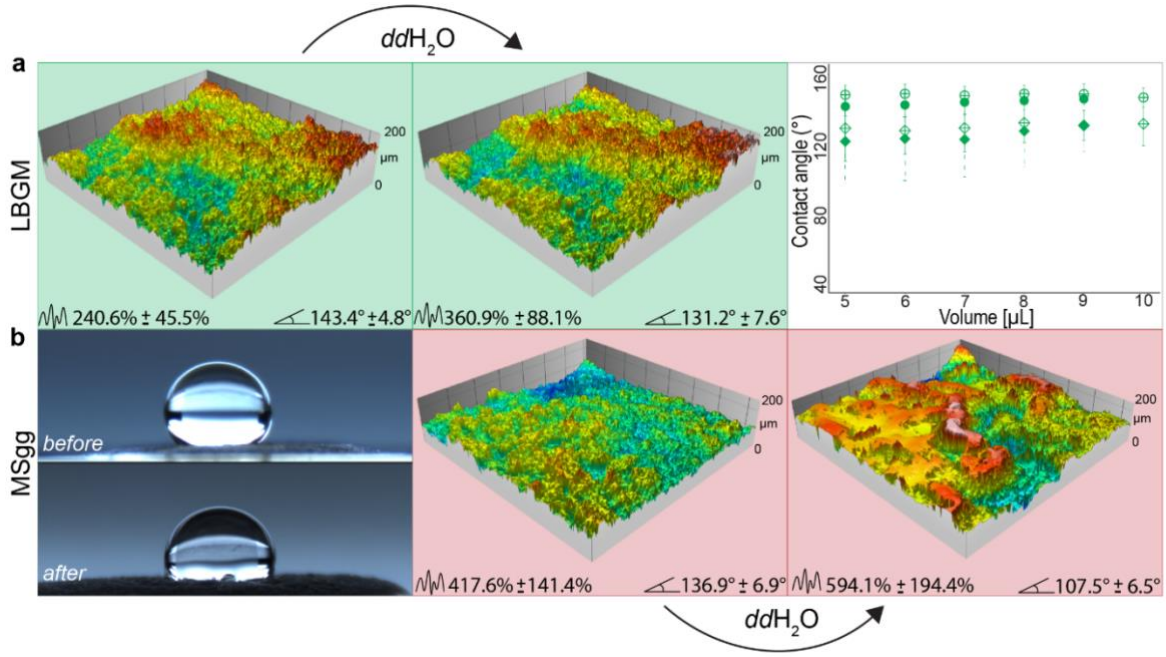

Figure 40 *Control measurements of P. putida biofilms exposed to ddH_2O for 18 h.* **a)** Profilometric images show a lotus-like hydrophobic *P. putida* biofilm before and after water exposure. In the far right, open symbols in the hysteresis diagram represent advancing CA values, whereas closed symbols represent receding CA values; circles correspond to untreated samples and diamonds to *dd*H_2O treated samples. **b)** Transversal and profilometric images of a *P. putida* biofilm with rose-like hydrophobicity before and after water exposure. **(a-b)** The numbers at the bottom of each profilometric image denote the average ***Sdr*** and CA values, respectively. The error values shown denote the standard deviation as calculated from at least 6 independent samples (N = 3, $n \geq 2$). The colors of background and symbols represent the biofilm wetting behavior: green – hydrophobic lotus, red – hydrophobic rose.

4.1.3 Erosion stability and antibiotic sensitivity of osmotically treated *vs*. non-treated biofilms

When trying to remove biofilms from surfaces with mechanical forces induced by flowing or dripping water, strongly hydrophobic surface properties can be a factor that contributes to the high resilience of a biofilm. Especially when exhibiting lotus-like behavior, the biofilm surface can efficiently avoid contact with an aqueous solution –at least on a nano- and micro-scopic length scales. Thus, it is expected that hydrophobic, lotus-like biofilms can resist erosion by water more efficiently than hydrophilic biofilms. The latter hypothesis was tested by comparing the erosion behavior of biofilms generated by *B. subtilis* B-1, *B. thailandensis*, and *P. putida* in their untreated (i.e., lotus-like hydrophobic) and ethanol treated (i.e., hydrophilic) state. First, the biofilms were exposed to dripping water and the eroded biofilm area was determined as a function of time (section 2.4.1, Fig. 9a). Indeed, as depicted in Fig. 41a, all three biofilm variants became more sensitive towards erosion by dripping water when their surfaces were

rendered hydrophilic by a short ethanol treatment. The strongest difference between untreated and ethanol treated samples was obtained for *B. subtilis* B-1 biofilms. However, this is not surprising considering that, among the three biofilm variants tested, this biofilm type resists erosion most efficiently: after 5 min of continuous water dripping, the eroded area of untreated B-1 biofilms is 5-10 times smaller than what is obtained for *B. thailandensis* and *P. putida* biofilms, respectively.

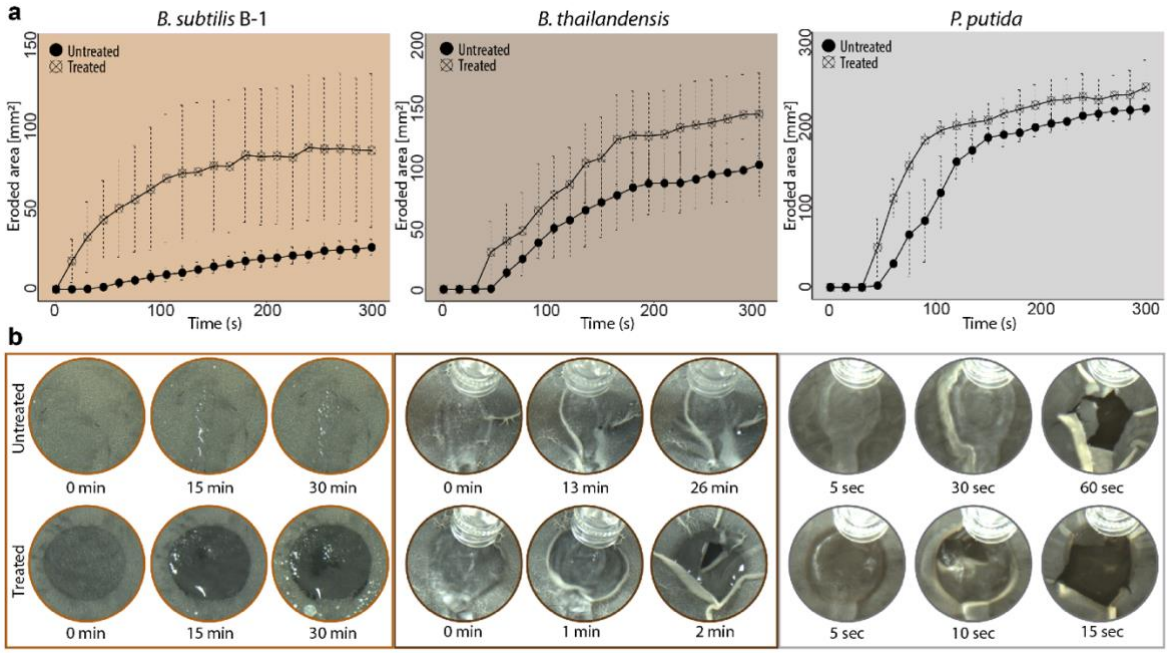

Figure 41 *Erosion stability of untreated vs. ethanol treated biofilm surfaces formed by B. subtilis* B-1, *B. thailandensis*, and *P. putida*. **a)** Erosion process in dripping water mode (section 2.4.1, Fig. 9a) of biofilms formed the three bacterial strains on MSgg agar (B-1) and LBGM agar *(putida* and *thailandensis*) as continuous layers (section 2.2.1.3). Error bars denote the standard deviation as calculated from at least 6 independent samples ($N = 3$, $n \geq 2$). **b)** Qualitative data showing the erosion process in flowing water mode (section 2.4.1, Fig. 9b) of the same type of biofilms as in **(a)**: top row images correspond to untreated biofilms, images in the bottom row to ethanol treated biofilms. The diameter of the images is ~30 mm. **a-b)** For both tests, the ethanol treatment was performed for 10 min.

Such a dripping water erosion test with impacting water droplets on the biofilm surface does not only probe the surface polarity of a biofilm but also its mechanical sturdiness. To reduce the contribution of the latter, which can differ among the biofilm variants, a second type of erosion experiment was performed where the biofilm surfaces were exposed to a continuous stream of flowing water (section 2.4.1, Fig. 9b). In this particular setup, all biofilm variants withstood erosion for much longer time intervals than in the dripping water tests (Fig. 41). However, also here, the ethanol treated biofilms became more susceptible to erosion as the onset of biofilm removal was clearly shifted to earlier time points compared to untreated samples (Fig. 41b).

Having established that altering the wetting properties of biofilms from lotus-like hydrophobic to hydrophilic enhances biofilm erosion by water, it was speculated that weakening the wetting resistance of biofilm colonies would also increase the efficiency of anti-microbial solutions.

To test this, an aqueous solution containing an antibiotic was chosen as a model for an anti-microbial liquid, and a live/dead staining kit (see section 2.4.2.1 for details) was selected for a quantitative assessment of the efficiency of the previous. First, a control experiment was performed to test the activity of the staining dyes on cells extracted from *Pseudomonas putida* biofilms. Two types of samples were tested: 'fresh' and 'heated' samples. 'Fresh' samples consisted of *P. putida* bacterial cells, which were extracted from untreated biofilms, suspended in sterile *dd*H_2O, and stained with a 1:1 solution of the two dyes propidium iodine and SYTO 9. 'Heated' samples were obtained in the same way, with the only difference that the cell suspension was heated in a boiling water bath for 5 min (to induce cell death) and then allowed to cool down to RT prior to staining. As observed in (Fig. 42c), a higher proportion of green cells in the heated samples shows that the dyes stain the cells in a counter-intuitive fashion: dead cells were stained green and live cells were stained read. Among others [172], this unusual staining outcome has already been reported before for *Pseudomonas aeruginosa* [173]. Therefore, live cells (stained red) are reported green and dead cells (stained green) are reported red hereafter for simplicity.

A second control was run afterwards; here, lotus-like *P. putida* biofilms were studied by exposing their surfaces to a solution containing 160 µg/mL of the clinically used broad-spectrum β-lactam antibiotic piperacillin (section 2.4.2, Fig. 10). After a 2 h incubation with this antibiotic solution, the percentage of live cells remained well above 80% (filled bars in Fig. 42a-b) and thus comparable to the control samples that were not exposed to the antibiotic (Fig. 42c). This demonstrates the poor efficiency of the antibiotic solution towards biofilm bacteria, even when such is suitable to kill planktonic *P. putida* bacteria [126]. Interestingly, virtually identical results were obtained when *P. putida* biofilms with rose-like hydrophobicity were treated with the antibiotic solution (filled bars in Fig. 42a-b).

In contrast, for biofilms that were osmotically treated before exposure to the antibiotic, the percentage of dead cells strongly increased (dashed bars in Fig. 42a-b). When a hydrophobic biofilm sample was rendered hydrophilic, either by a short ethanol treatment or a long KCl treatment, the percentage of dead cells was increased from 10 to 60% and from 15 to 50%, respectively (dashed bars in Fig. 42a-b). A similarly strong increase in the bacteria susceptibility to the antibiotic occurred when a lotus-like biofilm was converted into a rose-like biofilm, e.g. by exposure of the biofilm surface to a concentrated NaCl solution. Even though the biofilm surface remained hydrophobic in this case, the change of its wetting mode alone was sufficient to obtain an increase of dead bacterial cells from ~20 to 70% compared to the control (filled bars in Fig. 42a-b).

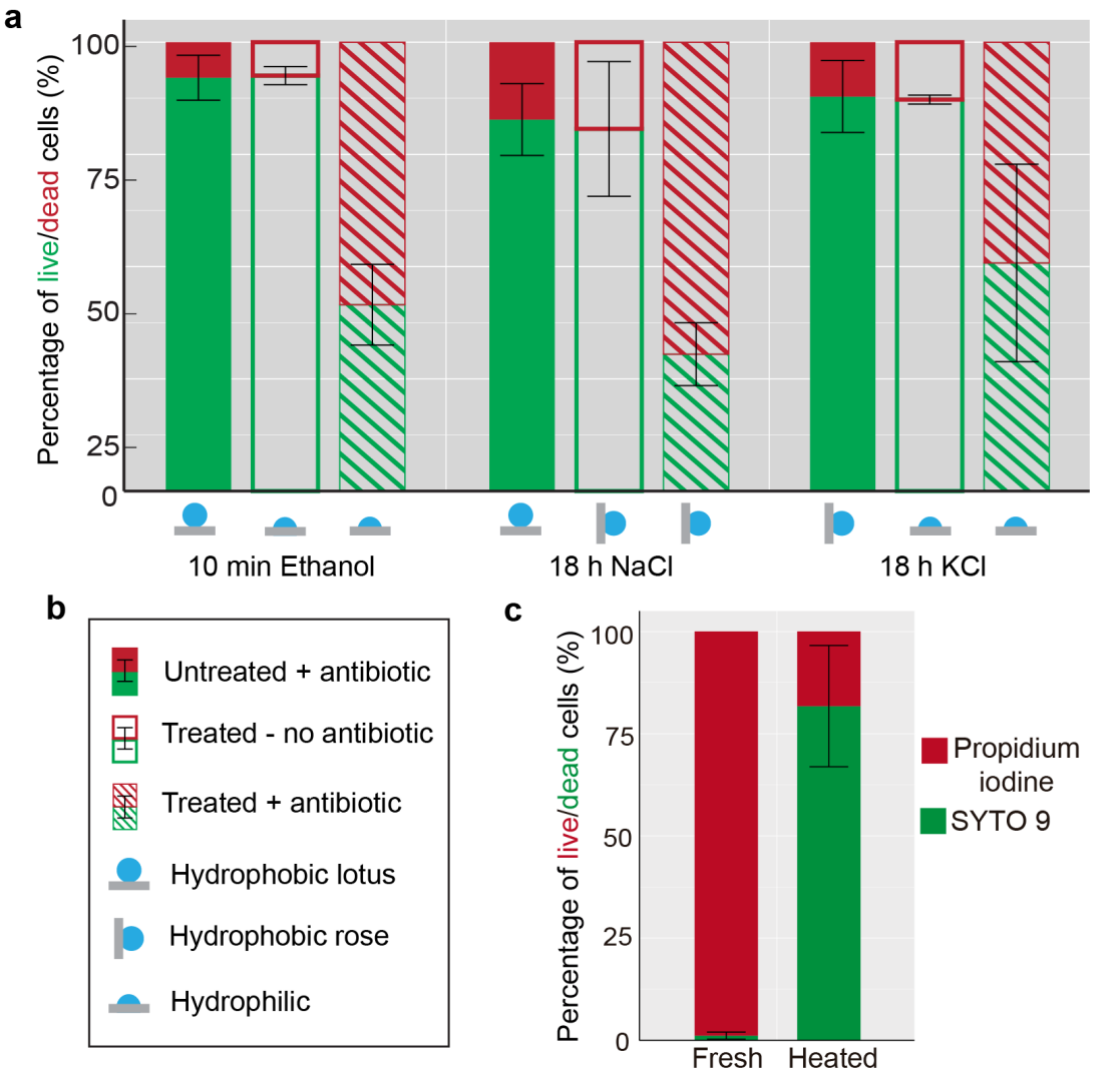

Figure 42 *Antibiotic sensitivity of untreated vs. osmotically treated biofilm surfaces formed by P. putida and fluorescence dyes controls.* **a)** Bar plots show percentage values of live (green) and dead (red) cells. 'Untreated' refers to biofilms exposed to air for the same time as their 'treated' counterparts. 'Treated' refers to samples exposed to an osmotic solution. The surfaces of the samples identified as '+ antibiotic' were incubated with piperacillin/tazobactam (section 2.4.2.1). **b)** Legends denoting the meaning of the symbols and color codes from **(a)**. **c)** Control experiment showing the proportion of live-to-dead bacterial cells from "fresh" and "heated" extracted cells from *P. putida* biofilms. **a-b)** Error bars denote the standard deviation as calculated from at least 6 independent samples ($N = 3$, $n \geq 2$).

To test for the effect of the individual osmotic agents on cell viability, the osmotic treatment was performed without subsequent antibiotic exposure. Here, the fraction of dead cells was similar for all solutions as for the control (open bars in Fig. 42a-b), demonstrating that the increased killing rate indeed originates from the antibiotic, and not from the osmotic agents. It is important to note that the high prevalence of live cells applies also for ethanol treated biofilms, underscoring biofilm resistance to disinfectants [174]. Such results suggest that the efficiency of the antibiotic solutions is linked to the detailed mode of wetting of the biofilm surfaces.

4.1.4 Summary of section 4.1 and implications of a biofilm osmotic treatment

It was shown here that the wetting resistance of omniphobic biofilm colonies can be altered by incubating the biofilm surface with either ethanol solutions or concentrated salt or sugar solutions. In parallel to the observed wetting alteration, topographical changes on the biofilm surfaces were detected, suggesting that mostly physical and not chemical mechanisms are responsible for the effects described here. As a result of these alterations, the erosion sensitivity and antibiotic efficiency of the tested biofilms was increased. Fig. 43 presents a general overview of the osmotic treatment proposed here, the alterations in the biofilm surfaces as a result of this treatment, and the implications on chemical and mechanical biofilm control strategies.

Although the particular wetting state obtained on a biofilm surface after the osmotic treatment depended both on the solution and the exposure time, the physical nature responsible for this effect suggests that such a treatment could be applicable to a broad range of hydrophobic biofilms. Furthermore, as demonstrated by experimentation with antibiotic solutions, already converting a lotus-like into a rose-like hydrophobic surface can be highly beneficial for increasing their efficiency. This result is interpreted such that, removing the ‘air cushion’ between the biofilm and the water phase (i.e. eliminating the Cassie-Baxter non-wetting state) and turning the wetting mode into an impregnated Cassie state, allows aqueous solutions to reach the biofilm surface on a microscopic level (Fig. 51). With such an approach, a treatment of biofilms with harmless solutions as presented here, could aid with the inactivation and removal of such materials from contaminated surfaces in both industrial and medical settings.

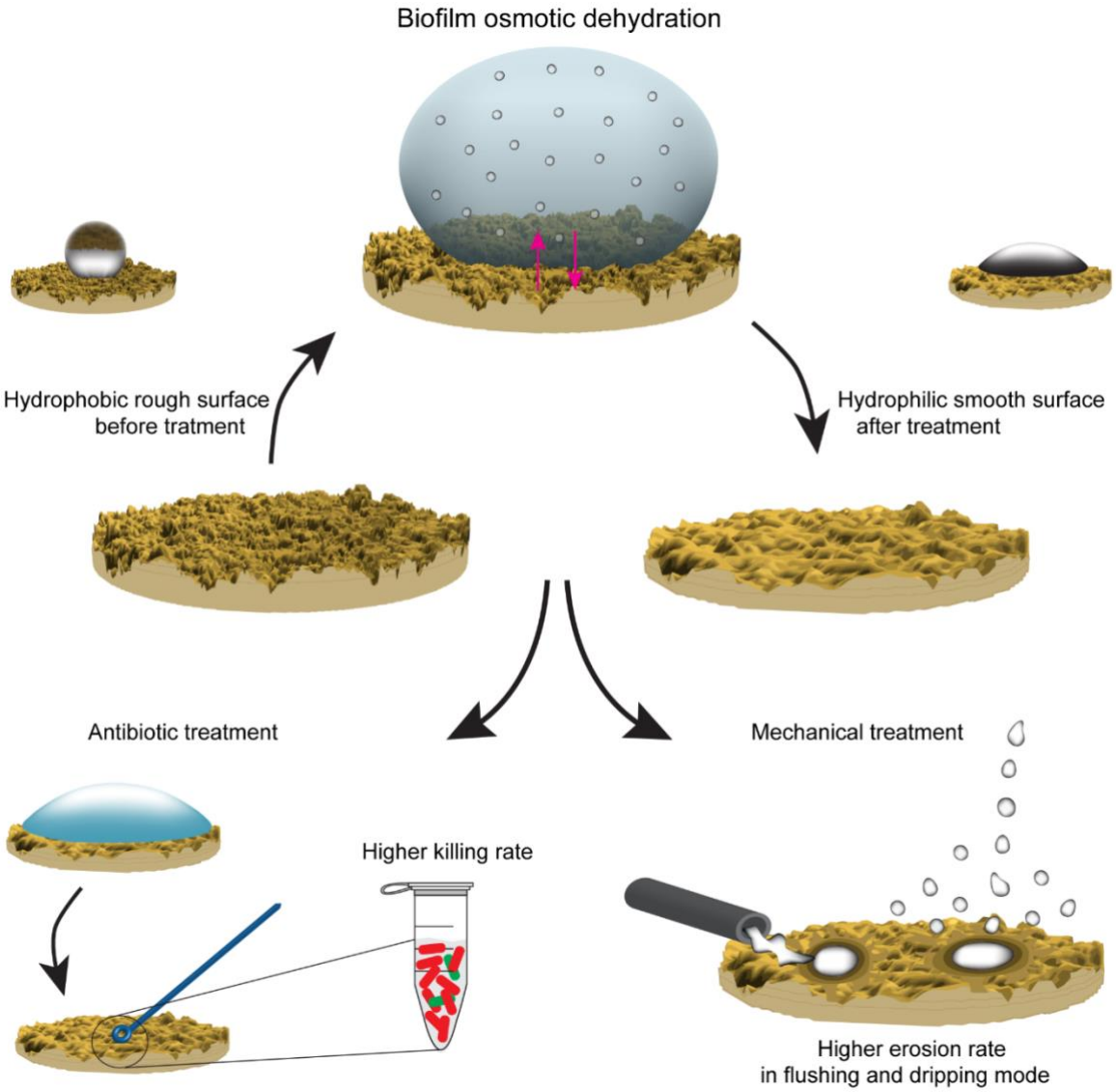

Figure 43 *Procedural summary*. The biofilm wetting resistance can be modified by incubating the biofilm surface with highly concentrated solutions that induce osmotic pressure. In parallel to this wetting modification, micro-topographical alterations of the biofilm surface occur. This suggests that mainly physical mechanisms are responsible for the observed alteration in wetting resistance. As a result of the osmotic treatment, a higher efficiency of antibiotic solutions towards biofilm bacteria is observed, and the biofilm samples show higher erosion rates when exposed to dripping or flowing water.

4.2 [e]Metal ion solutions as biofilm control agents against superhydrophobicity

As established before, surface superhydrophobicity makes bacterial biofilms very difficult to fight, and it is a combination of their matrix composition and complex surface roughness which synergistically protects these biomaterials from wetting. Although trying to eradicate biofilms with aqueous (antibiotic) solutions is common practice, it was shown in the previous section that this is a futile approach when biofilms have superhydrophobic properties. To date, most of the focus is aimed at developing strategies to inactivate the biofilm material without much consideration that their surfaces can remain impervious to such advances. In the previous section, a strategy where osmotic solutions were used as superhydrophobicity weakening agents was introduced. However, besides the latter, not many options are available to reduce the liquid repellency of biofilms or to prevent this material property from developing in the first place. Here, another solution to this challenge is presented using the model strain *Bacillus subtilis* NCIB 3610 and low concentrations of metal ions commonly found in the environment. Using a combination of microbiological and biophysical methods, it is demonstrated that the addition of metal ions such as copper and zinc during or after biofilm formation can render the surface of otherwise superhydrophobic biofilms completely wettable. An unspecific dampening of matrix promoting genes is observed for biofilms grown in the presence of metal ions, which might cause the formation of biofilm surfaces with almost unperceivable roughness features. As a result of the metal ion exposure presented here, these smoother, hydrophilic biofilms are more susceptible to aqueous antibiotics solutions. This strategy proposes a scalable and widely applicable step in a multi-faceted approach to eradicate biofilms.

4.2.1 Cultivation of NCIB 3610 biofilms in the presence of metal ions

Throughout this dissertation and some cases in literature, the formation of *B. subtilis* biofilms with strongly liquid-repellent surfaces has been reported at different growth conditions and on different liquid and semi-solid agar-substrates [26, 73, 77, 88]. Here, two biofilm types were selected as model systems to observe the effect of metal ions on biofilm surface and matrix characteristics: initially rose-like and initially lotus-like *B. subtilis* NCIB 3610 biofilms. Consistent with previous results (section 3.2), when NCIB 3610 bacteria were cultivated on LB medium at 30 °C for 24 h, biofilms with moderate surface roughness (***Sdr*** ~ 175 %) and rose-like wetting behavior were formed (Fig. 44a). In contrast, when the cultivation medium was enriched with glycerol and Manganese sulfate (= LBGM medium), biofilms with a higher surface complexity (***Sdr*** ~ 260 %) were obtained, and such biofilms behaved lotus-like hydrophobic (Fig. 44b). However, regardless of the original biofilm characteristics, when the medium in the agar-substrate was supplemented with $ZnCl_2$ or $CuSO_4$, the same bacterial cells almost always generated biofilms whose surface hydrophobicity was lost; at the same time, the roughness features on these biofilm surfaces were greatly reduced (Fig. 44a-c). Only for WT

[e] This section follows in part the publication: "*Effect of metal ions on B. subtilis NCIB 3610 biofilm surface hydrophobicity and antibiotic susceptibility*" submitted on 2019.

biofilms cultivated on LBGM medium, the presence of $ZnCl_2$ during biofilm growth led to colonies with a more variable wetting behavior (Fig. 44b): whereas colonies with hydrophilic surfaces were obtained in most cases, some colonies behaved hydrophobic. Still, also here, when compared to biofilms cultivated on standard LBGM agar, a significant reduction in the average surface hydrophobicity was achieved by the presence of $ZnCl_2$. Interestingly, the opposite effect was observed when the same bacteria were cultivated on $Al_2(SO_4)_3$ enriched agar; here, the biofilms showed increased surface complexity and their hydrophobic character was maintained (Fig. 44a-b).

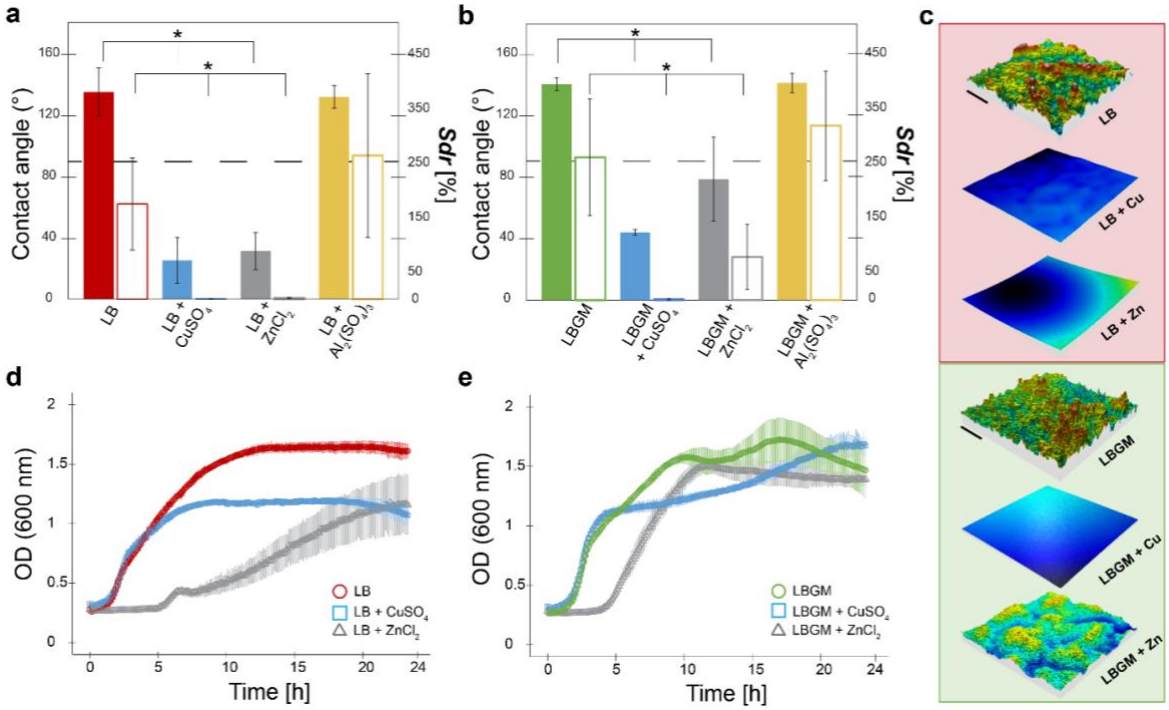

Figure 44 *Effect of metal ions on B. subtilis NCIB 3610 biofilms surface wetting and topography, and impact on growth kinetics of planktonic bacteria.* **a-b)** Contact angle (solid bars) and ***Sdr*** (empty bars) values for biofilms cultivated on LB **(a)** and LBGM **(b)** agar with and without one of the following metal ions: $CuSO_4$ (1.5 mM), $ZnCl_2$ (0.5 mM) or $Al_2(SO_4)_3$ (1.5 mM). The dashed line separates hydrophilic (< 90°) from hydrophobic (> 90°) behavior. Error bars denote the standard deviation as calculated from at least 9 independent samples ($N \geq 3$, $n \geq 3$). Stars denote statistical significant differences, where $p = 0.05$. **c)** Profilometric images of biofilms grown in normal and stress conditions, the scale bar denotes 0.2 mm in *x* and *y*; the *z* scale for LB samples (red background) is max. 110 µm and 150 µm for LBGM samples (green background). **d-e)** OD values determined for planktonic bacteria grown in LB **(d)** and LBGM **(e)** liquid media over time both at normal and stress conditions. Error bars denote the standard deviation as calculated from at least 12 independent samples ($N \geq 3$, $n \geq 4$).

Although the concentrations of $ZnCl_2$ and $CuSO_4$ used here (0.5 and 1.5 mM, respectively) are sufficiently high to affect the macroscopic properties of biofilms (Fig. 44c), at the same time, these low concentrations do not totally inhibit planktonic bacterial growth (Fig. 44d-e). Indeed, planktonic growth of *B. subtilis* only shows slightly altered kinetics when Copper or Zinc were present in the liquid media. In the case of LB medium, growth was retarded in the presence of Zinc whereas, in the presence of Copper, similar growth kinetics were measured as for the control –albeit with lower final OD values (Fig. 44d). A similar trend is observed for growth in LBGM medium: here, Zinc delayed the entry into exponential growth of WT *B. subtilis*,

whereas in the presence of Copper a similar curve was obtained as for the control. For all growth tests conducted in LBGM media, the final OD values are similar (Fig. 44e). Furthermore, when the same concentrations of metal ions were used to supplement the LB medium of planktonic WT bacterial cultures, incubation overnight resulted in similar ATP levels for all samples (Fig. 45). Both metal free and copper containing cultures show identical levels of ATP after planktonic growth, whereas Zinc-containing cultures show a slight but not significant reduction of this molecule (Fig. 45).

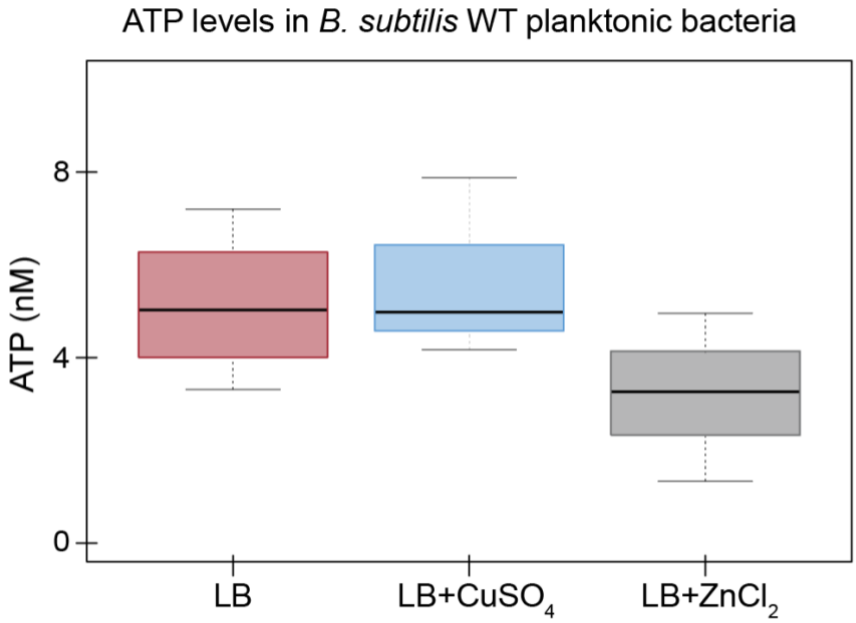

Figure 45 *Effect of metal ions on extracellular ATP of B. subtilis NCIB 3610 bacteria.* Boxes represent Q1-Q3, bold lines represent the median, and bars span from max. to min. ATP levels were determined from at least 6 independent samples ($n \geq 2$, $N = 3$). No statistically significant differences were found among the different samples, where $p = 0.05$. Metal ions were used in the following concentrations: 1.5 mM for $CuSO_4$ and 0.5 mM for $ZnCl_2$.

The metal ions used here for supplementation of the different media are essential for many cellular functions of the bacteria; nevertheless, in excess, they can also be lethal. An antimicrobial activity of Copper and Zinc ions has been widely reported with regard to protein binding, reactive oxygen species production, and membrane impairment [110]. Together, the previous observations show that the presence of subtoxic levels of selected metal ions during the cultivation of *B. subtilis* NCIB 3610 bacteria on agar substrates has a strong impact on the final morphological and physical characteristics of the formed biofilm. Also, these findings suggest that exposing mature biofilms to such metal ions could entail significant changes in the biofilm wetting resistance –and such a phenomenon could be used as a biofilm control strategy.

4.2.2 Effect of Copper and Zinc on NCIB 3610 biofilm matrix components

As discussed before in section 3.1, it is a combination of complex surface roughness and chemistry dictated by all matrix components –and not a single matrix component alone– that allows biofilms to establish their characteristic liquid repellency. Therefore, the next aim was to test if the presence of metal ions during biofilm growth disrupts the formation of hydrophobic biofilms by affecting the expression of genes responsible for the production of specific biofilm matrix components. For this purpose, *B. subtilis* strains harboring the P_{eps}-*gfp*, P_{bslA}-*gfp*, and P_{tapA}-*gfp* transcriptional reporters were used, which carry a promoter fusion to *gfp* gene (Table 1). To assess the general expression in the cells, a fourth reporter strain was used carrying a $P_{hyperspank}$-*gfp* construct (Table 1). First, as described above for the WT strain, these reporter strains were incubated in liquid media to assess the stress induced by the metal ions on the growth kinetics. Here, metal-induced stress altered the growth of all reporter strains in a similar way observed on the non-labelled WT (Figs. 46a and 47a). Next, the different reporter strains were grown on agar enriched with Copper (1.5 mM) or Zinc (0.5 mM), and the surfaces of the biofilm colonies were imaged with fluorescence microscopy. From those images, fluorescence intensity values were calculated and compared to normal growth conditions, i.e. to those obtained from biofilms grown on standard nutrient medium. As illustrated in Fig. 46, initially hydrophobic rose-like biofilms show the highest average fluorescence for the P_{bslA}-*gfp* strain, followed by the P_{tapA}-*gfp* and the P_{eps}-*gfp* strains, respectively.

When biofilms were grown in the presence of $CuSO_4$, a significant reduction in fluorescence was observed for biofilms formed by the P_{tapA}-*gfp* and the P_{bslA}-*gfp* strains, compared to those cultivated on standard LB-agar (Fig. 46b-c). In contrast, when grown in the presence of $ZnCl_2$, a significant reduction in fluorescence was only observed for the P_{tapA}-*gfp* strain, whereas the opposite trend was observed for the P_{bslA}-*gfp* strain (Fig. 46b-c). The P_{eps}-*gfp* strain was able to form biofilms with similar fluorescence –independent of the media the strain was grown on (Fig. 46b-c).

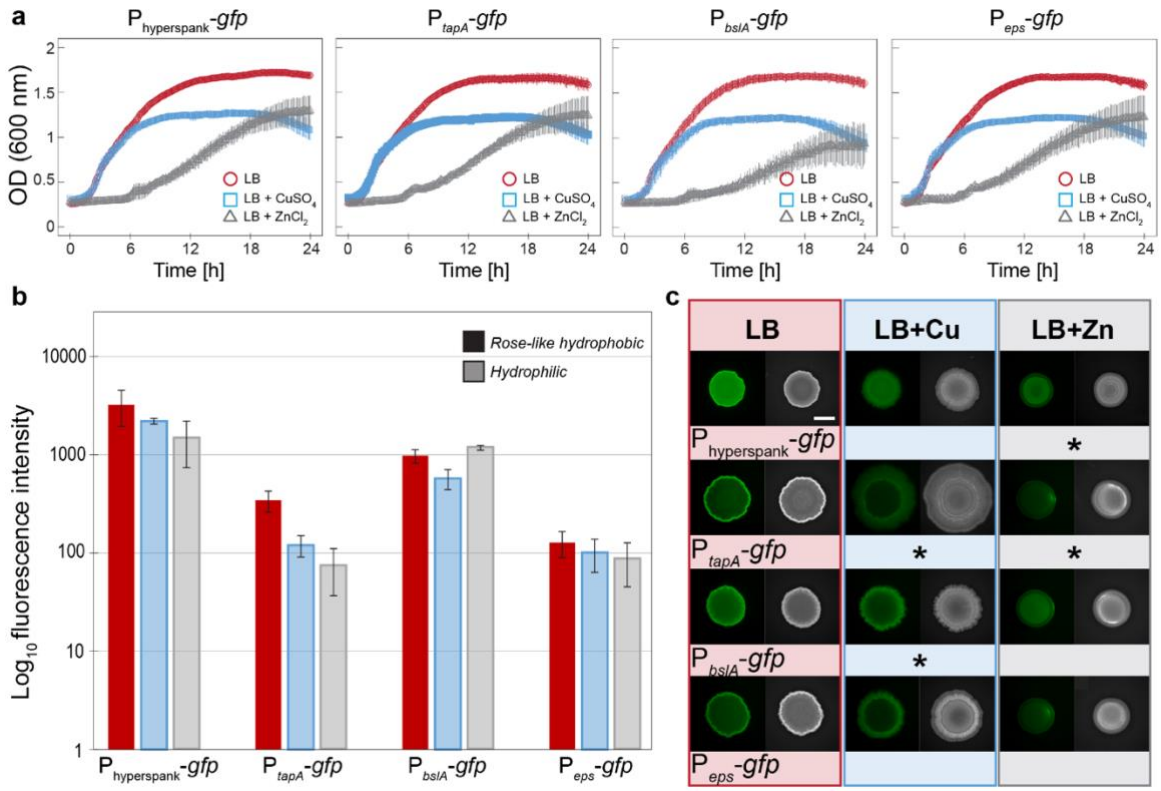

Figure 46 *Effect of $CuSO_4$ and $ZnCl_2$ on the planktonic growth kinetics of GFP-labelled B. subtilis NCIB 3610 strains in LB, and fluorescence of biofilm colonies generated by those strains on LB agar.* **a**) OD values were determined for planktonic bacteria at 600 nm. Bacteria were grown in LB liquid medium over ~24 h, both at normal and stress conditions. The error bars denote the standard deviation as determined from at least 6 independent samples ($n \geq 2$, $N \geq 3$). **b)** Relative fluorescence values determined for biofilm colonies grown on LB agar with and without $CuSO_4$ or $ZnCl_2$ ions, respectively. The error bars denote the standard deviation as calculated from 9 independent samples ($n = 3$, $N = 3$). **c)** Fluorescence and bright field images of the different biofilm colonies characterized in **(b)**; stars represent a significant reduction of fluorescence values when compared to biofilms grown on standard LB agar, where $p = 0.05$. Scale bar in **(c)** indicates 5 mm and is valid for all images. Throughout the figure, the colors indicate the type of media used for cultivation: red = LB; blue = LB + $CuSO_4$; grey = LB + $ZnCl_2$.

When the reporter strains were grown on LBGM agar where they generate lotus-like biofilms, a similarly high average fluorescence was measured for the P*tapA*-*gfp* and P*bslA*-*gfp* strains, whereas the P*eps*-*gfp* samples returned the lowest values (Fig. 47b). However, when these biofilms were grown in the presence of Copper or Zinc, an overall under-expression of matrix promoting genes was observed, and *tapA* and *eps* operons were most prominently affected (Fig. 47b-c). Importantly, the metal ions not only affected the expression of specific biofilm matrix components, but appear to have a general impact on fluorescent protein levels, including the control reporter strain (Phyperspank-*gfp*), in which similarly lower fluorescence values were detected when grown on agar enriched with Copper or Zinc compared to standard LB or LBGM agar, respectively (Figs. 46 and 47).

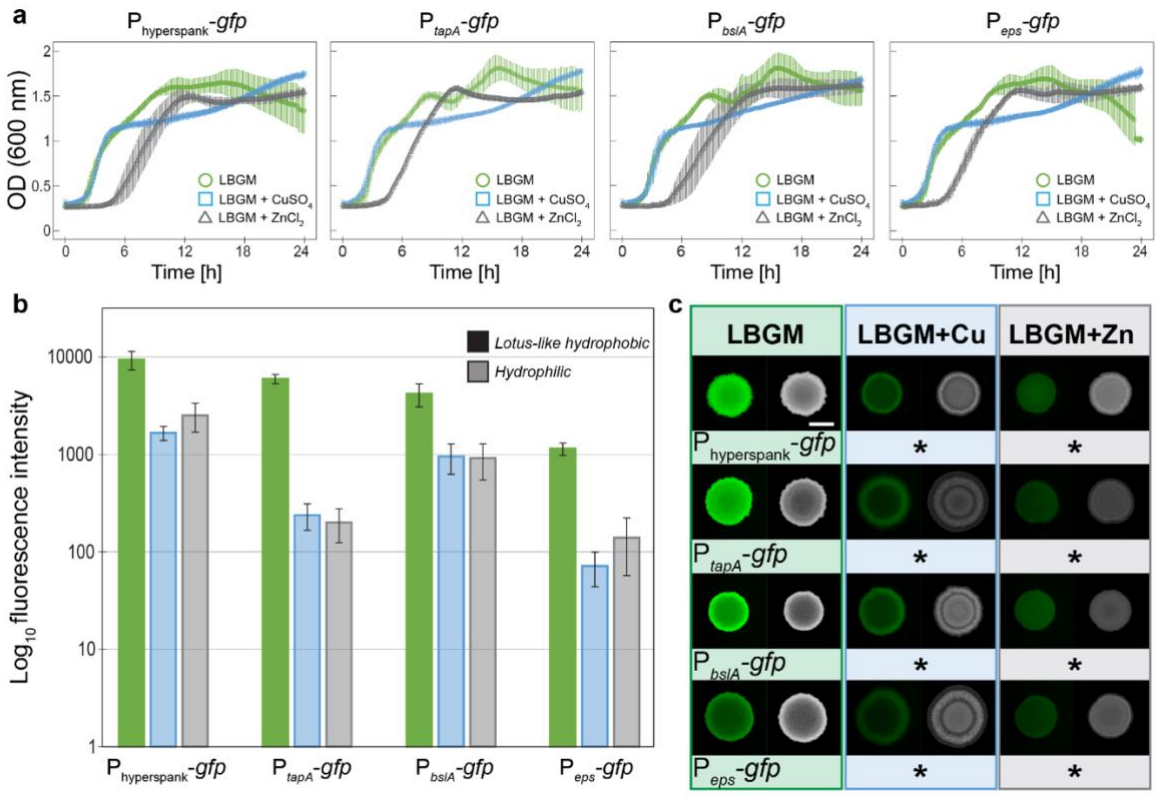

Figure 47 *Effect of $CuSO_4$ and $ZnCl_2$ on the planktonic growth kinetics of GFP-labelled B. subtilis NCIB 3610 strains in LBGM, and fluorescence of biofilm colonies generated by those strains on LBGM agar.* **a)** OD values were determined for planktonic bacteria at 600 nm. Bacteria were grown in LBGM liquid medium over ~24 h, both at normal and stress conditions. The error bars denote the standard deviation as calculated from at least 6 independent samples ($n \geq 2$, $N \geq 3$). **b)** Relative fluorescence values for biofilms grown on LBGM agar with and without $CuSO_4$ or $ZnCl_2$ ions, respectively. The error bars denote the standard deviation as calculated from 9 independent samples ($n = 3$, $N = 3$). **c)** Fluorescence and bright field images of the different biofilm colonies characterized in **(b)**; stars represent a significant reduction of fluorescence values when compared to biofilms grown on standard LBGM agar, where $p = 0.05$. Scale bar in **(c)** indicates 5 mm and is valid for all images. Throughout the figure, the colors indicate the type of media used for cultivation: green = LBGM; blue = LBGM + $CuSO_4$; grey = LBGM + $ZnCl_2$.

As an additional control ensuring that the alteration in biofilm colony fluorescence reported here is not a result from a direct influence of the metal ions on the green fluorescent protein, the stability of this protein was tested in the presence of Copper and Zinc. Of course, the pH of solutions containing either $CuSO_4$ or $ZnCl_2$ are acidic, but it is indicated in the literature that GFP should be stable in a pH range from 6 to 10 [175]. When the fluorescence of purified GFP mixed with $CuSO_4$ and $ZnCl_2$ solutions (at final concentrations of 1.5 and 0.5 mM, respectively) was analyzed both at acidic and neutral pH, it was observed that the fluorescence intensity of the protein was not affected when the metal ion containing solutions were neutralized with TRIS buffer (Fig. 48). Furthermore, the pH of the nutrient media (with and without agar) used for bacterial cultivation was determined to be ~6.2 with 1.5 mM $CuSO_4$ and ~6.7 with 0.5 mM $ZnCl_2$, which is still in the range of stability reported for GFP.

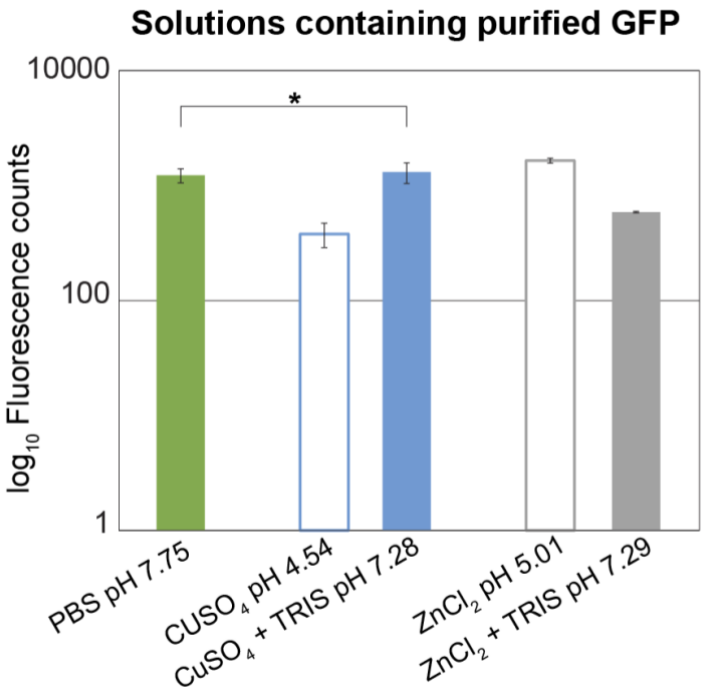

Figure 48 *Effect of pH induced by the addition of metal ion solutions on purified GFP.* Error bars denote the standard deviation as calculated from 6 individual samples (n = 6). Stars denote statistically significant differences, where p = 0.05. Here, only the fluorescence of the neutralized Copper solution is not significantly different to that of the purified GFP.

Together, these results suggest that biofilm cultivation under ionic stress is possible but –in most cases– suffers from an unspecific under-expression of genes, and this includes diminishing the production of biofilm matrix components. Together with the assessment of biofilm wetting and topography discussed above, it is indicated that this reduced availability of matrix components is responsible for a less developed surface topography and thus a reduced wetting resistance of the biofilm colonies.

4.2.3 Antibiotic sensitivity of NCIB 3610 biofilms grown in the presence of Copper and Zinc

As reported in section 4.1, biofilms with superhydrophobic surfaces are less susceptible to treatment with aqueous antibiotic solutions than biofilms with hydrophilic surfaces [73]. Hydrophilic biofilm surfaces allow for full wetting and, subsequently, enable the entrance of the antibiotic molecules into the biofilm matrix. This is a necessary step for the antibiotic to come in contact with the biofilm bacteria so it can take effect. On superhydrophobic biofilm surfaces, there is –in addition to a chemistry-based water repellency– a physical barrier provided by the roughness features. In the case of lotus-like superhydrophobicity, this complex topography entails the formation of a microscopic air cushion on the biofilm surface that largely prevents direct contact between the antibiotic and the biofilm bacteria. Thus, next it was tested if the two metal ions, Cu^{2+} and Zn^{2+}, as a direct consequence of preventing the formation of superhydrophobic biofilm surfaces, also increase the efficacy of two clinically relevant antibiotics (Tetracycline and Kanamycin) towards biofilm-embedded bacteria. In

brief, biofilms were cultivated on either LB or LBGM media (both, in the presence and absence of metal ions), and the mature biofilms were scraped from their substrate and treated for 1 h with antibiotic aqueous solutions (using antibiotic concentrations of 1.28 mg/mL each, corresponding to ~150x MIC_{90}). Then, CFUs were determined to assess the number of viable cells (section 2.4.2.2, Fig. 11).

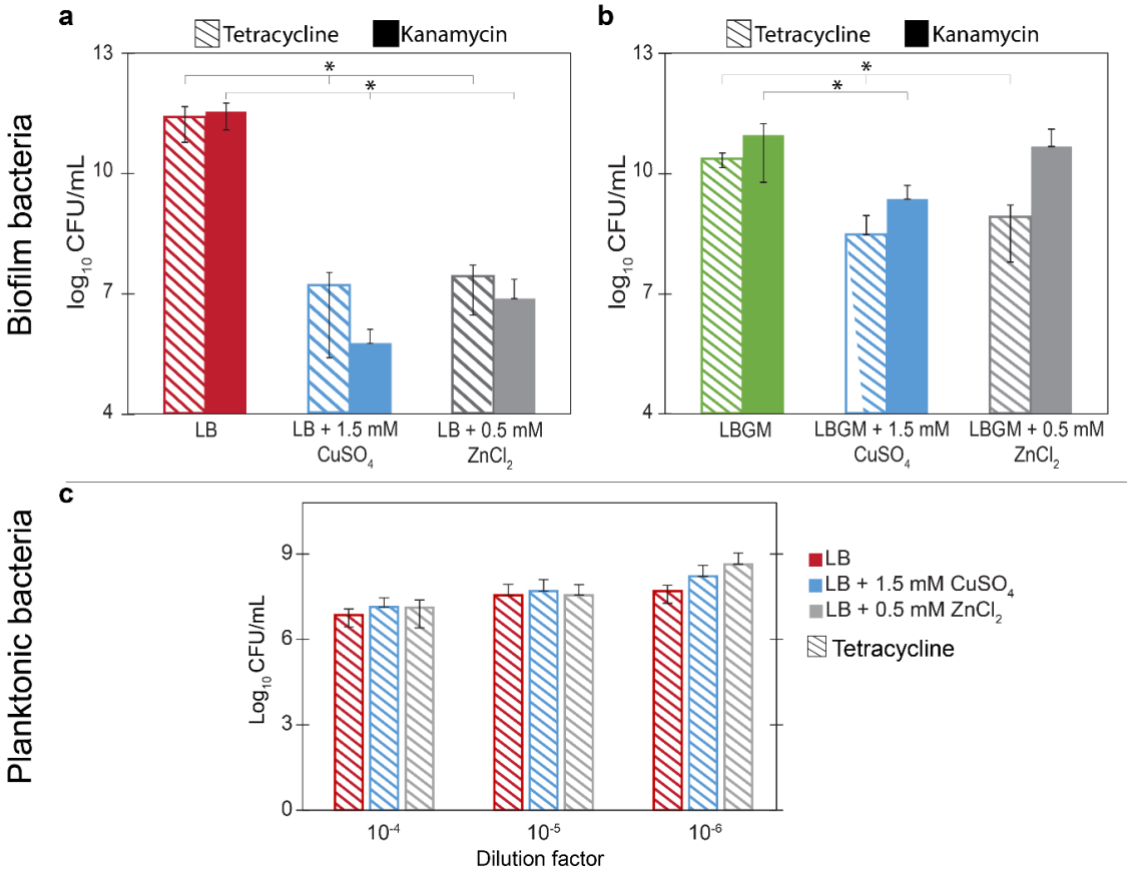

Figure 49 *Efficacy of aqueous antibiotic solutions on B. subtilis NCIB 3610 biofilms and planktonic bacteria cultivated in the presence of metal ions.* **a-b)** Log_{10} CFU/mL values determined after a 1 h treatment with either Tetracycline (dashed bars) or Kanamycin (solid bars) at a final concentration of 1.28 mg/mL. The tested biofilms were grown on LB **(a)** or LBGM **(b)** agar with and without $CuSO_4$ or $ZnCl_2$. Error bars denote the standard deviation as calculated from at least 6 independent samples ($N \geq 3$, $n \geq 2$). **c)** Log_{10} CFU/mL values after 1 h treatment with Tetracycline (8 µg/mL) on planktonic bacteria cultivated with and without $CuSO_4$ or $ZnCl_2$. Error bars denote the standard deviation as calculated from at least 9 independent samples ($N \geq 3$, $n \geq 3$). **(a-c)** Stars denote statistically significant differences, where $p = 0.05$.

In agreement with the expectations, cells retrieved from biofilms grown on LB agar and in the absence of Zn^{2+} or Cu^{2+} (i.e. for rose-like superhydrophobic biofilms) showed significantly improved survival (higher amount of viable bacterial cells) after an hour treatment with either Tetracycline or Kanamycin than cells retrieved from hydrophilic biofilms (Fig. 49a) that were generated in the presence of $CuSO_4$ or $ZnCl_2$. Similarly, treatment with Tetracycline on biofilms grown on LBGM medium showed a significantly higher amount of viable bacterial cells in the absence of the metal ions (lotus-like superhydrophobic biofilms) than in the presence of $CuSO_4$ or $ZnCl_2$ (hydrophilic biofilms) (Fig. 49b). In contrast, when the same LBGM-grown biofilms were treated with Kanamycin, a significant reduction in viable cells

was observed only for biofilms grown on $CuSO_4$ containing medium (Fig. 49b). The latter finding is not surprising considering that a more variable wetting behavior was detected for biofilms grown on LBGM agar containing $ZnCl_2$: for those samples, the biofilm surfaces were completely hydrophilic in some cases, but occasionally also slightly hydrophobic (Fig. 44b). Thus, it is suspected that the sample-to-sample variations obtained for biofilms cultivated in the presence of $ZnCl_2$ might be directly responsible for the variations in Kanamycin efficiency visible in Fig. 49b.

An increased occurrence of both, antibiotic resistance and bacterial persistence, in stress rich environments has been established, particularly for Copper and Zinc cations as they are generally found in the environment [176]. Even at subtoxic levels of Copper in contaminated soil, the occurrence of antibiotic resistance genes has been observed for certain bacteria [176]. To ensure that the increased antibiotic efficiency is a direct result from the reduced protection by the biofilm matrix and does not stem from a weakening effect that acted on the bacterial cells during planktonic growth under stress, the same antibiotic treatment method was applied to planktonic bacteria. Here, only Tetracycline was used as it showed the highest efficiency in the previous tests conducted with biofilm bacteria. Again, a similar CFU plating method was used to assess bacterial viability after the chemical challenge (section 2.4.2.2). Indeed, in agreement with the expectations, treatment of planktonic bacteria with Tetracycline resulted in no significant differences in viability – whether metal ions where present during planktonic growth or not (Fig. 49c). These results underscore the importance of the physical barrier conferred by the matrix on biofilm cells and how they rely on it for stress protection.

4.2.4 Effect of Copper and Zinc ions on mature NCIB 3610 biofilms

So far, it was tested if and under which circumstances the formation of superhydrophobic biofilms can be prevented by the presence of certain metal ions. However, such a strategy is only useful if the biofilms have not formed yet. The effect of metal ions on already formed biofilms has been studied mainly regarding their impact on the bulk mechanical properties but not much on the physical surface properties of biofilms. For instance, selected metal ions have been shown to affect the viscoelastic properties of biofilms protecting them from erosion [147, 177], and divalent ions increase the biofilm stiffness through a higher calcium carbonate content, which in turn, can form diffusion barriers that shelter the inner biofilm mass [178, 179]. Indeed, the latter examples actually describe protective effects provided by the metal ions, whereas, here, the focus is on the opposite effect.

In section 4.1, it was shown that altering the wetting properties of mature biofilms from superhydrophobic to hydrophilic can improve biofilm eradication methods which involve the use of aqueous solutions, and that this can be achieved by incubating the biofilm surfaces with concentrated solutions inducing osmotic surface dehydration effects [73]. Motivated by those previous findings, it was assessed next, whether the wetting resistance of already existing biofilms can also be altered if they are further cultivated but exposed to a liquid environment enriched with low concentrations of metal ions. For this purpose, *B. subtilis* NCIB 3610 biofilms with superhydrophobic surfaces were first generated on agar and then this agar

substrate carrying those mature (1 day old) biofilms was partially immersed into liquid media containing metal ions. In other words –different from the previous study, where the air-exposed surface of biofilms was brought into contact with a conditioning solution. Here, the metal ion enriched medium was allowed to diffuse into the biofilm matrix *via* the agar substrate. Experimentally, this was achieved by dedicated, porous sample holders which were used to carry both, the agar substrate and the cultivated biofilm (Section 2.2.3, Fig. 4).

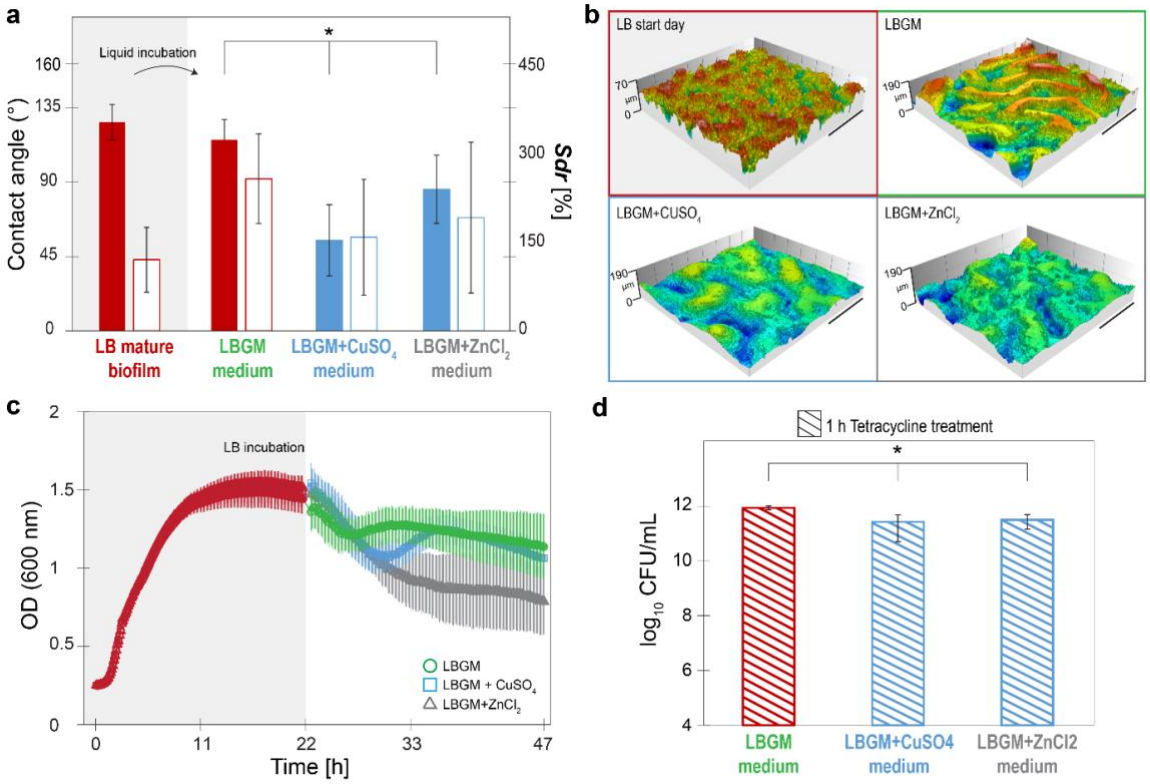

Figure 50 *Effect of metal ions diffusing through the substrate of mature B. subtilis NCIB 3610 biofilms on surface wetting and topography, planktonic growth kinetics, and antibiotic efficacy*. **a)** Contact angle (solid bars) and ***Sdr*** (empty bars) values of initially rose-like superhydrophobic mature biofilms before and after substrate-infusion with liquid LBGM medium with and without $CuSO_4$ or $ZnCl_2$. **b)** Profilometric images of the different biofilms characterized in **(a)**; the scale bar represents 0.3 mm in both the x- and y-axes. **c)** OD values determined at 600 nm for planktonic bacteria initially grown in liquid LBGM medium (for 22 h, red symbols) and then supplemented with LBGM liquid medium with and without $CuSO_4$ or $ZnCl_2$. **d)** Log10 CFU/mL values determined after 1 h treatment with Tetracycline. The tested mature biofilms were incubated with their agar substrate infused with LBGM medium infused with and without $CuSO_4$ or $ZnCl_2$. In **(a)** and **(d)**, stars denote statistically significant differences, where $p = 0.05$; bar color indicate the wetting behavior of the characterized samples; red=rose-like hydrophobic, blue=hydrophilic. In **(a)**, **(c)** and **(d)**; error bars denote the standard deviation as calculated from samples grown on at least three different days; **(a)**: ($n \geq 2$, $N \geq 6$), **(c)**: ($n = 32$, $N = 3$), **(d)**: ($n = 3$, $N = 3$).

Before determining the influence of metal ions on the wetting properties of biofilms, it was verified that the transfer procedure itself, i.e. growing the mature biofilms for another 24 h, does not alter their wetting behavior. Pre-tests showed, that, for rose-like hydrophobic biofilm samples grown on LB agar, a transfer into LBGM medium is necessary to maintain their rose-like wetting properties. As at those conditions the biofilm kept growing, the biofilm surface complexity was increased during this additional day of incubation (Fig. 50a). The same change

in nutrient media, and thus in growth conditions, was also applied to planktonic bacteria; although a slight decline in the growth curves was observed when the metal ions were added, the remaining OD was still reasonably high (Fig. 50c).

When initially rose-like mature biofilms were further cultivated in LBGM medium containing either 1.5 mM $CuSO_4$ or 0.5 mM $ZnCl_2$, the biofilms became wettable with contact angles < 90° (Fig. 50a). At the same time, those hydrophilic biofilms (compared to the ones that were further cultivated in standard LBGM) showed reduced surface roughness, which can be attributed to the presence of the metal ions (Fig. 50a-b). Again, a high variability in both, the measured contact angle and ***Sdr*** values was observed for mature biofilms exposed to $ZnCl_2$-containing LBGM liquid medium: some samples behaved slightly hydrophobic and others strongly hydrophilic (Fig. 50a). Yet, for all samples exposed to the metal ions, their superhydrophobic properties disappeared and –on average– their surface features were considerably lower than for the control samples (Fig. 50a-b). This shows that the effect of $CuSO_4$ and $ZnCl_2$ on preventing the formation of superhydrophobic biofilm surfaces is not limited to newly formed biofilms, but can also occur when a mature biofilm has already been established.

Finally, the efficacy of an antibiotic solution on mature biofilms whose surface wetting properties were tuned from rose-like superhydrophobic to hydrophilic was tested. For this purpose, the antibiotic that showed the strongest efficiency in the previous tests was chosen, i.e., Tetracycline. Also here, the entire treated biofilm mass was harvested from the substrate and exposed to an aqueous solution of 1.28 mg/mL Tetracycline for 1 h before determining CFUs. Interestingly, compared to biofilms cultivated on agar for one day only, mature biofilms that were further incubated for another day showed overall a stronger resilience towards the antibiotic, i.e., both, in the presence and absence of metal ions (Fig. 50d, Fig. 49a-b). One interpretation of this finding could be that there is a greater biological advantage for cells grown in normal conditions when they get exposed to a combination of stress and more nutrients – transfer from LB medium to LBGM medium provides such a situation where more nutrients are offered to a mature biofilm. Another interpretation would be that, after an additional day of incubation, there could be a higher amount of spores. However, if metal ions are added to the LBGM medium, into which the mature biofilms are transferred, two effects are observed: first, the biofilm surfaces become hydrophilic and, second, after an antibiotic challenge, significantly lower numbers of CFU/mL are found compared to the hydrophobic rose-like biofilms (Fig. 50d).

4.2.5 Would it be possible to design a one-step solution to efficiently eradicate bacterial biofilms?

It was shown here that the presence of the metal cations Cu^{2+} or Zn^{2+} during the cultivation of NCIB 3610 bacteria induces changes in the resulting biofilm matrix, and said changes alter the biofilm surface in such a way that otherwise superhydrophobic biofilms become completely wettable. Furthermore, the same low concentrations of metal ions induce very similar effects on mature biofilms when they are diffused through the substrate the biofilms are grown on. In both cases, an increased bacterial inactivation is observed when the entire biofilm material is treated with aqueous solutions containing antibiotics.

As discussed before, abolishing or at least weakening the superhydrophobic properties of biofilms can be an important step in fighting such sturdy materials: if successful, it allows for a more efficient accessibility of the embedded bacteria towards mechanical or chemical attack. Of course, finding a one-step, gold standard solution that is able to eliminate all kinds of biofilms would be optimal; yet, considering the broad variety of biofilm-forming microorganisms and the large differences in the molecular composition of the matrices they form, this appears unrealistic. Thus, a multi-faceted approach combining inhibition, pre-conditioning, inactivation and/or dispersal steps is likely to be the most efficient strategy to control biofilms. Pre-conditioning approaches, that is, treatment of the material before the use of antibiotics, can be a promising strategy for enabling a complete eradication of biofilms; other studies have shown that the effect of antibiotics can be enhanced in different ways: i.e. by using electrochemical scaffolds on chronic wounds [180] or by disrupting the EPS biopolymers [108]. Furthermore, not only chemical but also mechanical attack can be facilitated by pre-conditioning, as an enhanced biofilm erosion has been reported for hydrophilic and/or smooth biofilms compared to rough and/or hydrophobic ones [73, 181].

The method presented here introduces such a pre-conditioning strategy which targets a physical property of biofilms, i.e. their wetting resistance. The results presented here show that low concentrations of metal ions are sufficient to disturb the production of biofilm matrix components, and that this effect unspecifically targets different biomolecules at the same time. The latter indicates that the approach introduced here could also be applicable to biofilms generated by other bacterial species. As the metal ions can be applied to biofilms in the form of an aqueous solution, it should be possible to target different forms of biofilms at different stages of their development and in different growth environments.

5 Discussions & Outlook

In this dissertation, biofilm surface superhydrophobicity was described as a result of chemical and physical contributions provided by the matrix biomolecules, which in turn, give rise to topographical features that grant these bio-surfaces with different wetting behaviors. Furthermore, the knowledge acquired from the relation between biofilm surface topography and wetting was turned against these bio-surfaces, using it to target their liquid repellency.

Across a variety of bacterial strains and environmental conditions, three types of biofilm surfaces were found: hydrophilic, high-adhesion hydrophobic (rose-like), and low-adhesion hydrophobic (lotus-like). First, an extensive metrological characterization of their surface was performed in terms of their most pronounced features, i.e. the waviness of the two hydrophobic biofilms was assessed with both the ***Sal*** parameter and a Fourier analysis, resulting in similar impressions: highest waviness was found for lotus-like and lowest for both hydrophilic and rose-like biofilms. However, the spacing between smaller surface features was not discussed in detail even though it is an important parameter that can differentiate between rose-like and lotus-like surfaces; this is normally referred to as "pitch". It has been shown that hierarchical, rough surfaces with high adhesion towards water possess a larger pitch size within their microstructures, whereas surfaces with low-adhesion exhibit a smaller pitch size [3]. A surface parameter introduced in section 3.1.1, the root-mean-square surface slope, ***Sdq***, combines both roughness as well as spacing information; i.e. for two surfaces with identical roughness, a lower ***Sdq*** value indicates a texture which is spaced more widely. Indeed, rose-like hydrophobic biofilms showed significantly lower ***Sdq*** values than lotus-like biofilms indicating a larger pitch size between the micro-roughness of the former. This finding allows for the following interpretation: the larger spacing between the roughness features of rose-like biofilm surfaces allows liquids to penetrate into the microscale resulting in a "high adhesion" state; however, the nano-features still allow for high static CA values [3] and moderate liquid contact (Fig. 51). The highest liquid repellency is observed for lotus-like biofilms, which exhibit minimum contact with the surface, whereas hydrophilic biofilms show low repellency (Fig. 51). Hence, the greatest impact of such an exhaustive characterization of biofilm surfaces is the resolution that the levels of liquid repellency found here are directly related to the biofilm susceptibility towards antibiotic solutions and mechanical erosion with water (Fig. 51), and that this knowledge can be used to fight or prevent the onset of such sturdy surfaces.

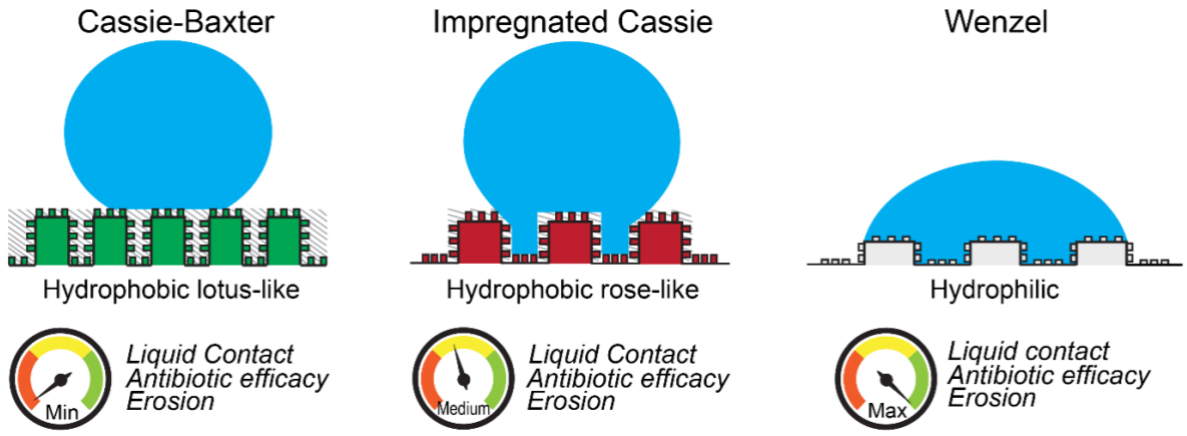

Figure 51 *Three different wetting behaviors were found on a wide variety of biofilm surfaces throughout this dissertation. Those wetting behaviors are directly related to topographical features of the biofilm surface, which confer different levels of protection from the environment.*

Nonetheless, when the analogy between surface topography and wetting behavior was extended, the delimitation among the three wetting regimes found here was slightly affected by the large variation in bacterial strains and environmental conditions (phase diagram in Fig. 25b). Certain overlap was found in the phase diagram depicting the surface complexity and CA values of several different biofilm surfaces exhibiting the three different wetting behaviors discussed before. Perhaps, using three levels of liquid repellency is a simplification of a possible multitude of wetting behaviors that can arise from such diverse samples. In fact, nine different wetting regimes have been identified in the literature for hierarchical rough surfaces [3] and their differences rely on the type of contact between the solid and the liquid phase. Thus, a topographical characterization coupled with liquid penetration studies could be used to quantify the fraction of biofilm surface area that can be wetted by liquids and, in turn, allow for a more sensitive categorization of these bio-surfaces in regard to their physical wetting regimes. The knowledge of relative values (e.g. percentages) of biofilm surface area in contact with liquids, for any given wetting behavior, could enable an estimation of the efficiency of biofilm treatment with aqueous antimicrobial solutions or mechanical erosion with liquids. Such an approach would further expand our understanding of the physical mechanisms behind the sturdy nature of bacterial biofilms and promote advances in fundamental research attempts to control them.

Regarding the compositional nature by which biofilms form superhydrophobic surfaces, it was demonstrated that disentangling the topography, wetting, and surface chemistry is not trivial. In fact, superhydrophobicity cannot take place without a topographical component, and the latter is not a result of only one protein. A time-resolved analysis of biofilms formed by *B. subtilis* NCIB 3610 revealed that the surface roughness is dictated by two main matrix biomolecules secreted by these bacteria; the BslA protein and the polysaccharide. It would be of great interest to extend such an analysis to bacterial strains with medical relevance and to study their surface topographical changes and wetting behavior over time. For instance, the strain *Vibrio cholerae* –a pathogenic microorganism, has been shown to form hydrophobic biofilms at the liquid air interface [182]. Additionally, several knock out

mutants lacking expression of specific matrix components have been identified for this strain [182, 183]. Therefore, with the method presented here, it should already be possible to use knock-out mutants of medically relevant strains to identify the biofilm matrix components responsible for an increased wetting resistance. The latter finding would help design more effective biofilm control strategies by targeting only those matrix components responsible for liquid repellency (Fig. 2). For instance, enzymatic degradation of biofilms is a common approach for exposing and targeting the bacteria within the matrix. Knowing which matrix components grant increased protection to the embedded bacteria could allow for designing more efficient enzymatic treatments.

Possibly, a time-resolved analysis of biofilm surfaces, could also allow for the identification of a time-point where the surface complexity development results in the onset of wetting resistance. Of course, not all bacteria can produce superhydrophobic biofilms, but due to the increased protection these microorganisms obtain when such property is present, it is important to recognize its development. For instance, five stages of biofilm development have been described in the literature; these stages have been thoroughly researched, and they have been accepted by the scientific community as the biofilm life-cycle [184]. As the study of biofilm wetting resistance is an area that remains underexplored, recognizing the onset of wetting resistance as a stage in biofilm development would allow for a deeper and more multidisciplinary understanding of these complex biomaterials (Fig. 52). The complexity of bacterial biofilms deserves attention from various disciplines, using descriptions and concepts that combine aspects from all disciplines would represent a step forward in an attempt to bring them closer.

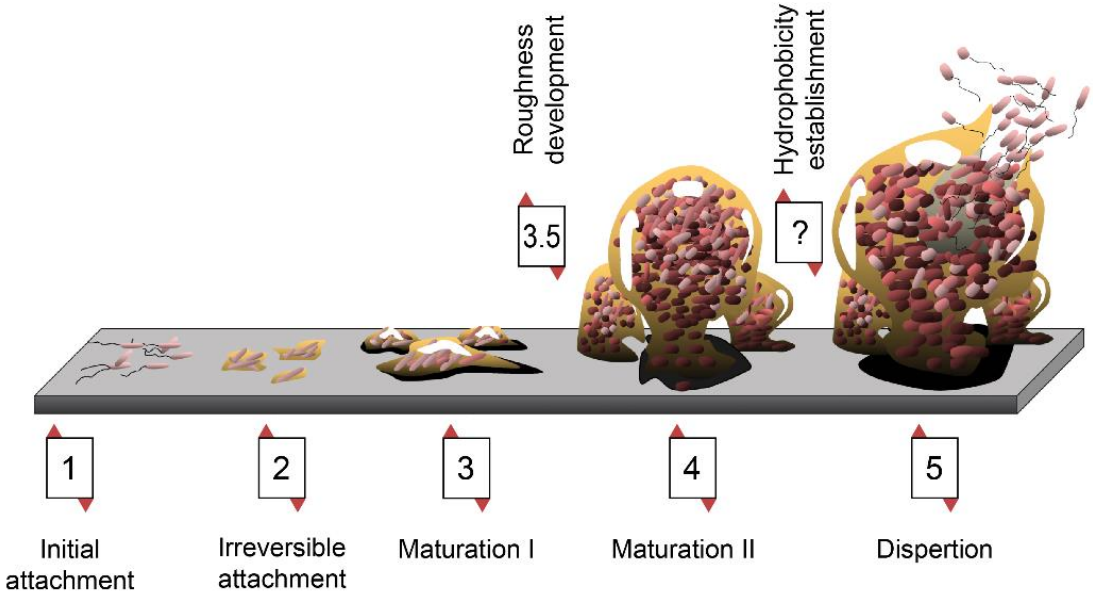

Figure 52 *Diagram showing the five stages of biofilm development (modified from Monroe, 2007 [184]).* Identifying the onset of surface hydrophobicity as one of the stages in biofilm development could allow for a deeper and more multidisciplinary insight into these biomaterials.

The key technique used throughout this dissertation for characterizing biofilms; light profilometry, allows for a fast, non-disruptive quantification of surface features. Here, coupled with wetting tests, it allowed to establish a link between the surface topography and the wetting behavior of biofilm colonies. Even for other biofilm forms i.e. pellicles formed at the liquid-air interface, such a link was also observed –albeit at lower overall roughness scales. Furthermore, this analogy was also useful in supporting findings from other areas of biofilm research like microbial evolution. In section 3.3, four products of diversification during evolution of *B. subtilis* NCIB 3610 were differentiated from each other and their ancestor *via* their biofilm surface characteristics. Hence, it would be interesting to see how far this analogy could go; although the technique should be fine-tuned for particular scenarios, it offers great potential. For instance, it was previously seen that for pellicle biofilms, which surfaces are smoother, parameters selected for quantifying the surface of biofilm colonies are not as efficient in describing such features. Hence, the study of evolved biofilms could require a new array of surface metrological parameters to be considered. Additionally, it was observed that small changes in the chemical compositions of the evolved biofilms can have a great impact on the studied surfaces; thus, methods that examine their composition, could be required. However, the flexibility and applicability of this analogy outweighs the efforts associated with the adaptation requirements. A possible application would be the study of bacterial evolution to antibiotic resistance in relation to biofilm morphology, surface topography, and wetting. Perhaps, genes that adapt to resist antibiotics could also be involved in physically fortifying the matrix; for instance, Dale *et al.* have shown that *Enterococcus faecalis* biofilms restructure in response to cellular stress induced by antibiotic exposure [185]. With regard to morphology, there are currently only a few studies indicating a relation between the structure of biofilms and antibiotic resistance. A study conducted by Farajzadeh Sheikh *et al*. with *Staphylococcus epidermidis* isolates showed a significant correlation between the capacity of biofilm formation and antibiotic resistance [186]. Whereas O'Connell *et al.* explored the influence of structure and antibiotic resistance on indirect pathogenicity of polymicrobial biofilms [187]. However, in both examples, a quantification of the biofilm structures was not performed. The latter observations indicate, that a quantitate study of biofilm morphological features such as height, surface topography and wetting (*via* light profilometry and wetting tests) in relation to antibiotic resistance (e.g. *via* genetic profiling) would be a novel approach to further advance the area of biofilm antibiotic resistance research.

Getting to know the biofilm surface in detail allows to exert control over these biomaterials. After identifying that surface topography has a great influence on the liquid repellency of biofilms, it was easy to hypothesize that there can be two routes to fight hydrophobicity: a chemical and a physical route (Fig. 2). In the last chapter of this dissertation, two strategies were presented that target biofilms' surface topography and as a result, their liquid repellency, representing examples of mainly physical treatment routes. First, a method using osmotic dehydration of biofilm surfaces with concentrated solutions of ethanol, salts, and sugar, showed a reduced liquid repellency of biofilms formed by three bacterial species with different matrix compositions –showing that the treatment method is not strain specific. However, this approach requires very high concentrations of ions or carbohydrates to take effect, and the incubation times needed for achieving a weakening of the biofilm wetting

resistance can be as high as 48 h. Also, high concentrations of salts or sugars can lead to unwanted side effects, such as accelerating corrosion on the biofilm-colonized material or serving as nutrients for other microorganisms. Hence, a second strategy, which makes use of metal ion solutions, was introduced next. Such method combines both physical, and in part, chemical routes, and could solve the problem of detrimental effects as the concentrations used here are very low and the metal ions are commonly found in the environment –making this strategy low-cost and low-risk. It was shown that exposure to Cu^{2+} and Zn^{2+} cations during or after biofilm formation can render the biofilm surfaces completely wettable. When the biofilms are incubated in the presence of the metal ions, this incubation process causes a dampening effect on the expression of matrix promoting genes –which, in turn, results in biofilms that have lost their characteristic surface roughness. Although this method was tested on one bacterial strain only, the effect on matrix gene expression was found to be unspecific, meaning that this treatment could yield similar results on other bacterial strains. Yet, further tests on other species would be needed to confirm the previous notion. Here, as well, long treatment times were required. Therefore, finding strategies such as the ones presented here that make use of mild biofilm control agents that can reduce biofilm liquid repellency after shorter exposure times would be ideal. For instance, the five-carbon sugar-alcohol xylitol shows both, solubility in water and antimicrobial activity [188]. This sugar-alcohol could be used as a more efficient osmotic agent to reduce biofilm hydrophobicity and, at the same time, induce chemical inactivation. For both strategies presented here, perhaps, inducing changes in temperature during treatment could help speed up the observed wettability changes.

Notably, both osmotic dehydration and metal ions exposure rendered the biofilms more susceptible to treatment with antibiotic solutions. The osmotic treatment also proved effective in enhancing biofilm erosion with water. Further tests would be required to confirm the efficiency of mechanical removal of biofilms exposed to metal ions –at both, early and late stages of biofilm growth. For the case of metal ion exposure since the beginning of cultivation, it is assumed that the formed biofilms could also be more susceptible to erosion than untreated ones due to a depleted biofilm matrix, which in turn, could have a weakening effect on the material's mechanical properties. A similar effect is expected to occur on mature biofilms exposed to metal ions; however, here, special care should be taken regarding the concentrations and types of metal ions used to induce changes in the material's surface hydrophobicity. It has been reported that selected metal ions induce ionic cross-linking of certain biofilm matrix components causing a fortification of the material's stiffness –as indicated by a higher elastic modulus, and in turn, its erosion stability [147, 158, 177]. Therefore, it is imperative to find an optimal combination of metal ions and concentrations capable of inducing changes in the biofilm wetting resistance but, at the same time, that avoid ionic cross-linking of the biofilm matrix components or a significant fortification of the matrix. Nevertheless, the findings obtained so far indicate that both methods introduced here: osmotic dehydration and metal ions exposure, entail surface pre-conditioning strategies capable of enhancing biofilm control attempts. The pre-conditioning strategies available in literature today are focused in promoting the efficiency of either chemical or mechanical biofilm removal; in contrast, the methods proposed here have the capacity to promote both.

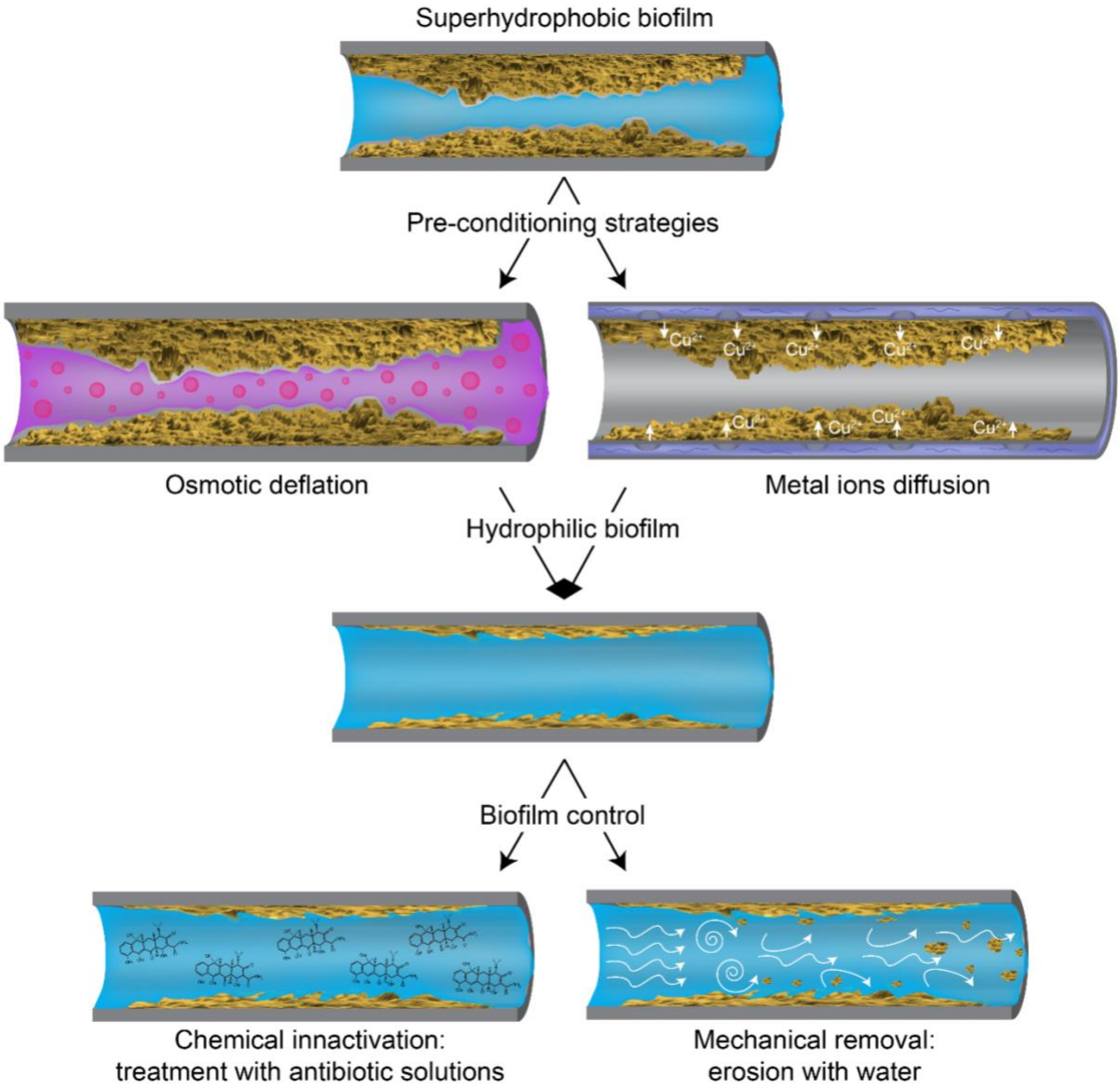

Figure 53 *Osmotic deflation and metal ions diffusion as mature superhydrophobic biofilm pre-conditioning strategies in pipe systems.*

It would be of interest to test if an enhanced mechanical removal can also be achieved when either method is applied to biofilms that are grown in the presence of water –often called *submerged* biofilms. These materials exhibit different mechanical properties than those grown exposed to air [189] and resemble real-life settings more closely, i.e. biofilms grown on pipes, catheters, water reservoirs, etc. The latter is of importance as, ideally, both pre-conditioning methods presented here could be applicable to such settings. As schematically illustrated in Fig. 53, for biofilms that have established in closed systems (such as pipes) an incubation step that includes the use of concentrated osmotic agents in the lumen, or diffusion of metal ions through a porous lining or hollow wall, could induce surface alterations and loss of hydrophobicity. Consequently, these biofilms would be rendered more susceptible to chemical inactivation and/or subsequent mechanical removal. Of course, applying either the osmotic deflation or metal ion treatments on existing systems would probably require adaptation of the

methods developed in the laboratory, the design of new systems, or the implementation of accessories to existing systems e.g. porous linings in existing tubing. However, the alternatives proposed here can be both, low cost and scalable.

In contrast to the line of argumentation followed so far, a detailed knowledge of biofilm surfaces also entails the opportunity to replicate them or to positively harness them. The design of bio-inspired artificial surfaces that mimic mechanisms found in nature is a novel topic with increasing interest from diverse areas. The conception of artificial materials that can have superhydrophobic properties is only possible due to observations from nature [10]. Having artificial surfaces that repel liquids to an extent that they are "self-cleaning" has been made possible by replicating the surfaces of lotus-leaves, this represents the most famous example of biomimicry and is referred to as the "lotus-effect". Like this, many other mechanisms found in nature have been selected, studied and replicated, for example: springtails that repel low-surface tension liquids, the *lupin* plant with water guidance mechanisms, mosquito eyes, which repel micrometer-sized droplets; among others [10]. Evidently, specific parts of those plants or animals exhibit a characteristic physical/chemical mechanism to repel or attract liquids; however, in the case of biofilms, the same biomaterial is capable of exhibiting several mechanisms at once. One general possibility where a biofilms could be of use would be for the large-scale design of superhydrophobic surfaces and/or surfaces with different degrees of wettability, through the replication of their distinct topographical features. Taking *Bacillus subtilis* NCIB 3610 biofilms as a model, for example, there are three main components that make these materials superhydrophobic: a hydrophobic protein coat, polysaccharides and amyloid fibers. One could further simplify this model by incorporating only a chemical component that confers hydrophobicity and a physical component that confers a hierarchical rough topography. For instance, Pan *et al.* have developed hierarchically structured surfaces using electrospinning of hydrophobic materials, the resulting coatings are able to repel both, low and high surface tension liquids [190]. Inspired by this, electrospinning could be used for the random deposition of hydrophobic fibers onto a substrate until a specific increase in its surface area is reached, allowing for the design of biofilm-like surfaces. The S***dr*** parameter, which describes the developed interfacial surface area ratio could make the design of biofilm-like surfaces possible. As discussed in chapter 3, the ***Sdr*** is able to distinguish between rose-like and lotus-like surfaces, for which a range of ~150-300% and values >300%, respectively, have been identified. Hence, using this parameter as a regulating measure or surface complexity, biofilm-like surfaces with high- and low-adhesion towards water can be designed. Interestingly, the ***Sdr*** parameter was not only able to characterize the superhydrophobicity of biofilms but also of rose-petals, which led to the conclusion that regardless of their detailed surface features and compositions, different biomaterials possess a parametric characteristic in common. Therefore, instead of molding or carefully crafting the details of specific bio-materials, a randomized replication of a given surface complexity (as defined by the ***Sdr*** parameter) could achieve a scalable and low-cost alternative to create liquid repellent surfaces. Furthermore, the sensitivity of the ***Sdr*** parameter could allow for the design of surfaces with heterogeneous liquid repellency, which possess increasingly varied applications, such as anti-fogging, anti-reflective, anti-icing, and anti-corrosion; to name a few [10].

Another area worth exploring is bioelectronics, where products from microorganisms are used as components for electronic devices as a sustainable and green approach [191]. Although electronics bring great advantages to society, the mining and processing of the materials required for the fabrication of electronic devices are energy intensive and environmentally invasive [191]. E-biologics is a great alternative to the waste associated with current electronics (e-waste) where non-toxic and degradable electronic materials are produced by biological sources [191]. Certain success has been achieved in this area but the use of biofilms as stand-alone living electronic devices is still in the making [191]. Advances have been made using naturally conductive biofilms formed by the strain *Geobacter sulfurreducens* in which the secreted pilin filaments show metallic like conductivity [192], and by incorporating motifs into the primary structural component of *Escherichia coli* biofilms, the curli fibers, in order to render them electrically conductive [193]. However, attempts have not been made yet using other bacterial strains as most secreted biomolecules are electrically insulating. In turn, the *E. coli* secreted curli fibers, which are amyloid proteins, have been widely studied for their application also as nanowires, i.e. assembled filaments decorated with metals to provide electrical conductivity [194, 195]. For instance, introduction of cysteine into the *E. coli*-expressed amyloid monomer yields a filament that binds gold and silver [194]. Although the model bacterium *Bacillus subtilis* is as recognized as *E. coli*, the former has not been explored as an alternative for e-biologics yet. In fact, it is known that *B. subtilis* NCIB 3610 expresses TasA, a protein that forms amyloid fibers [61], and genetic engineering has made it possible to produce strains that secrete that matrix component alone [67]. Furthermore, experimental evolution studies have shown that a *B. subtilis* NCB 3610 derivative strain lacking the ability to produce any other matrix component than TasA, evolve to include a cysteine residue in this protein [77]. Hence, it should be possible to obtain conductive biofilms formed by *Bacillus subtilis* strains that secrete only cysteine-containing TasA, and in turn, amyloid fibers, which can be decorated with metallic motifs. Furthermore, the capability of *B. subtilis* bacteria to produce liquid repellent biofilms could be exploited here as a stand-alone and insulated e-bioelectronics device. The latter indicates that the possibilities of harnessing bacterial biofilms hydrophobicity are broad and that more light should be shed in this area.

Lastly, special attention should be given to the super-omniphobic property displayed by certain biofilms. As presented in sections 3.1.1 and 4.1.1, biofilms formed by certain strains of the species *Bacillus subtilis*, *Pseudomonas*, and *Burkholderia* have the ability to repel water, low surface tension liquids, and oils. Such ability could be useful for applications with high environmental impact such as oil/water separation. Oil spill accidents and waste of oily wastewater are common events nowadays that are highly damaging to the environment. Until recently, scientific efforts to remedy such disastrous situation were rather scarce. Two approaches have been recently proposed: 'oli-removing' (with superhydrophobicity-superoleophilicity) and 'water-removing' (with superoleophobicity-superhydrophilicity) functional materials [196]. 'Oil-removing' materials are the most common, they efficiently provide a sponge-like system where oils are entrapped in a mesh or porous material, thereby removing this interface from the water-oil mixture [196, 197]. A drawback of 'oil-removing' materials is paradoxically their high affinity to oils, as the latter can easily foul and even block the material affecting its separation capacity [196, 197]. Recent advances in the development of

'water-removing' materials have shown promise in addressing the issues associated with 'oil-removing' ones [196-200]; however, different challenges arise here as well and the need for efficient, low-cost, scalable solutions still remains. Here, biofilms are proposed as an alternative for oil/water separation as these biomaterials can be superoleophobic, easily and economically produced, and do not incur damage to the environment. For instance, one of the surface properties exploited by 'water-removing' materials is their ability to retain water between their roughness features. The 'trapped' water serves as a cushion that allows the rough surface to efficiently repel oils, thus creating a solid-water-oil three-phase interface (underwater Cassie state) [196, 201]. Hence, it is expected that rose-like superhydrophobic biofilms, which are described by an impregnated Cassie state in-air (Fig. 51a), i.e. water can fill the micro-structures but not the nano-structures of the roughness features, will exhibit underwater superoleophobicity. Biofilms formed by the strains *B. subtilis* NCIB 3610 and *Pseudomonas putida* can form surfaces with rose-like wetting behavior under certain conditions [73, 88]. Furthermore, the strain *B. subtilis* B-1 can form superomniphobic biofilms in-air and, at the same time, shows high erosion stability towards dripping and flowing water [73]. Clearly, all these bacterial strains represent good candidates for oil/water separation. But, how can a biofilm functional material be created for this particular application?

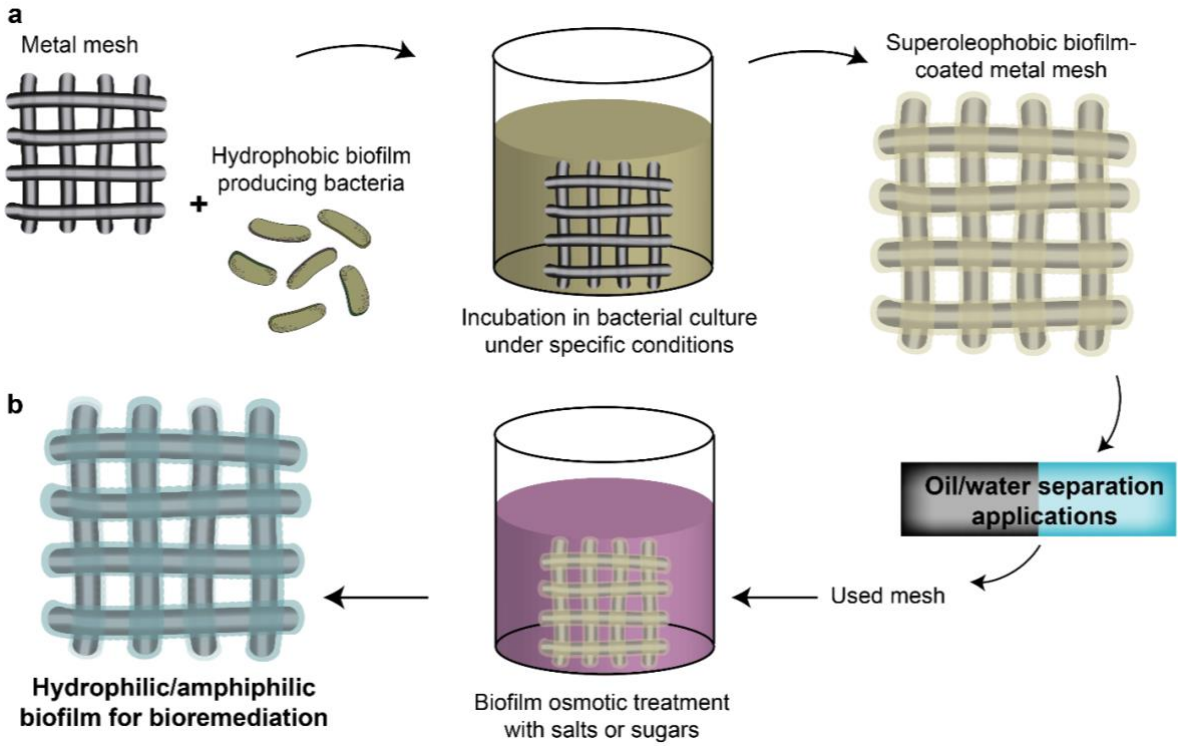

Figure 54 *The liquid repellency of biofilms could be harnessed for environmental applications, such as oil/water separation, by using them as hydrogel coatings on porous materials* ***(a)****. After usage, the same biomaterial could be osmotically treated to reduce its liquid repellency and used in bio-remediation* ***(b)****.*

Xue *et al.* introduced a hydrogel-coated mesh with superhydrophilic and underwater superoeleophobic properties [198]. The 'water removing' material consists of rough nanostructured hydrogel coatings and microscale metal substrates [198]. The polyacrylamide-coated stainless steel mesh can effectively (>99%) separate water from mixtures containing

vegetable oil, gasoline, and diesel [198]. Inspired by this, a biofilm-coated metal mesh is proposed here as a 'water removing' functional material for oil/water separation. The mesh would be incubated with NCIB 3610 or *putida* bacteria under selected nutrients, temperature, and humidity conditions to allow for the formation of rose-like superhydrophobic biofilms (Fig. 54a). For instance, a minimal salts medium (MSgg) combined with temperatures of 30 or 37 °C and low humidity allows for the formation of biofilms with such characteristics [73]. The pore-size of the mesh would be selected based on filtration and bacterial requirements. Both requirements are important as the former ensures throughput, and the latter can affect the formation of rough biofilms due to the bacteria's ability to sense and adapt to the substrate it grows on. However, biofilm cultivation requires low energy and costs and, as bacteria can form biofilms on virtually any substrate, other materials can be used and there is no need of cross-linking the coating with the substrate (as in many current applications). Lastly, biofilms have been shown to recover their mechanical properties after rupture [177], this, combined with the fact that they are living materials, entails self-mending and self-renewal capabilities.

Although the proposed biofilm-coated mesh for oil/water separation already promises great advantages compared to current strategies, a further beneficial application could be added to this material. Essentially, the same biofilm-coated mesh could be re-used for bio-remediation of the excluded oil or contaminated water. Inspired by the methods proposed in chapter 4 where superhydrophobic materials can be turned into completely wetting ones by an osmotic treatment [73] or exposure to metal ions, the wetting behavior of the biofilm-coated mesh could be switched to allow wetting by liquids. Of course, tests would be required to ensure that the osmotic treatment renders biofilms susceptible to wetting by low surface tension liquids as well as oils. However, the latter is expected, as when biofilms exhibit hydrophilic behavior, they are susceptible to all kinds of liquids. It is known that the first step in bio-remediation is the bioavailability of the compound to the bacterial cells [202]. Therefore, changes in the polarity of the biofilm material –through an osmotic treatment, would allow for contact between the cells and the contaminants and for the initiation of the bio-remediation process. Such application is of great importance as, although the biofilm material promises good tolerance to frequent use, like any other material, it has a limit. Re-using the biofilm-coated mesh for detoxification would add an additional functional step into its life-cycle. It is proposed that the used biofilm-coated mesh would be incubated in a solution containing an osmotic agent (Fig. 54b). For instance, rose-like *Pseudomonas putida* biofilms showed high wettability changes after treatment with KCl solutions, which would be a treatment option for metal meshes coated with this strain. Interestingly, *Pseudomonas putida* has been used for bioremediation of the hydrocarbon, 2,4 Dichlorophenol, when used in a rotating perforated tube bioreactor [202, 203]. The fact that the same bacterial strain has been shown to be effective in bio-remediation of hydrocarbons and also to form biofilms with desired characteristics for oil/water separation poses great promise for these biomaterials. Of course, the strategies proposed here are purely conceptual; however, the basis comes from tested methods, which allows to imagine their potential. The benefits that can be exploited from such complex and dynamic materials, like biofilms, are vast and what has been achieved so far is only the beginning.

6 Appendix

6.1 Appendix 1: Analysis of biofilm pellicles

6.1.1 List of strains

Appendix Table 1 *Strains used in section 3.2.2*

Name	Genotype	Reference
DK1042	NCIB 3610 comI^{Q12I}	[118]
TB601 (*Δeps)*	3610 comI^{Q12I} *eps::tet*	[204]
TB602 *(ΔtasA)*	3610 com^{IQ12I} *tasA::spec*	[65]

The strains used in section 3.2.2 originated from naturally competent derivatives of the undomesticated *B. subtilis* NCIB 3610 DK1042 strain [118], except for the WT NCIB 3610 strain used as control. *e+t* pellicles were constructed through the interaction of two partially deficient mutants, *Δeps* and *ΔtasA* that exchange matrix components with each other. *e4A+t4B* pellicles consist of an evolved strain isolated at the 4th transfer of the *e+t* mixture (see methods for evolution experiments in section 6.2.2.1). *wt6C* pellicles consist of an evolved strain isolated from the 6th transfer of the WT NCIB 3610 strain (see methods for evolution experiments in section 6.2.2.1).

6.1.2 Method for pellicle formation

Overnight cultures were generated as described in section 2.1.2, a cell suspension was prepared by centrifugation of the overnight culture (5000 rpm, 4 °C), then, the pellet was washed and resuspended in the base media, and the cell suspension was adjusted to an OD_{600} of 1. For pellicle formation, the base medium, in this case LBGM was inoculated with 1% (v/v) of the cell suspension. Pellicles were grown in LBGM medium statically in a 24-well plate at 30 °C for 48 h in 6 parallel replicates.

6.2 [d]Appendix 2: Diversification in *Bacillus subtilis* biofilms

6.2.1 List of strains

Appendix Table 2 *Strains used for the study of diversification in B. subtilis NCIB 3610 biofilms*

Name	Genotype	Reference
DK1042	NCIB 3610 comI^{Q12I}	118
NRS2243	3610 sacI::P$_{eps}$-*gfp* (Km^{R})	205
NRS2394	3610 sacI::P$_{tapA}$-*gfp* (Km^{R})	205
DTUB18	comI Rough sacI::P$_{eps}$-*gfp* (Km^{R})	77
DTUB19	3610 comI^{Q12I} Wrinkly sacI::P$_{eps}$-*gfp* (Km^{R})	77
DTUB20	3610 comI^{Q12I} Spreader sacI::P$_{eps}$-*gfp* (Km^{R})	77
DTUB21	3610 comI^{Q12I} Smooth sacI::P$_{eps}$-*gfp* (Km^{R})	77
DTUB22	3610 comI^{Q12I} Rough sacI::P$_{tapA}$-*gfp* (Km^{R})	77
DTUB23	3610 comI^{Q12I} Wrinkly sacI::P$_{tapA}$-*gfp* (Km^{R})	77
DTUB24	3610 comI^{Q12I} Spreader sacI::P$_{tapA}$-*gfp* (Km^{R})	77
DTUB25	3610 comI^{Q12I} Smooth sacI::P$_{tapA}$-*gfp* (Km^{R})	77

Appendix Table 2 describes the strains used for diversification studies. Strains were maintained in Lysogeny broth LB medium (LB-Lennox: Carl Roth, Karlsruhe, Germany) while MSgg was used for biofilm colony or pellicle biofilm induction [115].

6.2.2 Methods

6.2.2.1 Experimental evolution assays

Experimental evolution was performed using the natural competent derivative of the undomesticated *B. subtilis* NCBI 3610, DK1042 strain [118] grown in MSgg medium statically in a 24-well plate at 30 °C for 48 h in six parallel replicates. Mature pellicles were gently harvested from the surface of the liquid medium using a plastic inoculating loop. First, the edge of the pellicle was gently pierced to partially detach the biofilm from the wall of the plastic well. Second, the pellicle was collected by rapidly moving the loop clockwise, constantly keeping the loop at the liquid–air interface and touching the wall/edge of the pellicle. This allowed for harvesting of the entire biofilm, leaving the conditioned medium clear (optical density at 600 nm∼0). The material was then transferred to 2 mL Eppendorf tube containing 1 mL of 0.9% NaCl and 100 µL of glass sand and vortexed vigorously for 60 s. This allowed for efficient disruption of the material into single cells and small clumps, without the need for sonication that would highly increase the risk of contamination. Finally, the disrupted culture was reinoculated after a 100× dilution. After the 5th, 10th, 14th, 19th, 24th, 29th and 35th pellicle transfers, colony forming units (CFU)/mL in the pellicles described here as pellicle

[d] This section follows in part the publication: "*Evolution of exploitative interactions during diversification in Bacillus subtilis biofilms*" published on 2018, in FEMS Microbiology Ecology.

productivity were monitored and frozen (−80°C) stocks were preserved. Single isolates representing the four different morphotypes were isolated from population 1.

6.2.2.2 Colony morphology assay

Colony morphologies were examined on LB and MSgg medium with 1.5% agar. The plates were dried under laminar airflow conditions for 20 min after solidifying. 2 µL of the overnight grown cultures were spotted on the plate, and the lids were closed once the spotted culture had dried. The plates were incubated at 30 °C for 48 h.

6.2.2.3 Other

Light profilometry Contact angle measurements, and microscopy were performed the same way as described in sections 2.3.1, 2.3.2 and 2.3.5.

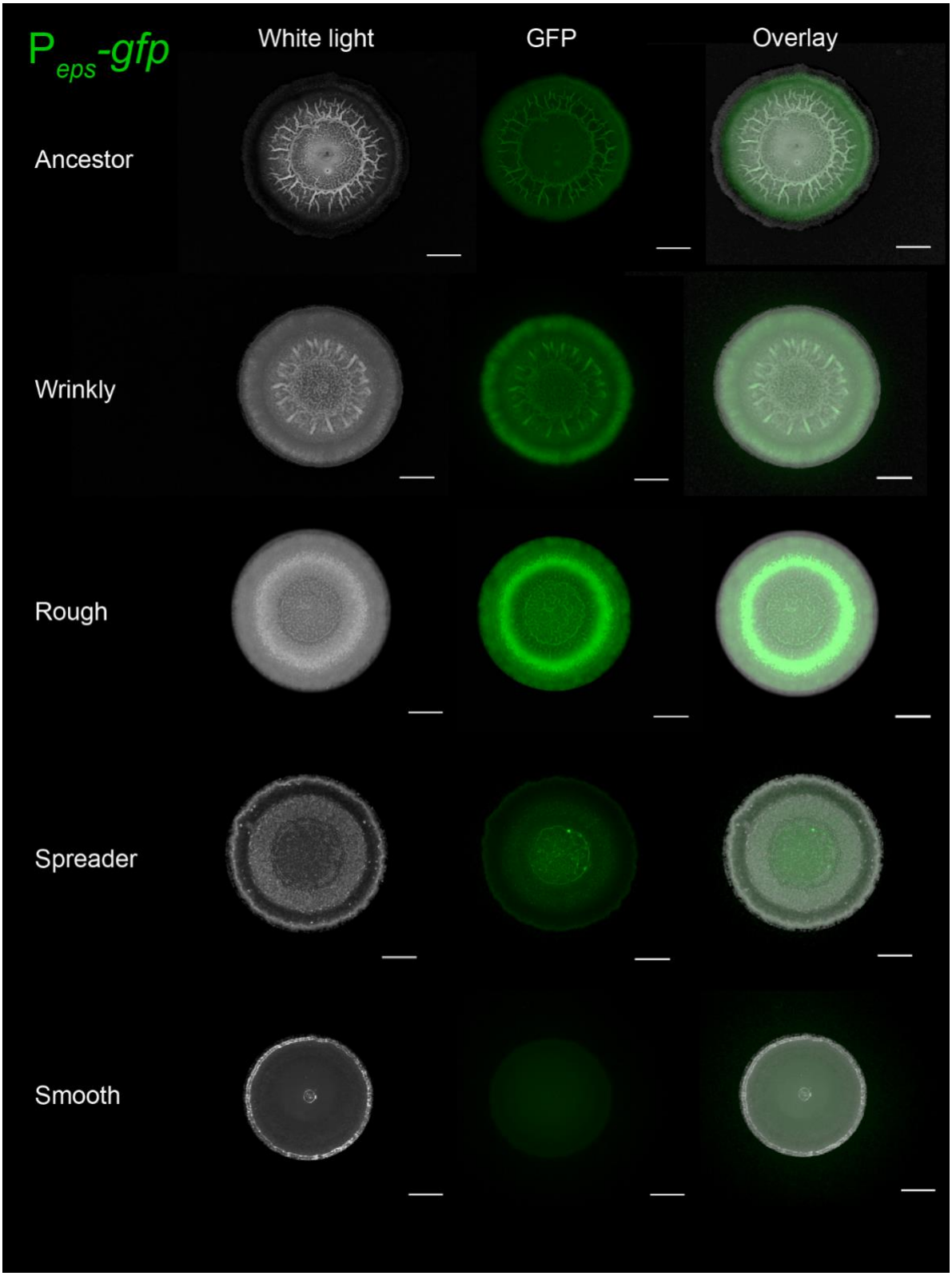

Appendix Figure 1 *Qualitative comparison of matrix-genes expression by different morphotypes.* Expression of *eps* was monitored in the ancestor and all morphotypes in colonies developed on MSgg agar using P_{eps}-*gfp* reporter fusion. Scale bar represents 2 mm.

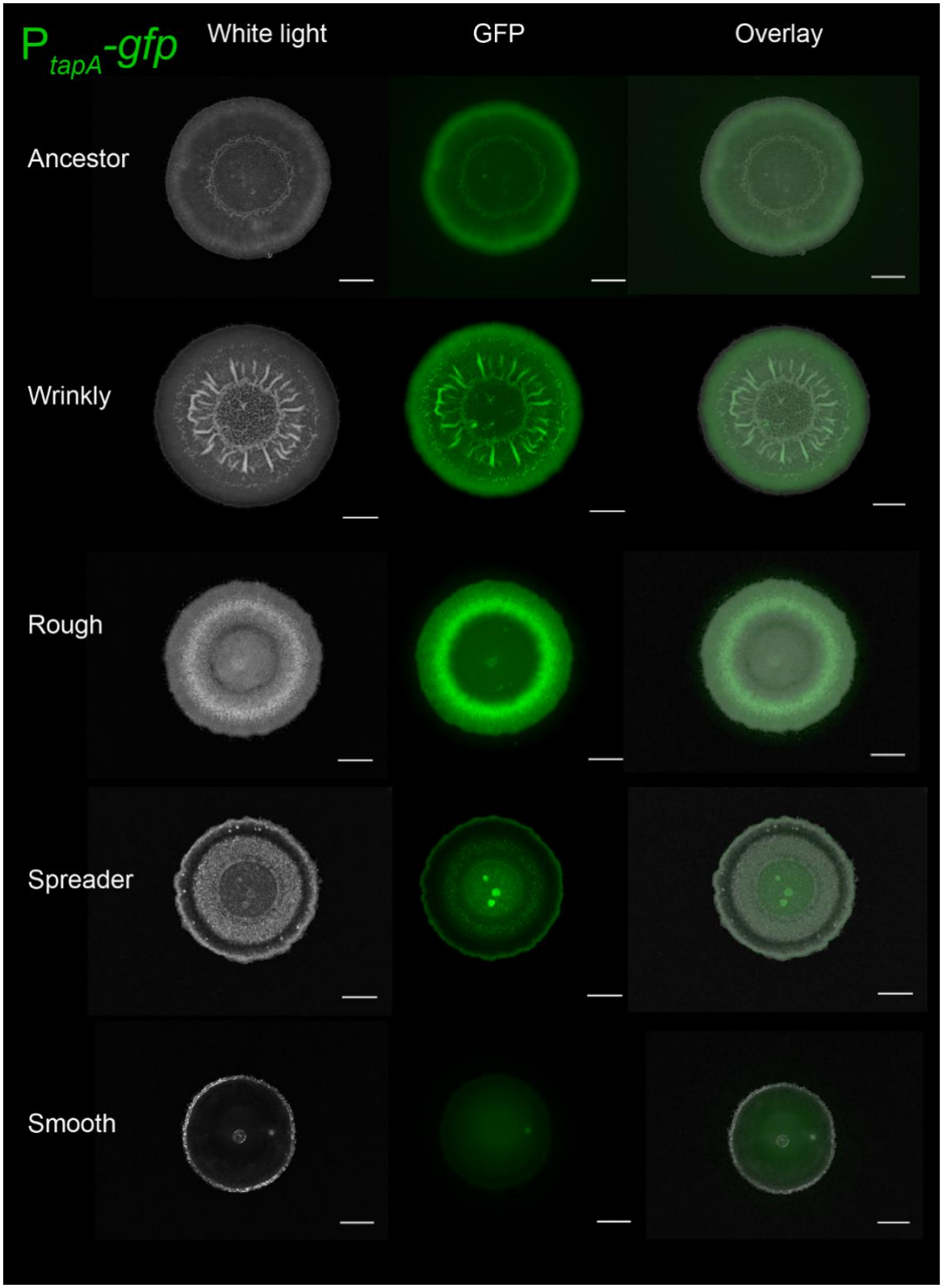

Appendix Figure 2 *Qualitative comparison of matrix-genes expression by different morphotypes.* Expression of *tapA* was monitored in the ancestor and all morphotypes in colonies developed on MSgg agar using P_{tapA}-*gfp* reporter fusion. Scale bar represents 2 mm.

7 Acknowledgements

First and foremost, I want to thank my supervisor Prof. Dr. Oliver Lieleg not just for giving me the opportunity to join his research group but for believing in me. For giving me his time, which I have learnt is our most valuable asset, his disposition to teach me and his guidance in all aspects of a scientist's life. I have learnt and grown so much since I started here, that I do not know how to thank you Oli, but I hope my efforts and this work are a good measure of my gratitude.

Special thanks to all the great scientists who worked with me and contributed to this dissertation: Alexandra Götz, Anna Dragoš, Akos T. Kovács, Madeleine Opitz, Sara Kesel, Moritz Werb; my students Markus Schönleitner and Felix Stangl. Thank you, Iris König-Decker and Christine Braig for your kind assistance in administrative and technical matters.

To my wonderful group: I never imagined I would meet such diverse, crazy, weird, awesome people at my work place that I would actually end up liking and loving so much. Thank you, Ben (a.k.a Osama Bün Labern), Ceran (a.k.a Seran Kimna x5), Marvin (a.k.a Morter Guy), Jian (a.k.a Juan), and Matthias (a.k.a Mattayas) for the beer breaks (btw, thank you Oli for even allowing beer breaks). Thank you, Carolin (a.k.a Rickster) and Theresa (a.k.a Törösa) for always having chocolate for me. Thank you, Benni for teaching me animal noises O>. And to all of you, thank you for your help with my dissertation and, of course, for your amazing friendship, I hope it lasts a lifetime.

Lastly, I want to thank my family. To my husband, Stephan Stromberger for loving me unconditionally and helping me get through this stage of my life –almost– sane and happy. Thank you, for understanding me (or least trying to), for supporting me, for lovingly taking care of me in situations where I did not even know I needed help, and for standing by my side even at my worst temper. I also want to show my gratitude to Anita and Wolfgang Stromberger for being there for me with love and advice whenever needed and for supporting me and Stephan in all our decisions.

Este trabajo como todo lo valioso en mi vida está dedicado a mi abuelo, Jesús Falcón, porque sin sus enseñanzas de trabajo arduo, humildad y respeto nunca hubiera llegado hasta esta página. Nunca olvidaré ese día que te conté mis planes de estudiar en el extranjero, no lo sabia pero esa conversación cambiaría mi vida. El orgullo que me demostraste con tus ojos y el apoyo incondicional con tus palabras quedarán grabados en mi memoria y corazón por siempre. Gracias a mis dos abuelos, también a Jesús García, por demostraterme una fortaleza sobrehumana que me motiva día a día.

Lo mismo para mis padres: Marisol y Juan José, su amor y apoyo incondicional me acompañan siempre. Gracias por nunca apresurarme ni cuestionar mis decisiones, al contrario, aceptarlas con orgullo y felicidad, lo cual considero la prueba de amor más grande que existe. En realidad no tengo palabras para agradecerles todo lo que me han dado, solo puedo decir que les amo infinitamente papi y mami.

Gracias hermanitos Marcela y Alain por distraerme y hacerme feliz en momentos difíciles, por no juzgarme (que yo sepa :D) al decidir irme lejos para perseguir mis sueños. Yo sé que en algun momento mis decisiones les afectaron de alguna manera y aun así nuestro amor y el apoyo que nos damos es inmenso. Gracias a Paulina y Regina, por ser ellas, nadamás; mi más grande fuente de alegría.

Gracias cuñados Adrian y Jocelyne; tíos Lili, Loli y Fachi, Primos: Chris, Elian, Ali, Mauro, Elva y Alex; abuelita Elba; sobrinos: Vale, Mariano y Leo; por estar ahí siempre que los necesito, por esperarme con ansias cada que regreso a casa y simplemente por hacer mi vida extraordinaria. A mi familia elegida: Julián y Cesar, gracias amigos por demostrarme una amistad que no ve distancias y por echarme Porras siempre.

Y cómo olvidar a mis angelitos: Filadelfa González, Mauro Alcudia, y Aurora López, mil gracias y besos hasta el cielo.

8 List of publications

C. Falcón García, M. Schönleitner, C. N. Lozano-Andrade, A. Dragoš, A. T. Kovács, O. Lieleg
Effect of metal ions on *B. subtilis* NCIB 3610 biofilm surface hydrophobicity and antibiotic susceptibility
Submitted

C. Falcón García, F. Stangl, A. Götz, W. Zhao, S. A. Sieber, M. Opitz, O. Lieleg
Topographical alterations render bacterial biofilms susceptible to chemical and mechanical stress
Biomat. Sci., **7**, 220-232 (2019)

A. Dragoš, M. Martin, **C. Falcón Garcia**, L. Kricks, P. Pausch, T. Heimerl, B. Bálint, G. Maróti, G. Bange, D. López, O. Lieleg, A. T. Kovács
Collapse of genetic division of labour and evolution of autonomy in pellicle biofilms
Nat. Microbiol., **3**(12), 1451-1460 (2018)

A. Dragoš, N. Lakshmanan, M. Martin, B. Horváth, G. Maróti, **C. Falcón García**, O. Lieleg, A. T. Kovács
Evolution of exploitative interactions during diversification in *Bacillus subtilis* biofilms
FEMS Microbiol. Ecol., **94**(1), fix155 (2018)

S. Kesel, B. von Bronk[#], **C. Falcón García**[#], A. Götz, O. Lieleg, M. Opitz
Matrix composition determines the dimensions of *Bacillus subtilis* NCIB 3610 biofilm colonies grown on LB agar
RSC Adv., 7(51), 31886-31898 (2017)

M. Werb[#], **C. Falcón García**[#], N. C. Bach, S. Grumbein, S. A. Sieber, M. Opitz, O. Lieleg
Surface topology affects wetting behavior of *Bacillus subtilis* biofilms
npj biofilms and microbiomes, **3**(1), 11 (2017)

[#] Authors contributed equally.

9 References

1. C. Neinhuis and W. Barthlott, *Annals of Botany*, 1997, **79**, 667-677.
2. L. Feng, S. Li, Y. Li, H. Li, L. Zhang, J. Zhai, Y. Song, B. Liu, L. Jiang and D. Zhu, *Advanced Materials*, 2002, **14**, 1857-1860.
3. B. Bhushan and M. Nosonovsky, *Philosophical Transactions of the Royal Society A-Mathematical Physical and Engineering Sciences*, 2010, **368**, 4713-4728.
4. Q. Xu, Y. Wan, T. S. Hu, T. X. Liu, D. Tao, P. H. Niewiarowski, Y. Tian, Y. Liu, L. Dai, Y. Yang and Z. Xia, *Nature Communications*, 2015, **6**, e8949.
5. X. Gao and L. Jiang, *Nature*, 2004, **432**, e36.
6. T. Wagner, C. Neinhuis and W. Barthlott, *Acta Zoologica*, 1996, **77**, 213-225.
7. Z. Wang, M. Elimelech and S. Lin, *Environmental Science & Technology*, 2016, **50**, 2132-2150.
8. C.-H. Xue, S.-T. Jia, J. Zhang and J.-Z. Ma, *Science and Technology of Advanced Materials*, 2010, **11**, e033002.
9. I. U. Vakarelski, N. A. Patankar, J. O. Marston, D. Y. C. Chan and S. T. Thoroddsen, *Nature*, 2012, **489**, 274-277.
10. T. Darmanin and F. Guittard, *Journal of Materials Chemistry A*, 2014, **2**, 16319-16359.
11. A. C. Lima and J. F. Mano, *Nanomedicine*, 2015, **10**, 271-297.
12. S. Shin, J. Seo, H. Han, S. Kang, H. Kim and T. Lee, *Materials*, 2016, **9**, e116.
13. A. Gauthier, S. Symon, C. Clanet and D. Quere, *Nature Communications*, 2015, **6**, e8001.
14. J. C. Bird, R. Dhiman, H.-M. Kwon and K. K. Varanasi, *Nature*, 2013, **503**, 385-388.
15. A. Marmur, *Langmuir*, 2004, **20**, 3517-3519.
16. A. B. D. Cassie and S. Baxter, *Transactions of the Faraday Society*, 1944, **40**, 546-551.
17. Z. Guo, W. Liu and B.-L. Su, *Journal of Colloid and Interface Science*, 2011, **353**, 335-355.
18. E. Celia, T. Darmanin, E. Taffin de Givenchy, S. Amigoni and F. Guittard, *Journal of Colloid and Interface Science*, 2013, **402**, 1-18.
19. A. Mitchinson, *Nature*, 2007, **445**, e373.
20. A. Nakajima, *NPG Asia Materials*, 2011, **3**, 49-56.
21. J. Lee and K. Yong, *NPG Asia Materials*, 2015, **7**, e201.
22. H. Yang, F. Liang, Y. Chen, Q. Wang, X. Qu and Z. Yang, *NPG Asia Materials*, 2015, **7**, e176.
23. J. Lv, Y. Song, L. Jiang and J. Wang, *ACS Nano*, 2014, **8**, 3152-3169.
24. A. K. Kota, G. Kwon and A. Tuteja, *NPG Asia Materials*, 2014, **6**, e109.
25. T.-S. Wong, S. H. Kang, S. K. Y. Tang, E. J. Smythe, B. D. Hatton, A. Grinthal and J. Aizenberg, *Nature*, 2011, **477**, 443-447.
26. A. K. Epstein, B. Pokroy, A. Seminara and J. Aizenberg, *Proceedings of the National Academy of Sciences*, 2011, **108**, 995-1000.
27. E. Drenkard and F. M. Ausubel, *Nature*, 2002, **416**, 740-743.
28. R. N. Wenzel, *Industrial and Engineering Chemistry*, 1936, **28**, 988-994.

29. A. Heydorn, A. T. Nielsen, M. Hentzer, C. Sternberg, M. Givskov, B. K. Ersbøll and S. Molin, *Microbiology*, 2000, **146**, 2395-2407.
30. H. Beyenal, C. Donovan, Z. Lewandowski and G. Harkin, *Journal of Microbiological Methods*, 2004, **59**, 395-413.
31. C. Larimer, J. D. Suter, G. Bonheyo and R. S. Addleman, *Journal of Biophotonics*, 2016, **9**, 656-666.
32. C. Ya-Wen, A. F. Alexandros, M. M. Samantha, D. K. Harold, E. A. Thomas and F.-N. Alberto, *New Journal of Physics*, 2015, **17**, e033017.
33. J. Dervaux, J. C. Magniez and A. Libchaber, *Interface Focus*, 2014, **4**, e20130051.
34. M. Nosonovsky and B. Bhushan, *Advanced Functional Materials*, 2008, **18**, 843-855.
35. A. Lafuma and D. Quere, *Nature Materials*, 2003, **2**, 457-460.
36. H. C. Flemming and J. Wingender, *Nature Reviews Microbiology*, 2010, **8**, 623-633.
37. M. Marvasi, P. T. Visscher and L. Casillas Martinez, *FEMS Microbiology Letters*, 2010, **313**, 1-9.
38. I. Sutherland, *Microbiology*, 2001, **147**, 3-9.
39. C. D. Nadell, K. Drescher, N. S. Wingreen and B. L. Bassler, *The Isme Journal*, 2015, **9**, 1700-1709.
40. H. Vlamakis, Y. Chai, P. Beauregard, R. Losick and R. Kolter, *Nature Reviews Microbiology*, 2013, **11**, 157-168.
41. L. Hobley, C. Harkins, C. E. MacPhee and N. R. Stanley-Wall, *FEMS Microbiology Reviews*, 2015, **39**, 649-669.
42. V. Berk, J. C. N. Fong, G. T. Dempsey, O. N. Develioglu, X. W. Zhuang, J. Liphardt, F. H. Yildiz and S. Chu, *Science*, 2012, **337**, 236-239.
43. C. Hung, Y. Zhou, J. S. Pinkner, K. W. Dodson, J. R. Crowley, J. Heuser, M. R. Chapman, M. Hadjifrangiskou, J. P. Henderson and S. J. Hultgren, *MBio*, 2013, **4**, e00645-00613.
44. Q. Wei and L. Z. Ma, *International Journal of Molecular Sciences*, 2013, **14**, 20983-21005.
45. J. Valle, C. Latasa, C. Gil, A. Toledo-Arana, C. Solano, J. R. Penades and I. Lasa, *PLoS Pathogens*, 2012, **8**, e1002843.
46. A. P. Stapper, G. Narasimhan, D. E. Ohman, J. Barakat, M. Hentzer, S. Molin, A. Kharazmi, N. Hoiby and K. Mathee, *Journal of Medical Microbiology*, 2004, **53**, 679-690.
47. H. Koo, J. Xiao, M. I. Klein and J. G. Jeon, *Journal of Bacteriology*, 2010, **192**, 3024-3032.
48. J. Xiao, M. I. Klein, M. L. Falsetta, B. Lu, C. M. Delahunty, J. R. Yates, 3rd, A. Heydorn and H. Koo, *PLoS Pathogens*, 2012, **8**, e1002623.
49. D. O. Serra, A. M. Richter and R. Hengge, *Journal of Bacteriology*, 2013, **195**, 5540-5554.
50. D. O. Serra, A. M. Richter, G. Klauck, F. Mika and R. Hengge, *mBio*, 2013, **4**, e00103-00113.
51. K. Drescher, J. Dunkel, C. D. Nadell, S. van Teeffelen, I. Grnja, N. S. Wingreen, H. A. Stone and B. L. Bassler, *Proceedings of the National Academy of Sciences*, 2016, **113**, E2066-E2072.

52. P. Gupta, S. Sarkar, B. Das, S. Bhattacharjee and P. Tribedi, *Archives of Microbiology*, 2016, **198**, 1-15.
53. M. Simoes, L. C. Simoes and M. J. Vieira, *LWT - Food Science and Technology*, 2010, **43**, 573–583.
54. H. C. Flemming, J. Wingender, U. Szewzyk, P. Steinberg, S. A. Rice and S. Kjelleberg, *Nature Reviews Microbiology*, 2016, **14**, 563-575.
55. X. Wang, G. Wang and M. Hao, *Computational and Mathematical Methods in Medicine*, 2015, **2015**, e581829.
56. W. Zhang, A. Seminara, M. Suaris, M. P. Brenner, D. A. Weitz and T. E. Angelini, *New Journal of Physics*, 2014, **16**, e015028.
57. T. E. Angelini, M. Roper, R. Kolter, D. A. Weitz and M. P. Brenner, *Proceedings of the National Academy of Sciences*, 2009, **106**, 18109-18113.
58. M. Ardré, H. Henry, C. Douarche and M. Plapp, *Physical Biology*, 2015, **12**, e066015.
59. J. van Gestel, H. Vlamakis and R. Kolter, *PLoS Biology*, 2015, **13**, e1002141.
60. X. Zhang, X. Wang, K. Nie, M. Li and Q. Sun, *Physical Biology*, 2016, **13**, e046002.
61. S. S. Branda, F. Chu, D. B. Kearns, R. Losick and R. Kolter, *Molecular Microbiology*, 2006, **59**, 1229-1238.
62. K. Kobayashi and M. Iwano, *Molecular Microbiology*, 2012, **85**, 51-66.
63. H. Vlamakis, C. Aguilar, R. Losick and R. Kolter, *Genes & Development*, 2008, **22**, 945-953.
64. Á. T. Kovàcs, J. van Gestel and O. P. Kuipers, *Molecular Microbiology*, 2012, **85**, 8-11.
65. S. Arnaouteli, A. S. Ferreira, M. Schor, R. J. Morris, K. M. Bromley, J. Jo, K. L. Cortez, T. Sukhodub, A. R. Prescott, L. E. P. Dietrich, C. E. MacPhee and N. R. Stanley-Wall, *Proceedings of the National Academy of Sciences*, 2017, **114**, E6184-E6191.
66. L. Hobley, A. Ostrowski, F. V. Rao, K. M. Bromley, M. Porter, A. R. Prescott, C. E. MacPhee, D. M. F. Van Aalten and N. R. Stanley-Wall, *Proceedings of the National Academy of Sciences*, 2013, **110**, 13600-13605.
67. S. Kesel, B. von Bronk, C. Falcón García, A. Götz, O. Lieleg and M. Opitz, *RSC Advances*, 2017, **7**, 31886-31898.
68. D. Romero, C. Aguilar, R. Losick and R. Kolter, *Proceedings of the National Academy of Sciences*, 2010, **107**, 2230-2234.
69. M. Morikawa, S. Kagihiro, M. Haruki, K. Takano, S. Branda, R. Kolter and S. Kanaya, *Microbiology-Sgm*, 2006, **152**, 2801-2807.
70. P. Cescutti, B. Cuzzi, Y. Herasimenka and R. Rizzo, *Carbohydrate Polymers*, 2013, **94**, 253-260.
71. M. Tallawi, M. Opitz and O. Lieleg, *Biomaterials Science*, 2017, **5**, 887-900.
72. M. Toyofuku, T. Inaba, T. Kiyokawa, N. Obana, Y. Yawata and N. Nomura, *Bioscience, Biotechnology, and Biochemistry*, 2016, **80**, 7-12.
73. C. Falcón García, F. Stangl, A. Götz, W. Zhao, S. A. Sieber, M. Opitz and O. Lieleg, *Biomaterials Science*, 2019, **7**, 220-232.
74. L. S. Cairns, L. Hobley and N. R. Stanley-Wall, *Molecular Microbiology*, 2014, **93**, 587-598.

75. R. Gallegos-Monterrosa, E. Mhatre and Á. T. Kovács, *Microbiology*, 2016, **162**, 1922-1932.
76. T. Hölscher, B. Bartels, Y.-C. Lin, R. Gallegos-Monterrosa, A. Price-Whelan, R. Kolter, L. E. P. Dietrich and Á. T. Kovács, *Journal of Molecular Biology*, 2015, **427**, 3695-3708.
77. A. Dragoš, M. Martin, C. Falcón Garcia, L. Kricks, P. Pausch, T. Heimerl, B. Bálint, G. Maróti, G. Bange, D. López, O. Lieleg and Á. T. Kovács, *Nature Microbiology*, 2018, **3**, 1451-1460.
78. A. Dragoš, N. Lakshmanan, M. Martin, B. Horváth, G. Maróti, C. Falcón García, O. Lieleg and Á. T. Kovács, *FEMS Microbiology Ecology*, 2018, **94**, fix155.
79. M. Martin, T. Hölscher, A. Dragoš, V. S. Cooper and Á. T. Kovács, *Journal of Bacteriology*, 2016, **198**, 2564-2571.
80. P. B. Rainey and M. Travisano, *Nature*, 1998, **394**, 69-72.
81. C. C. Traverse, L. M. Mayo-Smith, S. R. Poltak and V. S. Cooper, *Proceedings of the National Academy of Sciences*, 2013, **110**, E250-E259.
82. S. R. Poltak and V. S. Cooper, *The Isme Journal*, 2010, **5**, 369-378.
83. G. Koch, A. Yepes, K. U. Förstner, C. Wermser, S. T. Stengel, J. Modamio, K. Ohlsen, K. R. Foster and D. Lopez, *Cell*, 2014, **158**, 1060-1071.
84. W. Kim, S. B. Levy and K. R. Foster, *Nature Communications*, 2016, **7**, e10508.
85. H. P. Steenackers, I. Parijs, A. Dubey, K. R. Foster and J. Vanderleyden, *FEMS microbiology reviews*, 2016, **40**, 373-397.
86. C. N. Ellis, C. C. Traverse, L. Mayo-Smith, S. W. Buskirk and V. S. Cooper, *Evolution; international journal of organic evolution*, 2015, **69**, 283-293.
87. K. M. Flynn, G. Dowell, T. M. Johnson, B. J. Koestler, C. M. Waters and V. S. Cooper, *Journal of bacteriology*, 2016, **198**, 2608-2618.
88. M. Werb, C. Falcón García, N. C. Bach, S. Grumbein, S. A. Sieber, M. Opitz and O. Lieleg, *npj Biofilms and Microbiomes*, 2017, **3**, e11.
89. S. Arnaouteli, C. E. MacPhee and N. R. Stanley-Wall, *Current Opinion in Microbiology*, 2016, **34**, 7-12.
90. M. Morikawa, *Journal of Bioscience and Bioengineering*, 2006, **101**, 1-8.
91. R. Hayat, S. Ali, U. Amara, R. Khalid and I. Ahmed, *Annals of Microbiology*, 2010, **60**, 579-598.
92. G.-P. Sheng, H.-Q. Yu and X.-Y. Li, *Biotechnology Advances*, 2010, **28**, 882–894.
93. *Biofilms in Wastewater Treatment*, IWA Publishing, London, UK, 2003.
94. B. Halan, K. Buehler and A. Schmid, *Trends in Biotechnology*, 2012, **30**, 453-465.
95. *Biofilms in Bioremediation*, Caister Academic Press, Norfolk, UK, 2016.
96. S. K. Behera, M. Manjaiah, S. Sekar, S. K. Panda, M. Vuyo and A. F. Mulaba-Bafubiandi, *Geomicrobiology Journal*, 2017, **35**, 447-459.
97. L. Hall-Stoodley, J. W. Costerton and P. Stoodley, *Nature Reviews Microbiology*, 2014, **2**, 95-108.
98. *Biofilms in Medicine, Industry and Environmental Biotechnology*, IWA Publishing, London, UK, 2003.
99. C. R. Arciola, D. Campoccia and L. Montanaro, *Nature Reviews Microbiology*, 2018, **16**, 397-409.

100. D. McDougald, S. A. Rice and S. Kjelleberg, *Nature Reviews Microbiology*, 2012, **10**, 39-50.
101. J. B. Kaplan, *Journal of Dental Research*, 2010, **89**, 205-218.
102. H. Koo, R. N. Allan, R. P. Howlin, P. Stoodley and L. Hall-Stoodley, *Nature Reviews Microbiology*, 2017, **15**, 740-755.
103. X. Zhu and X. J. Loh, *Biomaterials Science*, 2015, **12**, 1505-1518.
104. G. Hazell, P. W. May, P. Taylor, A. H. Nobbs, C. C. Welchc and B. Sua, *Biomaterials Science*, 2018, **6**, 1424-1432.
105. S. Bierbaum, S. Mulansky, E. Bognár, I. Kientzl, P. Nagy, N. E. Vrana, M. Weszl, E. Boschke, D. Scharnwebera and C. Wolf-Brandstetter, *Biomaterials Science*, 2018, **6**, 1390-1402.
106. T. L. Wood, T. Gong, L. Zhu, J. Miller, D. S. Miller, B. Yin and T. K. Wood, *npj Biofilms and Microbiomes*, 2018, **4**, e22.
107. J. Y. Co, G. Cárcamo-Oyarce, N. Billings, K. M. Wheeler, S. C. Grindy, N. Holten-Andersen and K. Ribbeck, *npj Biofilms and Microbiomes*, 2018, **4**, e23.
108. L. C. Powell, M. F. Pritchard, E. L. Ferguson, K. A. Powell, S. U. Patel, P. D. Rye, S.-M. Sakellakou, N. J. Buurma, C. D. Brilliant, J. M. Copping, G. E. Menzies, P. D. Lewis, K. E. Hill and D. W. Thomas, *npj Biofilms and Microbiomes*, 2018, **4**, e13.
109. M. Simoes, M. O. Pereira and M. J. Vieira, *Water Research*, 2005, **39**, 5142-5152.
110. J. A. Lemire, J. J. Harrison and R. J. Turner, *Nature Reviews Microbiology*, 2013, **11**, 371-384.
111. T. L. Dinh, G. R. Akhmetova, D. S. Martykanova, N. L. Rudakova and M. R. Sharipova, *BioNanoScience*, 2019, **9**, 521-527.
112. A. Sirelkhatim, S. Mahmud, A. Seeni, N. H. M. Kaus, L. C. Ann, S. K. M. Bakhori, H. Hasan and D. Mohamad, *Nano-Micro Letters*, 2015, **7**, 219-242.
113. C. L. Dupont, G. Grass and C. Rensing, *Metallomics*, 2011, **3**, 1109-1118.
114. Y.-H. Hsueh, W.-J. Ke, C.-T. Hsieh, K.-S. Lin, D.-Y. Tzou and C.-L. Chiang, *PLOS ONE*, 2015, **10**, e0128457.
115. S. S. Branda, J. E. González-Pastor, S. Ben-Yehuda, R. Losick and R. Kolter, *Proceedings of the National Academy of Sciences*, 2001, **98**, 11621-11626.
116. A. Goto and M. Kunioka, *Bioscience, Biotechnology, and Biochemistry*, 1992, **56**, 1031-1035.
117. M. Albano, J. Hahn and D. Dubnau, *Journal of Bacteriology*, 1987, **169**, 3110-3117.
118. M. A. Konkol, K. M. Blair and D. B. Kearns, *Journal of Bacteriology*, 2013, **195**, 4085-4093.
119. I. Seccareccia, Á. T. Kovács, R. Gallegos-Monterrosa and M. Nett, *Microbiological Research*, 2016, **192**, 231-238.
120. E. Mhatre, A. Sundaram, T. Hölscher, M. Mühlstädt, J. Bossert and Á. T. Kovács, *Microorganisms*, 2017, **5**, e7.
121. M. Shemesh and Y. Chai, *Journal of Bacteriology*, 2013, **195**, 2747-2754.
122. J. Frohn, *Optical quality control for industry: applicable in laboratory up to inline-inspection*, NanoFocus AG, https://docplayer.net/7910616-Optical-quality-control-for-industry-applicable-in-laboratory-up-to-inline-inspection-dr-josef-frohn-nanofocus-ag-oberhausen-ettlingen.html, 2010.

123. N. AG, µsurf technology, www.nanofocus.com, (accessed 21.06, 2019).
124. ISO, ISO 25178-2:2012(en), https://www.iso.org/obp/ui/#iso:std:iso:25178:-2:ed-1:v1:en, 2018).
125. J. Cox and M. Mann, *Nature Biotechnology*, 2008, **26**, 1367-1372.
126. D. M. Johnson, D. J. Biedenbach and R. N. Jones, *Diagnostic Microbiology and Infectious Disease*, 2002, **43**, 49-60.
127. P. C. B. Turnbull, N. M. Sirianni, C. I. LeBron, M. N. Samaan, F. N. Sutton, A. E. Reyes and L. F. Peruski, *Journal of Clinical Microbiology*, 2004, **42**, 3626-3634.
128. D. B. Adimpong, K. I. Sorensen, L. Thorsen, B. Stuer-Lauridsen, W. S. Abdelgadir, D. S. Nielsen, P. M. Derkx and L. Jespersen, *Applied and Environmental Microbiology*, 2012, **78**, 7903-7914.
129. M. D. Macia, E. Rojo-Molinero and A. Oliver, *Clinical Microbiology and Infection*, 2014, **20**, 981-990.
130. O. Ciofu, E. Rojo-Molinero, M. D. Macià and A. Oliver, *APMIS*, 2017, **125**, 304-319.
131. CLSI, *Journal*, 2015, **M07-A10**.
132. N. Cerca, S. Martins, F. Cerca, K. K. Jefferson, G. B. Pier, R. Oliveira and J. Azeredo, *Journal of Antimicrobial Chemotherapy*, 2005, **56**, 331-336.
133. S. Tyanova, T. Temu, P. Sinitcyn, A. Carlson, M. Y. Hein, T. Geiger, M. Mann and J. Cox, *Nature Methods*, 2016, **13**, 731-740.
134. S. Maere, K. Heymans and M. Kuiper, *Bioinformatics*, 2005, **21**, 3448-3449.
135. D. B. Kearns, F. Chu, S. S. Branda, R. Kolter and R. Losick, *Molecular Microbiology*, 2005, **55**, 739-749.
136. A. Ostrowski, A. Mehert, A. Prescott, T. B. Kiley and N. R. Stanley-Wall, *Journal of Bacteriology*, 2011, **193**, 4821-4831.
137. F.-M. Chang, S.-J. Hong, Y.-J. Sheng and H.-K. Tsao, *Applied Physics Letters*, 2009, **95**, e064102.
138. L. Feng, Y. Zhang, J. Xi, Y. Zhu, N. Wang, F. Xia and L. Jiang, *Langmuir*, 2008, **24**, 4114-4119.
139. T. Young, *Philosophical Transactions - Royal Society of London*, 1805, **95**, 65-87.
140. M. W. Wong, *Discrete Foruier Analysis*, Springer Science & Business Media, 2011.
141. K. Ueda, T. Seki, T. Kudo, T. Yoshida and M. Kataoka, *Journal of Bacteriology*, 1999, **181**, 78-82.
142. D. T. Verhamme, E. J. Murray and N. R. Stanley-Wall, *Journal of Bacteriology*, 2009, **191**, 100-108.
143. H. Takamatsu, Y. Chikahiro, T. Kodama, H. Koide, S. Kozuka, K. Tochikubo and K. Watabe, *Journal of Bacteriology*, 1998, **180**, 2968-2974.
144. T. Shida, H. Hattori, F. Ise and J. Sekiguchi, *Bioscience, Biotechnology, and Biochemistry*, 2000, **64**, 1522-1525.
145. R. L. Smith, L. J. Thompson and M. E. Maguire, *Journal of Bacteriology*, 1995, **177**, 1233-1238.
146. S. Kesel, S. Grumbein, I. Gümperlein, M. Tallawi, A.-K. Marel, O. Lieleg and M. Opitz, *Applied and Environmental Microbiology*, 2016, **81**, 2424-2432.
147. S. Grumbein, M. Opitz and O. Lieleg, *Metallomics*, 2014, **6**, 1441-1450.

148. A. Seminara, T. E. Angelini, J. N. Wilking, H. Vlamakis, S. Ebrahim, R. Kolter, D. A. Weitz and M. P. Brenner, *Proceedings of the National Academy of Sciences*, 2012, **109**, 1116-1121.
149. M. Asally, M. Kittisopikul, P. Rué, Y. Du, Z. Hu, T. Çağatay, A. B. Robinson, H. Lu, J. Garcia-Ojalvo and G. M. Süel, *Proceedings of the National Academy of Sciences*, 2012, **109**, 18891-18896.
150. N. J. Shirtcliffe, G. McHale and M. I. Newton, *Langmuir*, **2009**, **25**, 14121-14128.
151. J. Ju, H. Bai, Y. Zheng, T. Zhao, R. Fang and L. Jiang, *Nature Communications*, 2012, **3**, e1247.
152. W. J. Hamilton and M. K. Seely, *Nature*, 1976, **262**, 284-285.
153. Y. Zheng, H. Bai, Z. Huang, X. Tian, F.-Q. Nie, Y. Zhao, J. Zhai and L. Jiang, *Nature*, 2010, **463**, 640-643.
154. H. Bai, X. Tian, Y. Zheng, J. Ju, Y. Zhao and L. Jiang, *Advanced Materials*, 2010, **22**, 5521-5525.
155. J. Ju, Y. Zheng and L. Jiang, *Accounts of Chemical Research*, 2014, **47**, 2342-2352.
156. A. R. Parker and C. R. Lawrence, *Nature*, 2001, **414**, 33-34.
157. M. Nosonovsky and B. Bhushan, *Lotus versus rose: Biomimetic surface effects*, Springer, Berlin, Heidelberg, 2012.
158. M. Klotz, M. Kretschmer, A. Goetz, S. Ezendam, O. Lieleg and M. Opitz, *RSC Advances*, 2019, **9**, 11521-11529.
159. A. Marmur, *Biofouling*, 2006, **22**, 107-115.
160. P. Zhang, L. Lin, D. Zang, X. Guo and M. Liu, *Small*, 2016, **13**, e1503334.
161. Nonjabulo P. Gule, Nusrat M. Begum and B. Klumperman, *Critical Reviews in Environmental Science and Technology*, 2015, **46**, 535-555.
162. A. Harwood and J. C. Coates, *Current Opinion in Cell Biology*, 2004, **16**, 470-476.
163. T. R. Garrett, M. Bhakoo and Z. B. Zhang, *Progress in Natural Science*, 2008, **18**, 1049-1056.
164. S. B. Surman, J. T. Walkerb, W. Weaver, A. Skinnere, D. T. Goddardc, K. Hansonf, L. H. G. Mortond, D. Caldwellf, C. W. Keevilb and J. Kurtz, *Journal of Microbiological Methods*, 1996, **25**, 57-70.
165. R. N. Biswal and N. L. Maguer, *Journal of Food Process Engineering*, 1989, **11**, 159-176.
166. M. P. Herrling, J. Weisbrodt, C. M. Kirkland, N. H. Williamsone, S. Lacknera, S. L. Codd, J. D. Seymour, G. Guthausen and H. Horn, *Biotechnology and Bioengineering*, 2017, **12**, 2857-2867.
167. N. L. Kavanaugh and K. Ribbeck, *Applied and Environmental Microbiology*, 2012, **78**, 4057-4061.
168. O. Borugă, C. Jianu, C. Mişcă, I. Goleţ, A. Gruia and F. Horhat, *Journal of Medicine and Life*, 2014, **7**, 56-60.
169. G. Vazquez, E. Alvarez and J. M. Navaza, *Journal of Chemical and Engineering Data*, 1995, **40**, 611-614.
170. A. I. Toryanik and V. G. Pogrebnyak, *Journal of Structural Chemistry*, 1977, **17**, 464-465.

171. A. K. Yadav and S. V. Singh, *Journal of Food Science and Technology*, 2014, **51**, 1654–1673.
172. S. M. Stocks, *Cytometry Part A* 2004, **2**, 189-195.
173. P. Stiefel, S. Schmidt-Emrich, K. Maniura-Weber and Q. Ren, *BMC Microbiology*, 2015, **15**, e36.
174. A. Bridier, R. Briandet, V. Thomas and F. Dubois-Brissonnet, *Biofouling*, 2011, **27**, 1017-1032.
175. T. N. Campbell and F. Choy, *Molecular Biology Today*, 2001, **2**, 1-4.
176. K. Poole, *Trends in Microbiology*, 2017, **25**, 820-832.
177. O. Lieleg, M. Caldara, R. Baumgartel and K. Ribbeck, *Soft Matter*, 2011, **7**, 3307-3314.
178. Y. Shen, P. C. Huang, C. Huang, P. Sun, G. L. Monroy, W. Wu, J. Lin, R. M. Espinosa-Marzal, S. A. Boppart, W.-T. Liu and T. H. Nguyen, *npj Biofilms and Microbiomes*, 2018, **4**, e15.
179. A. Keren-Paz, V. Brumfeld, Y. Oppenheimer-Shaanan and I. Kolodkin-Gal, *npj Biofilms and Microbiomes*, 2018, **4**, e8.
180. S. T. Sultana, D. R. Call and H. Beyenal, *npj Biofilms and Microbiomes*, 2016, **2**, e2.
181. Y. Shen, G. L. Monroy, N. Derlon, D. Janjaroen, C. Huang, E. Morgenroth, S. A. Boppart, N. J. Ashbolt, W.-T. Liu and T. H. Nguyen, *Environmental Science & Technology*, 2015, **49**, 4274-4282.
182. E. C. Hollenbeck, J. C. N. Fong, J. Y. Lim, F. H. Yildiz, G. G. Fuller and L. Cegelski, *Biophysical journal*, 2014, **107**, 2245-2252.
183. J. C. N. Fong, K. Karplus, G. K. Schoolnik and F. H. Yildiz, *Journal of bacteriology*, 2006, **188**, 1049-1059.
184. D. Monroe, *PLOS Biology*, 2007, **5**, e307.
185. J. L. Dale, J. L. Nilson, A. M. T. Barnes and G. M. Dunny, *npj Biofilms and Microbiomes*, 2017, **3**, e15.
186. A. Farajzadeh Sheikh, A. Asareh Zadegan Dezfuli, T. Navidifar, S. S. Fard and M. Dehdashtian, *Infection and Drug Resistance*, 2019, **12**, 1771-1782.
187. H. A. O'Connell, G. S. Kottkamp, J. L. Eppelbaum, B. A. Stubblefield, S. E. Gilbert and E. S. Gilbert, *Applied and Environmental Microbiology*, 2006, **72**, 5013-5019.
188. E. M. Decker, G. Maier, D. Axmann, M. Brecx and C. von Ohle, *Quintessence International*, 2008, **39**, 17-22.
189. B. W. Peterson, Y. He, Y. Ren, A. Zerdoum, M. R. Libera, P. K. Sharma, A.-J. van Winkelhoff, D. Neut, P. Stoodley, H. C. van der Mei and H. J. Busscher, *FEMS microbiology reviews*, 2015, **39**, 234-245.
190. S. Pan, A. K. Kota, J. M. Mabry and A. Tuteja, *Journal of the American Chemical Society*, 2013, **135**, 578-581.
191. D. R. Lovley, *mBio*, 2017, **8**, e00695-00617.
192. N. S. Malvankar, M. Vargas, K. P. Nevin, A. E. Franks, C. Leang, B.-C. Kim, K. Inoue, T. Mester, S. F. Covalla, J. P. Johnson, V. M. Rotello, M. T. Tuominen and D. R. Lovley, *Nature Nanotechnology*, 2011, **6**, 573-579.
193. P. Q. Nguyen, Z. Botyanszki, P. K. R. Tay and N. S. Joshi, *Nature Communications*, 2014, **5**, e4945.

194. T. Scheibel, R. Parthasarathy, G. Sawicki, X.-M. Lin, H. Jaeger and S. L. Lindquist, *Proceedings of the National Academy of Sciences*, 2003, **100**, 4527-4532.
195. A. Lakshmanan, S. Zhang and C. A. E. Hauser, *Trends in Biotechnology*, 2012, **30**, 155-165.
196. J. Yong, F. Chen, Q. Yang, J. Huo and X. Hou, *Chemical Society Reviews*, 2017, **46**, 4168-4217.
197. X. Gao, L.-P. Xu, Z. Xue, L. Feng, J. Peng, Y. Wen, S. Wang and X. Zhang, *Advanced Materials*, 2014, **26**, 1771-1775.
198. Z. Xue, S. Wang, L. Lin, L. Chen, M. Liu, L. Feng and L. Jiang, *Advanced Materials*, 2011, **23**, 4270-4273.
199. Q. Wen, J. Di, L. Jiang, J. Yu and R. Xu, *Chemical Science*, 2013, **4**, 591-595.
200. Y.-Q. Liu, Y.-L. Zhang, X.-Y. Fu and H.-B. Sun, *ACS Applied Materials & Interfaces*, 2015, **7**, 20930-20936.
201. I. E. Palamà, S. D'Amone, V. Arcadio, D. Caschera, R. G. Toro, G. Gigli and B. Cortese, *Journal of Materials Chemistry A*, 2015, **3**, 3854-3861.
202. R. Singh, D. Paul and R. K. Jain, *Trends in Microbiology*, 2006, **14**, 389-397.
203. F. Kargi and S. Eker, *Process Biochemistry*, 2005, **40**, 2105-2111.
204. E. J. Murray, T. B. Kiley and N. R. Stanley-Wall, *Microbiology*, 2009, **155**, 1-8.
205. E. J. Murray, M. A. Strauch and N. R. Stanley-Wall, *Journal of bacteriology*, 2009, **191**, 6822-6832.